2021

Exploring the Dopamine Transporter Utilizing a Two-Pronged Approach with Novel Cathinone Analogs and Mutant Dopamine Transporters

Charles B. Jones III
Virginia Commonwealth University

EXPLORING THE DOPAMINE TRANSPORTER UTILIZING A TWO-PRONGED APPROACH WITH NOVEL CATHINONE ANALOGS AND MUTANT DOPAMINE TRANSPORTERS

A thesis submitted in partial fulfillment of the requirements for the degree of Master of Science at Virginia Commonwealth University.

by

Charles Bernard Jones IIII

Bachelor of Science in Chemistry, University of Central Florida 2014

Director: MAŁGORZATA DUKAT

Associate Professor, Department of Medicinal Chemistry

Virginia Commonwealth University

Richmond, Virginia

July, 2021

Acknowledgement

I would like to thank Dr. Dukat for taking me on as a student. She has allowed me to finally do work that I am truly passionate about and her guidance and patience have been paramount in my journey to become a medicinal chemist. Thank you to Dr. Glennon for all of his insights and help. He really pushed me to think critically about all aspects of my projects. Thank you to my lab mates Preeth and Jeremy who have supported and encouraged me not only in the lab but in life as well. Thank you to Dr. Eltit for teaching me all the biology used for my projects and for helping me not to over stress about work. I would also like to thank his entire lab especially Vy and Sebastian who helped teach me cell culturing and biological assays. Thank you to Dr. Fernando and everyone at the Unimin R&D group, without their tutelage I could not be where I am at today. A special thank you to Sara. There are not words for what you mean to me, you support me in every way. You believe in me and help me be the person I want to be. Finally, I would like to thank my family, my sister for being able to provide support for when I cannot be there, my father for showing me how to have integrity and for being strong, and my mother for encouraging me and always letting me chase my dreams.

Table of Contents

List of Tables……vii

List of Figures……..…ix

List of Schemes…….xiv

List of Abbreviations……..xv

Abstract……...xvii

I. Introduction……..…1

II. Background……..…4

A. Monoamine Transporters (MATs) ……..…4

B. Structure of MATs……..…7

C. Pharmacology of MATs……...11

D. Transporter Ligands and Drugs of Abuse……13

1. Releasers……15

2. Inhibitors……..17

3. Partial Releasers……18

E. Assay Methods……19

1. APP^+ Assay……20

2. Ca^{2+} Flux Assay……..21

F. Cathinone SAR……22

1. Aryl Substitution……..24

2. α-Methyl Modification……26

3. Amine Modification……27

4. Inhibitor Cathinone Deconstruction……28
5. Inhibitor Cathinone Elaboration……30
G. Methylphenidate SAR……..33
1. Aryl Substitution……..35
2. Amine Substitution……38
3. Ester Modifications……40
4. Ring Modifications……..41
H. New Methylphenidate/Cathinone Hybrids……43
III. Specific Aims and Rationale ……..48
A. Project 1……..48
Aim 1. Construct a new hDAT homology model……....48
Aim 2. Elucidate factors determining the potency of 3,4-disubstituted cathinone/methylphenidate hybrids ……....49
a. Synthesis……49
b. Biological Studies……..……..53
c. Docking……54
B. Project 2..……54
Aim. Evaluate binding modes of selected cathinones at DAT mutant transporters utilizing 3D molecular modeling…..…..54
IV. Results and Discussion……..57
A. Project 1……..57
Aim 1. Construction of a new hDAT homology model……..57
Aim 2. Synthesis and evaluation of cathinone/methylphenidate hybrids...62

a. Synthesis……62

b. Biological Studies……..……..75

c. Docking……81

B. Project 2……..86

Aim. Evaluate binding modes of selected cathinones at DAT mutant transporters utilizing 3D molecular modeling ……..……....86

a. Interactions at *subpocket A*……..……95

b. Interactions at *subpocket B*……..96

c. Interactions at *subpocket C*……..99

V. Conclusion……...101

VI. Experimental……...103

A. Molecular modeling……103

B. Synthesis……104

1. 2-(3,4-Dichlorobenzoyl)piperidine Hydrochloride (**119**)……..…..105
2. 2-(3,4-Dimethylbenzoyl)piperidine Hydrochloride (**120**)……..….106
3. 2-(Naphtho-2-yl)piperidine Hydrochloride (**121**)……....107
4. *N*-Boc-pipecolic acid (**123**)……108
5. *N*-Boc-pipecolate *N*-(methylmethoxyl)amide (**124**)……...108
6. 2-(1-Pentoyl)piperidine Hydrochloride (**132**)…..……....109

C. APP^+ uptake assay……110

1. Preparation of HEK293 cells……110
2. Imaging solution for experiment……...110
3. Agents……..110

4. Live-cell imaging……111

5. Analysis……111

VII. Bibliography……...112

VIII. Vita……..125

List of Tables

Table 1. dDAT crystal structures……..…….8

Table 2. hSERT crystal structures……..……10

Table 3. Association of SLC6 family members with substrate and human disease……12

Table 4. Inhibition of [^{3}H]dopamine uptake by elaborated analogs of α-PVP (**11**)……..31

Table 5. DAT binding affinity (IC_{50}, nM) and uptake inhibition potency (IC_{50}, nM) of aryl substituted methylphenidate (**9**) analogs **51-79**……36

Table 6. [^{3}H]WIN 35,428 binding affinities of methylphenidate (**9**) analogs with amine substituents……39

Table 7. [^{3}H]WIN 35,428 binding affinities (IC_{50}, nM) of ester-modified methylphenidate (**9**) analogs.……41

Table 8. DAT binding affinity (IC_{50}, nM) and uptake inhibition potency (IC_{50}, nM) of piperidine ring modified methylphenidate (**t9**) analogs **108-111**.……42

Table 9. DAT uptake inhibition potency (IC_{50}, nM) of aryl ring modified hybrid (i.e., **112**) compounds and DAT binding affinity (IC_{50}, nM) of corresponding aryl-ring modified methylphenidate (**9**) analogs……46

Table 10. Lipophilic (π), electronic (σ), steric (Vol), hydrogen bond (HB) acceptor, and halogen bond formation properties of compounds **119**-**121**……..……51

Table 11. HINT table of highest scoring **dt9** solution with scores for each type of molecular interaction……..61

Table 12. Uptake inhibition (IC_{50}, nM) values of methylphenidate (**t9**) and hybrid compounds **119**-**121** in the APP+ uptake assay at hDAT……78

Table 13. HINT scores in descending order of compounds **119**-**121** and **dt9**…….83

Table 14. Potency of MDPV (**10**), α-PVP (**11**), and MDPPP (**39**) inhibiting DA-induced Ca^{2+} signals at the indicated transporters……..……..88

Table 15. Amino acid residues corresponding to the *A*, *B*, and *C* subpockets that make up the S1 central binding site in *wt* dDAT, dDAT (i.e., quadruple) mutant, and hDAT...93

Table 16. Gold and HINT scores for docking solutions of the agents MDPV (**10**), α-PVP (**11**), and MDPPP (**39**) in the *wt* dDAT, dDAT mutant, and hDAT models……..94

Table 17. Tabulated positive, negative, and sum total HINT interactions of docked solutions for the agents MDPV (**10**), α-PVP (**11**), and MDPPP (**39**) in the *wt* dDAT, dDAT (i.e., quadruple) mutant, and hDAT models……..……95

List of Figures

Figure 1. Topology of monoamine transporters depicting 12 transmembrane domains connected by intracellular and extracellular loops……..4

Figure 2. A) schematic representation of monoaminergic synaptic terminals. B) chemical structures of the endogenous substrates for SLC6 neurotransmitter transporters (NTTs) and ion coupling stoichiometry for neurotransmitter reuptake……..6

Figure 3. Representation of uptake versus releaser efflux cycle. T_o is the transporter facing outward. T_i is the transporter facing inward.....14

Figure 4. Structures of selected releasing agent drugs of abuse……...…...15

Figure 5. A) A field of khat plants. B) A bundle of fresh khat leaves.……16

Figure 6. Structures of selected reuptake inhibitor drugs of abuse……...17

Figure 7. Structures of selected partial releasing agents……19

Figure 8. Structure of APP^+ (**14**) and fluorescence of HEK293 cells stably expressing hDAT exposed to APP^+…….21

Figure 9. Releasers (e.g., AMPH, **4**) cause Ca^{2+} efflux by Ca^{2+} channel activation through cellular depolarization. Inhibitors (e.g., MDPV, **10**) do not activate Ca^{2+} channels……...22

Figure 10. Structures of the two isomers of cathinone (**6**)……..23

Figure 11. Structure of cathinone (**6;** R_1=R_3=H, R_2=CH_3) and numbering and position of substituents……23

Figure 12. Structure of cathinone analogs with selected aryl substitutions……....24

Figure 13. Structure of methcathinone analogs with selected aryl substitutions…….25

Figure 14. Structure of cathinone analogs with selected α-methyl modifications……...26

Figure 15. Structure of cathinone analogs with selected amine modifications……..…..27

Figure 16. Deconstruction of MDPV (**10**). IC_{50} values represent potency to block reuptake of DA. Each arrow represents one structural modification.…….……...29

Figure 17. Four stereoisomers of methylphenidate (**9**)……...33

Figure 18. (A) Global minimum of *d-threo*-methylphenidate (**dt9**) (B) Solved crystal structure of *l-threo*-methylphenidate (**lt9**)…….……..34

Figure 19. SAR features that have been quantitatively explored for (**dt9**)…..……....35

Figure 20. Cathinone (**6**)/methylphenidate (**t9**) hybrid compound **112**…....44

Figure 21. Ca^{2+} efflux assay of selected hybrid compound **112** showing inhibitor properties…….45

Figure 22. Correlation (r = 0.91) of APP^+ uptake assay data of hybrid (i.e., **112**) compounds and binding data of methylphenidate (**t9**) analogs.....47

Figure 23. Structures of hybrid compound **112**, potent hybrid compound **119**, and two proposed new compounds **120** and **121**.…….……...……...50

Figure 24. Representation of positive and negative electrostatic interactions involving a halogen bonds (above) and aromatic rings (below)…….....53

Figure 25. Structures of agents to be examined at dDAT mutant transporters: MDPV (**10**), α-PVP (**11**), and MDPPP (**39**)…….55

Figure 26. Summary of two-pronged approach to better understand DAT……56

Figure 27. hDAT homology model (cartoon) with labeled transmembrane (TM) helices……..59

Figure 28. hDAT homology model (cartoon, green) with possible binding pose of methylphenidate (**dt9**, sticks, white) forming salt bridge (dotted line, yellow) with D79..60

Figure 29. ^{1}H NMR spectrum of compound **119**……..67

Figure 30. ^{1}H NMR spectrum of compound **132**……...70

Figure 31. ^{1}H NMR spectrum of compound **120**……..74

Figure 32. ^{1}H NMR spectrum of compound **121**……..75

Figure 33. Dose-response curves of **t9** and hybrid compounds **119**-**121** in an APP^{+} uptake assay at hDAT ……..……77

Figure 34. Correlation between the binding data of **t9** analogs (x-axis) and APP^{+} uptake assay data (y-axis) for the corresponding methylphenidate hybrid compounds (r = 0.91, n = 8). Predicted pIC_{50} activity for compound **121** analog (red)……..80

Figure 35. Correlation between the binding data of **t9** analogs (x-axis) and APP^+ uptake assay data (y-axis) for the corresponding methylphenidate hybrid compounds (r = 0.89, n = 9). Predicted pIC_{50} binding for dimethyl **t9** analog (red)……81

Figure 36. hDAT homology model (cartoon, green) with possible binding poses of S isomer hybrids **119** (sticks, purple), **120** (sticks, cyan), and **121** (sticks, magenta)……82

Figure 37. Sequence and alignment of hSERT, dDAT, and hDAT. Highlighted areas form the S1 central binding site and boxed amino acids are selected sites of dDAT mutations……87

Figure 38. hDAT homology model (Connolly surface, green) with MDPV (**10**, sticks, yellow) in the S1 central binding pocket (Connolly surface, red)……..……90

Figure 39. Divided *A*, *B*, and *C* subpockets with possible binding pose of MDPV (**10**, sticks, yellow), α-PVP (**11**, sticks, orange), and MDPPP (**39**, sticks, wheat) in hDAT (lines and cartoon, cyan) S1 central binding site……..92

Figure 40. Amino acid residues (lines) that make up *subpocket A* for hDAT (cyan), dDAT mutant (green), and *wt* dDAT (purple). MDPV (**10**, sticks, yellow) shown as a reference……..96

Figure 41. Amino acid residues (lines) that make up *subpocket* B for hDAT (cyan), dDAT mutant (green), and *wt* dDAT (purple). MDPV (**10**, sticks, yellow) shown as a reference……..97

Figure 42. Amino acid residues (lines) that make up *subpocket C* for hDAT (cyan), dDAT mutant (green), and *wt* dDAT (purple). MDPV (**10**, sticks, yellow) shown as a reference……...……...100

List of Schemes

Scheme 1. General procedure for target compound synthesis……..62

Scheme 2. Synthesis of intermediate **123**……....63

Scheme 3. Synthesis of intermediate **124**……64

Scheme 4. Synthesis of intermediate **128**……65

Scheme 5. Synthesis of intermediate compound **131**……66

Scheme 6. Synthesis of target compound **119**……68

Scheme 7. Failed synthesis of target compound **120**……..69

Scheme 8. Synthesis of off target compound **132**……71

Scheme 9. Successful synthesis of target compound **120**……72

List of Abbreviations

5-HT	Serotonin
α-PVP	α-Pyrrolidinovalerophenone
ADHD	Attention deficit hyperactivity disorder
AMPH	Amphetamine
APP^+	4-(4-Dimethylamino)phenyl-1-methylpyridinium
BOP	Benzotriazol-1-yloxytris(dimethylamino)phosphonium hexafluorophosphate
DA	Dopamine
DAT	Dopamine transporter
dDAT	*Drosophila melanogaster* dopamine transporter
EL	Extracellular loop
GFP	Green fluorescent protein
GPCR	G protein coupled receptor
HB	Hydrogen bond
hDAT	Human dopamine transporter
HEK	Human embryonic kidney
HMPA	Hexamethylphosphoramide

hSERT	Human serotonin transporter
LeuT	Leucine Transporter
LGIC	Ligand gated ion channel
MAT	Monoamine Transporter
MDMA	*N*-Methyl-1-(3,4-methylenedioxyphenyl)-2-aminopropane
MDPPP	3,4-Methylenedioxy-α-pyrrolidinopropiophenone
MDPV	Methylenedioxypyrovalerone
NE	Norepinephrine
NET	Norepinephrine transporter
NPS	New Psychoactive Substance
NSS	Neurotransmitter sodium symporter
NTT	Neurotransmitter transporter
PBD	Protein Data Bank
ROI	Region of interest
SERT	Serotonin transporter
SLC6	Solute carrier 6
SPL	SYBYL's programing language
TLC	Thin layer chromatography

Abstract

EXPLORING THE DOPAMINE TRANSPORTER UTILIZING A TWO-PRONGED APPROACH WITH NOVEL CATHINONE ANALOGS AND MUTANT DOPAMINE TRANSPORTERS

By Charles Jones

A thesis submitted in partial fulfillment of the requirements for the degree of Master of Science at Virginia Commonwealth University.

Virginia Commonwealth University, 2021

Major Director: Małgorzata Dukat, Associate Professor

Department of Medicinal Chemistry

The dopamine transporter (DAT) is responsible for the removal of the neurotransmitter from the synaptic gap and a therapeutic target for a multitude of drugs. While the ortholog *Drosophila melanogaster* dopamine transporter (dDAT) and human serotonin transporter (hSERT) have resolved structures, the human dopamine transporter (hDAT) does not. A 3-D computational homology model of hDAT was constructed for the study of molecular interactions with agents within the central binding site (S1) of the transporter.

Synthetic cathiones are a class of abused stimulant drugs that primarily target DAT. Greater than 150 cathinones have been identified on the clandestine market but there is not much known about the structure-activity relationship (SAR) of these abused compounds. A dichloro substituted benzoylpiperdine compound, part of novel series of benzoylpiperdine cathinones, was found to be a potent DAT inhibitor. Two new disubstituted compounds were computationally modelled, synthesized, and biologically evaluated to investigate the effect of these substituents in DAT inhibitor potency. It was found that all compounds were active and that the hybrids with electron donating substituents were weaker compared to the hybrids with electron withdrawing substituents tested.

Cathinones based on the pyrrolidinophenone scaffold, such as 3,4-methylenedioxypyrovalerone (MDPV), α-pyrrolidinopentiophenone (α-PVP), and 3,4-methylenedioxy-α-pyrrolidinopropiophenone (MDPPP), are established illicit psychostimulants. These compounds are potent inhibitors of hDAT but have little to no activity at dDAT. In collaboration with Dr. Eltit's lab (VCU) gain-of-function studies and in silico modeling using mutant DAT transporters were performed. Four non-conserved amino acid residues critical for MDPV's high potency activity as a reuptake inhibitor at hDAT were identified. These residues can drive MDPV selectivity not only by stabilizing binding, but also by controlling access to its binding site.

I. Introduction

Monoamine transporters (MATs) are a family of transporters that regulate the concentration of neurotransmitters in the synaptic gap.[1] Dysfunction of these transporters are responsible for a number of neuropsychiatric disorders.[1] MATs are a target for therapeutic agents that can treat these disorders but is also a primary target for drugs of abuse.[1] Of the three MATs, the dopamine transporter (DAT) is a specific target of abused stimulant drugs due to dopamine's (DA) reward pathways.[1]

Human DAT (hDAT) does not have a solved crystal structure therefore computational modelling studies of this transporter must make use of homology models. Less than 20 years ago the bacterial ortholog leucine transporter had been crystallized and was essential for the first developed homology models for hDAT.[2] Even more recently *drosophila* DAT dDAT had been crystallized followed by hSERT.[3,4] With the newer, more closely related crystallized transporter structures available, a more accurate homology model will be developed to conduct molecular modeling studies of hDAT.

Synthetic cathinones are a vast class of stimulant compounds structurally related to the naturally occurring stimulant cathinone found in the leaves of the khat plant.[5] This group of compounds is responsible for the majority of stimulant new psychoactive substances (NPS) and more are emerging every year on the clandestine market.[5] While there are numerous cathinones that are being abused, little is known about the SAR of these compounds. Methylphenidate which is a well-known and prescribed drug for attention

deficit hyperactivity disorder (ADHD) has extensive SAR established.[6] Efforts have successfully been made to correlate a novel series of benzoylpiperdine cathinones that share features with methylphenidate with known methylphenidate analogs in order to use the known methylphenidate SAR to inform cathinone SAR.[7] In this series, it was found that the 3,4-dichloro substituted benzoylpiperdine was the most potent, even more potent than methylphenidate.[7] To expand on SAR understanding of hDAT and to determine which aspects cause the high potency of this disubstituted compound, two new benzoylpiperdine compounds with varying electronic and lipophilic character will be prepared and studied.

dDAT, which can be considered a hDAT mutant, functions the same under normal conditions. Abused stimulant cathinones such as MDPV are highly active at hDAT but have little to no activity at dDAT. These two transporters are closely related and share over 50% sequence identity.[3] In collaboration with Dr. Eltit's lab, a series of mutant dDATs were studied and it was found that with only 4 point mutations of dDAT to hDAT amino acid residues, MDPV gained activity in the mutant dDAT similar to what is observed in hDAT. Modelling will be performed in order to determine which amino acids are important in these interactions and what the cause of gain-of-function is for the mutant.

Utilizing this two pronged approach where hDAT will be studied using new compounds (cathinone hybrids) as well as using new transporters (dDAT mutants), a better understanding of the innerworkings of hDAT can be established which is essential for the

development of new medications for psychostimulant dependence, attention deficit hyperactivity, and other neuropsychiatric disorders associated with dopamine dysregulation.

II. Background

A. Monoamine Transporters (MATs)

The biogenic amine (monoamine) transporters or MATs are part of the neurotransmitter sodium symporter (NSS) and solute carrier 6 (SLC6) family.[1] They are a 12 transmembrane helix protein (Figure 1) that are Na^+/Cl^- dependent.[1] These transporters are found on neurons and glial cells, and are responsible for regulation of synaptic monoamines (serotonin (5-HT), dopamine (DA), and norepinephrine (NE)) that activate G protein coupled receptors (GPCRs) and ligand gated ion channels (LGICs).[1,8,9]

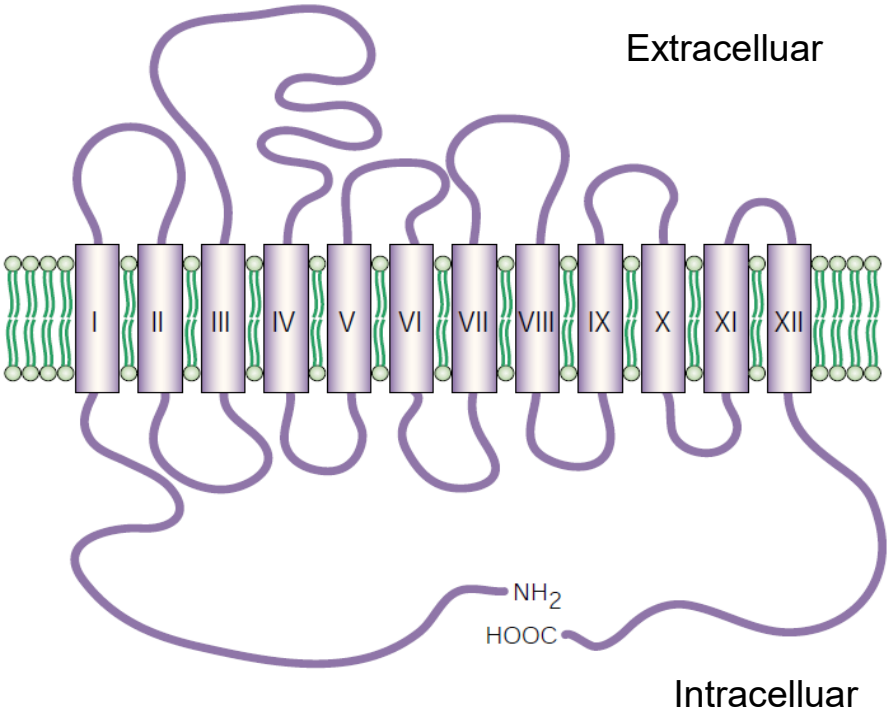

Figure 1. Topology of monoamine transporters depicting 12 transmembrane domains connected by intracellular and extracellular loops.[10]

Regulation occurs by the use of an electrochemical gradient to actively remove the monoamines from the extracellular space back into the presynaptic neuron through the transporter.[1] A different transporter is primarily responsible for each corresponding monoamine.[11] SERT is responsible for 5-HT (**1**), NET for NE (**2**), and DAT for DA (**3**) (Figure 2).[11] Each transporter moves the appropriate neurotransmitter along with different molar equivalent ions.[1] NET uses one Na^+ ion and one Cl^- ion. DAT uses two Na^+ ions and one Cl^- ion. SERT uses one Na^+ ion, one Cl^- ion, and counter transports one K^+ ion.[1] The intercellular potassium ion is transported to the extracellular space after the ligands (5-HT, Na^+, and Cl^-) have been released intercellularly and the transporter is changing conformation to its original state.[12]

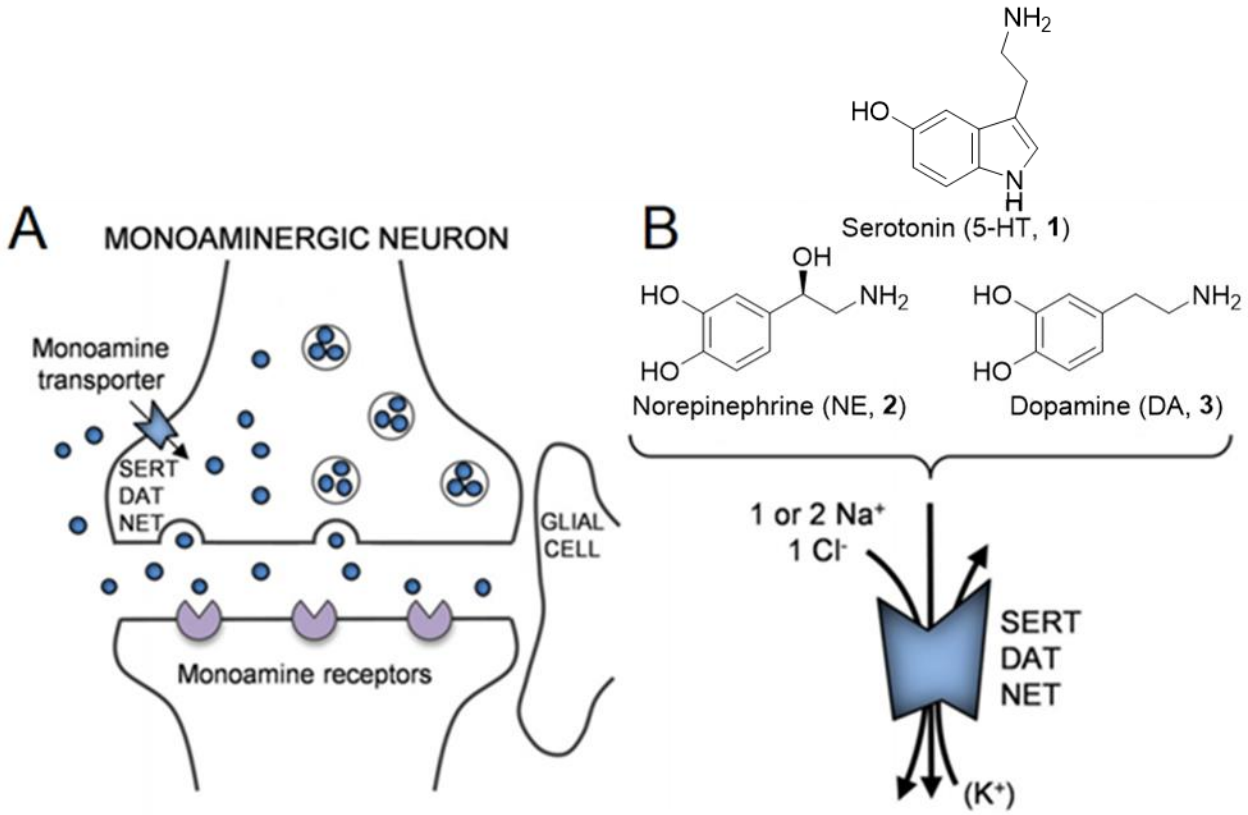

Figure 2. A) Schematic representation of monoaminergic synaptic terminals. B) Chemical structures of the endogenous substrates for SLC6 neurotransmitter transporters (NTTs) and ion coupling stoichiometry for neurotransmitter reuptake.[13]

These transporters play a role in neuropsychiatric disorders such as attention deficit hyperactivity disorder (ADHD), depression, orthostatic intolerance, epilepsy, Parkinsonism, schizophrenia, and drug abuse.[1] In 1961, Hertting and Axelrod were the first to describe the concept of the reuptake of NE (**2**) by sympathetic nerve terminals.[8] It was postulated that the reuptake of neurotransmitters by a transporter was essential for their deactivation.[8] DA and 5-HT were also later shown to have similar mechanisms.[10] Countless studies have since been conducted on the function of the monoamine uptake transporters. By the 1990s, the genes that code for the monoamine transporter proteins

were determined due to progress in molecular cloning techniques.[14] This facilitated the discovery of the localization, structural and functional domains, and contributions to brain function of the transporters using a variety of techniques such as heterologous expression systems, mutagenesis, in vivo imaging, and animal models with disrupted monoamine transporter genes.[10]

B. Structure of MATs

The first homologue of a monoamine transporter to be crystallized was the leucine transporter (LeuT) from the bacterium *Aquifex aeolicus*.[2] This transporter was crystallized in 2005 and has 12 transmembrane helices with a pseudo-2-fold axis in the membrane plane.[2] This protein shares 20% identity with the eukaryotic NSSs.[2] There are currently 22 published crystal structures of LeuT with multiple drugs that are in various states of the transport cycle. DAT, the first of the monoamine transporters to be crystallized in 2013, was crystallized from the fruit fly *Drosophila melanogaster* (i.e., dDAT).[3] Several point mutations (V74A, V275A, V311A, L415A, and G538L) and modifications were used to induce the transporter to crystallize.[3] Amino acid residues 1-20 as well as extracellular loop 2 (EL2) 164-206 were removed.[3] Amino acids 602–607 were replaced by a C-terminus green fluorescent protein (GFP–His8) tag with a thrombin cleavage site (LVPRGS).[3] Recombinant Human Anti-Dopamine transporter antibody antigen binding fragment (Fab) 9D5 at a ratio of DAT:Fab 1:1.1 was also used to enhance crystallization.[3] There are 14 current crystal structures of the *Drosophila* dopamine transporter (dDAT) bound to both releasing agents and uptake inhibitors (Table 1). All structures are either in the outward facing state (from inhibitors) or in the partially occluded state (from

releasing agents). The inward facing and occluded conformations have still not been crystallized. The uptake inhibitors that have been crystallized are nisoxetine, reboxetine, RTI55, win35428, cocaine, and nortriptyline.[3,15] The releasing agents are 3,4-dichlorophenethylamine, methamphetamine, and dextroamphetamine.[15] DA, the endogenous ligand, has also been crystallized with dDAT.[15] The dDAT crystal structure was a leap forward in modeling the human dopamine transporter (hDAT) as it shares greater than 50% identity.[3]

Table 1. dDAT crystal structures.[3,15,16]

PDB ID[a]	Resolution (Å)[b]	Agents	Mutation	Reference
Inhibitors				
4M48	2.96	Nortriptyline	V74A/V275A/ V311A/G538L/ L415A	Penmatsa 2013
4XNU	2.98	Nisoxetine	V74A/V275A/ V311A/G538L/ L415A	Penmatsa 2015
4XNX	3.00	Reboxetine	V74A/L415A	Penmatsa 2015
4XP5	3.30	RTI55	V74A/L415A	Wang 2015

4XPG	3.21	Win35428	D121G/S426M	Wang 2015
4XPB	3.05	Cocaine	D121G/S426M	Wang 2015
4XPF	3.27	RTI55	D121G/S426M	Wang 2015
4XP4	2.80	Cocaine	V74A/L415A	Wang 2015
Releasers				
4XPH	2.9	3,4-Dichloro phenethylamine	D121G/S426M	Wang 2015
4XP6	3.10	Methamphetamine	V74A/L415A	Wang 2015
4XPT	3.36	3,4-Dichloro phenethylamine	D121G/S426M	Wang 2015
4XPA	2.95	3,4-Dichloro phenethylamine	V74A/L415A	Wang 2015
4XP9	2.80	Dextroamphetamine	V74A/L415A	Wang 2015
Endogenous				
4XP1	2.89	Dopamine	V74A/L415A	Wang 2015

[a]Protein Data Bank ID; [b]X-ray.

The human serotonin transporter (hSERT) was first crystallized in 2016.[4] There are currently three different constructs of the crystallized transporter. There is the N- and C-terminally truncated wild-type (ΔN72, ΔC13), ts3 which contains the thermostabilizing mutations Y110A, I291A, and T439S, and ts2 which is identical to ts3 without the Y110A mutation.[4] Both ts2 and ts3 also have had mutations of the surface-exposed cysteines C554A, C580A, and C622A.[4] These constructs are then fused to a C-terminus GFP and

then tagged with twin Strep and a decahistadine for purification.[4] Two different recombinant antibody fragments have also been used to help crystallization, Fab 8B6 and 15B8.[4] Only Apo-state hSERT and reuptake inhibitors bound in hSERT have been crystallized. These inhibitors are Br-citalopram, (*S*)-citalopram (escitalopram), paroxetine, sertraline, fluvoxamine, Br-paroxetine, and levoparoxetine.[4,17-19]

Table 2. hSERT crystal structures.[4,17-19]

PDB ID	Method	Resolution (Å)	Agents	Mutation	Reference
5I6Z	X-ray	4.53	Apo	ts2	Coleman 2016
5I74	X-ray	3.395	Br-Citalopram	ts3	Coleman 2016
5I73	X-ray	3.24	Escitalopram	ts3	Coleman 2016
5I75	X-ray	3.49	Escitalopram, Br-Citalopram	ts3	Coleman 2016
5I6X	X-ray	3.14	Paroxetine	ts3	Coleman 2016
5I71	X-ray	3.15	Escitalopram	ts3	Coleman 2016
6AWO	X-ray	3.534	Sertraline	ts3	Coleman 2018
6AWN	X-ray	3.62	Paroxetine	S439T	Coleman 2018
6AWQ	X-ray	4.046	Sertraline	ts3	Coleman 2018
6AWP	X-ray	3.8	Fluvoxamine	ts3	Coleman 2018
6W2B	X-ray	4.7	Br-Paroxetine	ts2	Coleman 2020
6W2C	X-ray	6.3	Levoparoxetine	ts2	Coleman 2020

6DZW	Cryo-EM	4.3	Paroxetine	ts2	Coleman 2019
6DZV	Cryo-EM	4.2	Ibogaine	WT	Coleman 2019
6DZY	Cryo-EM	4.1	Ibogaine	ts2	Coleman 2019
6DZZ	Cryo-EM	3.6	Ibogaine	WT	Coleman 2019
6VRK	Cryo-EM	4.1	Br-Paroxetine	WT	Coleman 2020
6VRL	Cryo-EM	3.8	Levoparoxetine	WT	Coleman 2020
6VRH	Cryo-EM	3.3	Paroxetine	WT	Coleman 2020

Not only are there X-ray crystal structures but also cryo-EM structures for hSERT. Because of cryo-EM and the non-competitive inhibitor ibogaine, all conformations (outward facing, partially occluded, occluded, and inward facing) of hSERT have been reported.[17] Also due to citalopram orthosteric and allosteric sites of hSERT are known.[4] There are currently 19 published structures of hSERT (Table 2). NET has still not been crystallized to date. Other unexplored crystal structures are SERT with releasing agents, human DAT (hDAT), DAT with its occupied allosteric site, DAT occluded, DAT inward facing, and any of the above transporter with a partial releaser.

C. Pharmacology of MATs

The regulation of the transporters has been associated with multiple neuropsychiatric and other disorders (Table 3). [1] There are several pieces of evidence that support this association. The first is that therapeutic agents used to treat mood disorders target DAT,

NET, and SERT.[10] Second, monoamine transporter over expression/under expression have been shown to be prevalent in psychiatric and neurological disorders such as ADHD, depression, and Parkinson's disease.[10] This has been determined both through binding techniques in post mortem brain samples and brain imaging techniques.[10]

Table 3. Association of SLC6 family members with substrate and human disease.[1]

Transporter	Human Gene	Substrate	Disease Association
NET	SLC6A2	Norepinephrine	ADHD, Anorexia nervosa, Depression, Orthostatic intolerance, Cardiovascular disease
DAT	SLC6A3	Dopamine	Addiction, ADHD, Major affective disorder, Parkinson’s disease, Tourette’s syndrome
SERT	SLC6A4	Serotonin	Anxiety, Autism, Depression, Gastrointestinal disorders, Obesity, OCD, Premature ejaculation, Schizophrenia

D. Transporter Ligands and Drugs of Abuse

All agents that are affiliated with the monoamine transporters work under three modes of action. First, the endogenous ligands are substrates for the transporters and are co-transported with ions through the transporter into the cell.[13] The second type are inhibitors that will bind to the transporter in its outward facing state and prevent the transition to an occluded state.[13] The third type of agent's, known as releasers, mode of action is substrate-like but they also induce a reverse function of the transporter causing an efflux of endogenous monoamine neurotransmitters extracellularly (Figure 3).[20] Once the transporter is in the inward state releasing the agent intracellularly, endogenous ligands are then transferred in the reverse direction extracellularly.[20] There is a subclass of these releasers that are known as partial releasers.[21] They function like releasers but are not nearly as efficacious.[21]

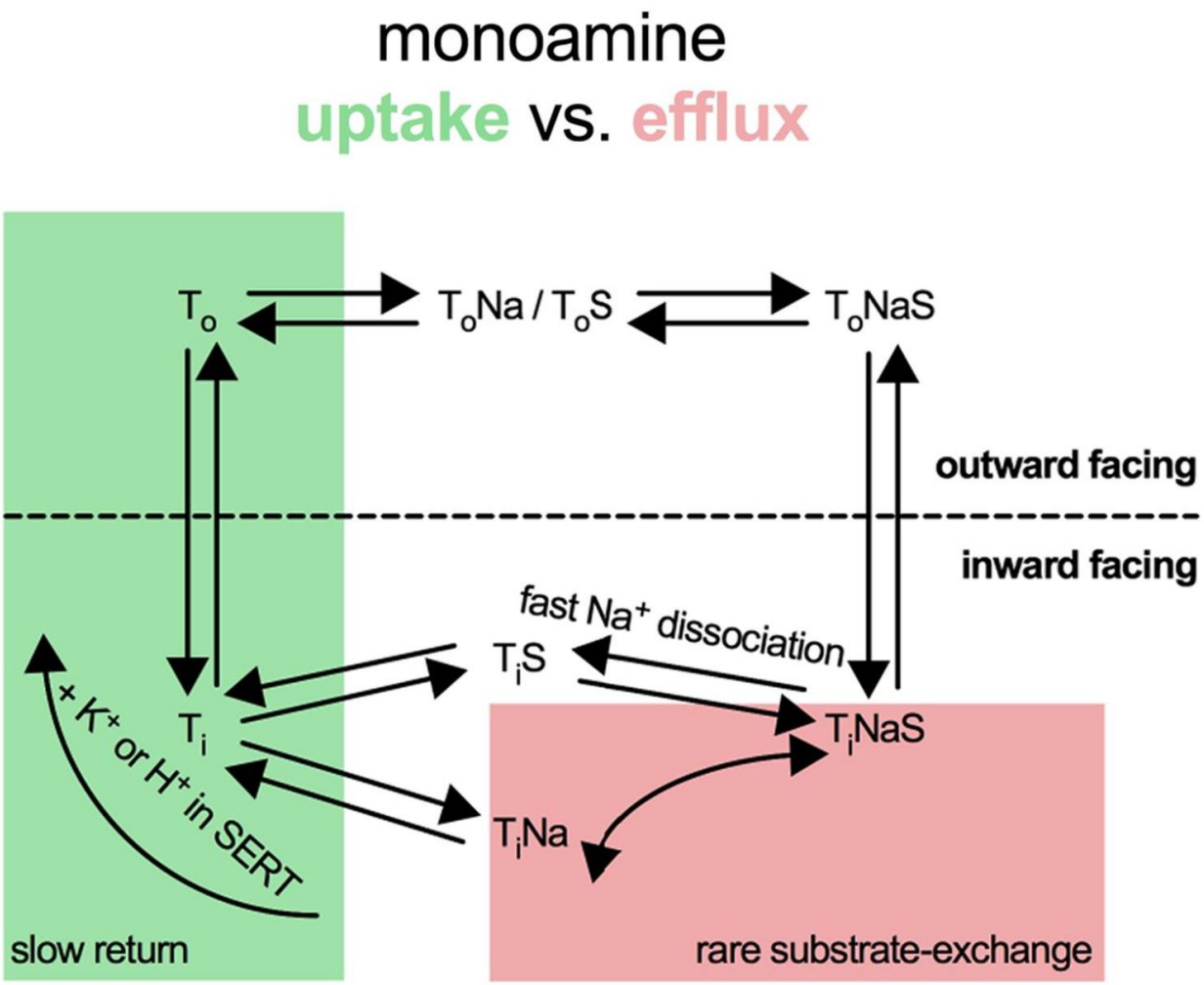

Figure 3. Representation of uptake versus releaser efflux cycle. T_o is the transporter facing outward. T_i is the transporter facing inward.[21]

The inhibitors make up the largest variety of these agents on the market. Many drugs of abuse directly affect the transporters. Of this category of drugs, all act either as a releaser or an inhibitor. Both types of agents have the same outcome with an overall increase in synaptic concentration of neurotransmitter.

1. Releasers

The most widely abused and infamous releasers are amphetamine (AMPH, **4**) and methamphetamine (**5**). Both these agents are Schedule II in the United States. As such, they have limited medical use but a high potential for abuse, with use potentially leading to psychological or physical dependance.[22] The severe behavioral effects of these agents are related to the release of excess DA into the synaptic cleft of dopaminergic neurons.[23] N-Methylated AMPH, that is, methamphetamine (**5**), has been shown to have increased potency compared to AMPH.[23]

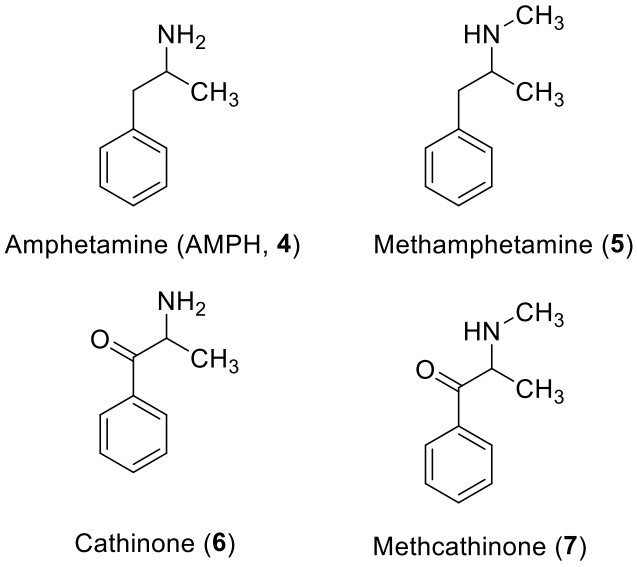

Figure 4. Structures of selected releasing agent drugs of abuse.

The chewing of khat leaves (Figure 5) has been practiced for hundreds of years in middle eastern countries to produce a stimulant effect.[24] The stimulant effects are primarily due

to the chemical agent cathinone (**6**), a naturally occurring psychoactive alkaloid that is a beta ketone analog of amphetamine (**4**) as well as a potent releasing agent.[24]

A. **B.**

Figure 5. A) A field of khat plants. B) A bundle of fresh khat leaves.[25]

The first synthetic cathinone derivative reported was methcathinone (**7**) in 1928,[26] although the term “methcathinone” was not coined until 1987.[27] Like amphetamine (**4**) increasing in potency with N-methylation to methamphetamine (**5**), methcathinone (**7**) was considered in the same vein with N-methylation of cathinone (**6**).[27] The recreational use of methcathinone (**7**) has been mostly reported in former USSR countries but gained popularity in the USA during the 1990s.[24,28] Recently the majority of new psychoactive substances (NPS) that effect the monoamine transporters are synthetic cathinones.[29]

They are usually sold as "legal highs" and multiple synthetic cathinone analogs have gained prominence starting around 2007.[29]

2. Inhibitors

The most infamous inhibitor drug of abuse is cocaine (**8**) which is the major active stimulant of the coca leaf (*Erythroxylon coca*).[30,31] The leaf is widely used and chewed in South America as an anti-fatigue agent.[30] While cocaine itself is a Schedule II drug with legitimate medical use, there is a worldwide drug abuse problem with it.[31] Cocaine (**8**) is a nonselective inhibitor across all three MATs, but the main action that contributes to cocaine's (**8**) and all inhibitor drug of abuse's abuse potential is the inhibition of DAT allowing for an increase of DA concentration in the synaptic cleft of dopaminergic neurons.[31]

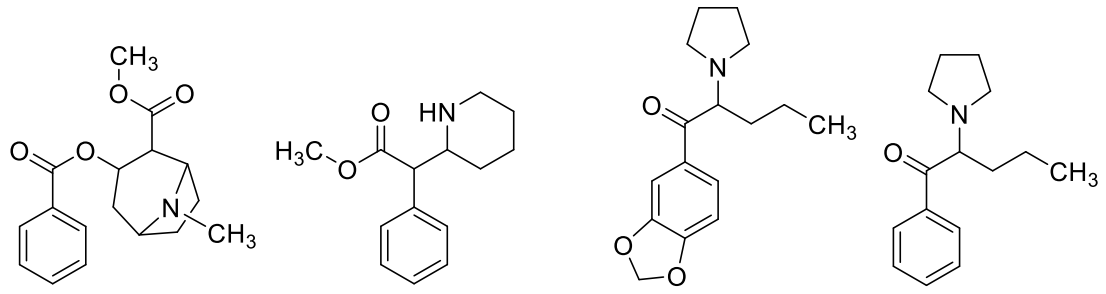

Figure 6. Structures of selected reuptake inhibitor drugs of abuse.

Methylphenidate (**9**) is another well-known inhibitor drug with high potential for abuse.[32] Like cocaine, it is Schedule II.[33] It differs in the fact that it has little to no activity at SERT and is much more selective for the other two MATs, DAT and NET.[34] Synthetic cathinones have been found to be inhibitor drugs of abuse as well. 3,4-Methylenedioxypyrovalerone (MDPV, **10**) was the first popularly abused synthetic cathinone found to be an inhibitor.[35] MDPV (**10**) is more potent than both cocaine (**8**) and methylphenidate (**9**) at DAT and was placed under Schedule I as of 2011. [33,36,37] α-PVP (**11**), the des-methylenedioxy analog of MDPV (**10**), started appearing more often on the clandestine market after the ban on MDPV and its sale was first restricted in 2014.[33,38] α-PVP (**11**) is about equipotent to MDPV (**10**) and like both methylphenidate (**9**) and MDPV (**10**) is highly selective for DAT and NET.[39]

3. Partial Releasers

Partial releasers, a sub class of releasers, display their partial release characteristics due to inducing neurotransmitter efflux at a slower rate than full releasers.[40] This unique property presents compounds with lower E_{MAX} which is the maximum response an agent can produce compared to the full releaser *D*-amphetamine.[40] Compounds **12** and **13** have both been identified as partial releasers.[40] Compound **12** has an EC_{50} of 622 nM but its E_{MAX} is only 61%.[40] Likewise, **13** presents an EC_{50} of 1207 nM and an E_{MAX} of 66%.[40] The E_{MAX} of both compounds is much lower when compared with the full releaser AMPH with an E_{MAX} of 103%.[40]

The exact mechanism underlying the action of partial releasers remains unknown. However, the “partial release” by certain agents might be assay related. For example, some substituted AMPH analogs that behave as partial releasers in a synaptosome assay were shown to act as reuptake inhibitors in a two-electrode voltage clamp assay using hDAT.[41]

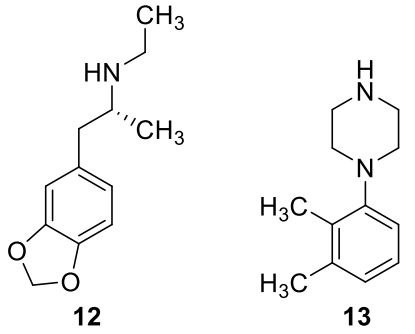

Figure 7. Structures of selected partial releasing agents.[40]

The possible therapeutic applications of partial releasers are still undetermined. Partial releasers have been shown to display less abuse liability.[41] These types of compounds have the potential to be developed into useful drugs due to their lower abuse potential.

E. Assay Methods

A variety of methods have been used to characterize MAT releasing agents and reuptake inhibitors. The information that each assay exhibits makes up the majority of what is known about DAT and agents that act at DAT. Here only two methods will be described

in detail. The first assay is the APP^+ inhibition assay.[42] It allows the characterization of both inhibitors and releasers but does not differentiate between the two.[42] The second assay is the Ca^{2+} flux assay.[43] This assay is a more recent development and allows for the differentiation between releasers and inhibitors.[43]

1. APP+ ASSAY

One method for examining possible emerging stimulant drugs of abuse is using an APP^+ inhibition assay. This assay uses human embryonic kidney (HEK) 293 cells with an overexpression of the transporter of interest. 4-(4-Dimethylamino)phenyl-1-methylpyridinium (APP^+, **14**) is a fluorescent compound that is a substrate for the monoamine transporters (Figure 8).[44] It is only fluorescent when transported within the cell.[44] This is primarily due to the conformation the molecule takes intracellularly which increases its conjugation and lowers the excitation band gap.[45] The assay proceeds by exposing the cells to an agent of interest followed by a mixture of the agent and APP^+ (**14**).[42] If a dose dependent decrease of fluorescence is observed the agent of interest is competitively inhibiting APP^+ from interacting with the transporter.[42] Through this method both releasing agents and inhibitors are able to be examined for functional activity but not differentiated. Figure 8 depicts the fluorescence of APP^+ when interacting with HEK293 cells stably expressing hDAT. Each amorphous circle is a cell and the bright white color is the fluorescence emitted at a wave length of 540 nm using an excitation wave length of 460 nm pictured through the microscope.

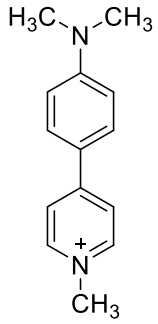

APP$^+$ (**14**)

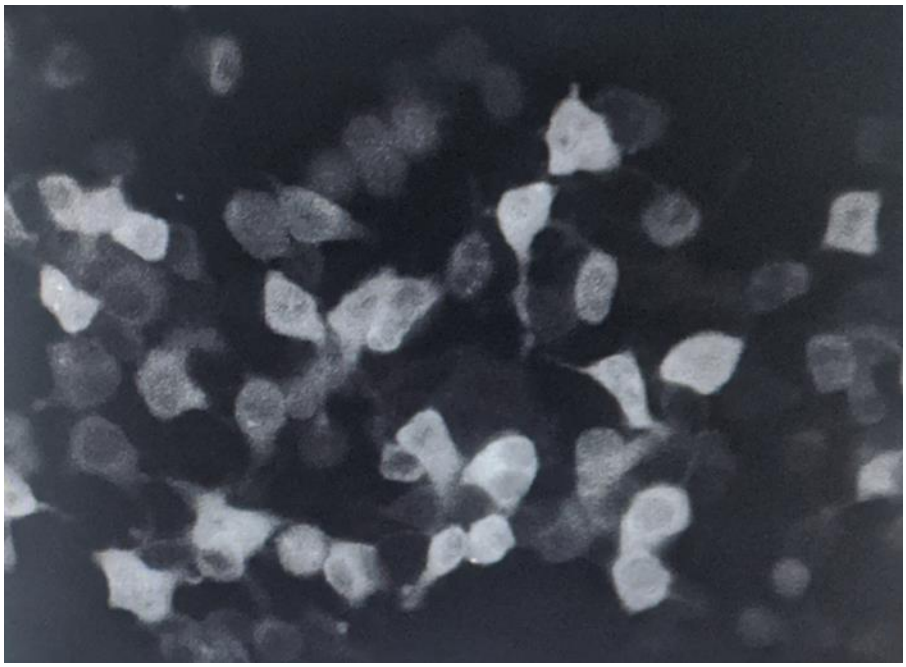

Figure 8. Structure of APP$^+$ (**14**) and fluorescence of HEK293 cells stably expressing hDAT exposed to APP$^+$.

2. Ca^{2+} Flux Assay

A calcium flux assay can be used to distinguish the two types of agents. In this assay HEK293 cells expressing the MAT transporter of interest are also transiently transfected with voltage gated calcium channels ($Ca_V1.2$) .[43] Fura2 is a membrane permeable fluorescent dye that only fluoresces upon binding to intracellular calcium ions.[43] The assay is carried out by exposing the cells to fura2 and then washing away the excess solution.[43] The agent of interest is then perfused to the cell and fluorescence is measured using a fluorescence microscope.[43] Upon a substrate being transported intercellularly, the cell becomes depolarized causing the calcium channels to open and a flux of calcium ions enter the cell (Figure 9).[46] These ions interact with the intracellular fura2 and cause

fluorescence to occur.[43] Inhibitors however, block the transporter thereby disallowing any depolarization to occur and the calcium channels stay closed.[43] No fluorescence is observed for the inhibitors.[43] The potency of inhibitors can be measured by inhibition of DA.

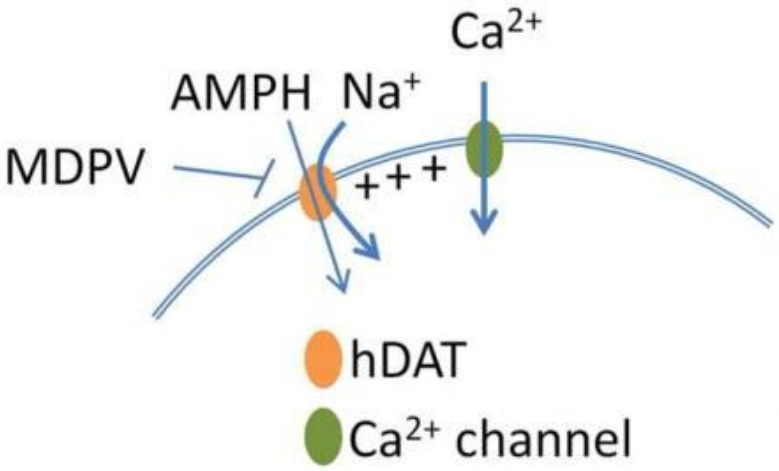

Figure 9. Releasers (e.g., AMPH, **4**) cause Ca^{2+} efflux by Ca^{2+} channel activation through cellular depolarization. Inhibitors (e.g., MDPV, **10**) do not activate Ca^{2+} channels.[46]

F. Cathinone SAR

After the discovery of the stimulant effects of cathinone from the khat plant several other synthetic cathinone compounds were found to have stimulant effects.[5,47] Early studies using rabbit synaptosomes pretreated with [^{3}H]DA showed that cathinone (**6**) was a

releasing agent.[48] Later it was found that of the two possible isomers of cathinone (**6**) the S isomer **6s** was more potent than the R isomer **6r** in drug discrimination studies.[49]

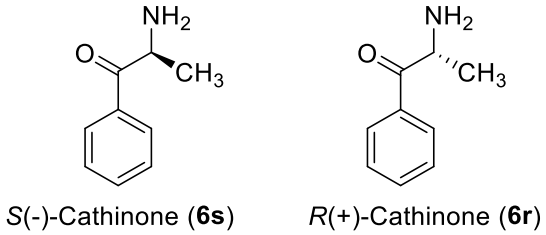

Figure 10. Structures of the two isomers of cathinone (**6**).

The first synthetic cathinone, methcathinone (**7**) was found to be even more potent than cathinone.[27] Many other synthetic cathinones have been examined for activity with modifications at the phenyl ring (R_1), alpha carbon (R_2), and the amine (R_3) (Figure 11).[5]

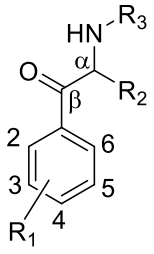

Figure 11. Structure of cathinone (**6;** R_1=R_3=H, R_2=CH_3) and numbering and position of substituents.

1. Aryl Substitution

Few ring substitutions have been examined for cathinone (**6**). Of the agents tested **15**-**18**, all failed to produce locomotor stimulation in mice.[50] Compound **19** failed to generalize in rats trained to discriminate cathinone (**6**) from saline vehicle while **20** showed partial generalization.[51]

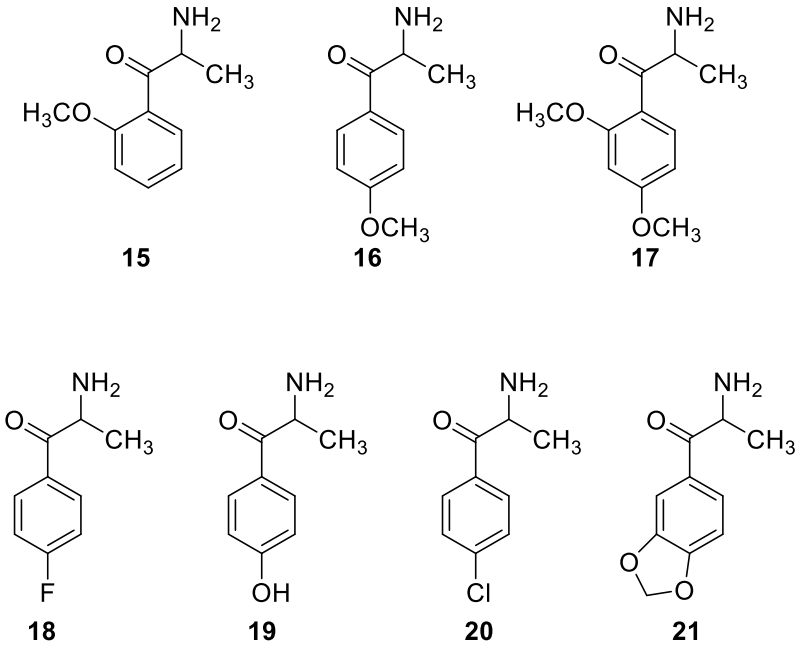

Figure 12. Structure of cathinone analogs with selected aryl substitutions.

Compound **21** produced partial generalization for amphetamine (**4**) trained rats but fully substituted in rats trained with the empathogen *N*-methyl-*1*-(3,4-methylenedioxyphenyl)-

2-aminopropane (MDMA).[52] Several ring substitutions have been examined for methcathinone (**7**) as well.[30]

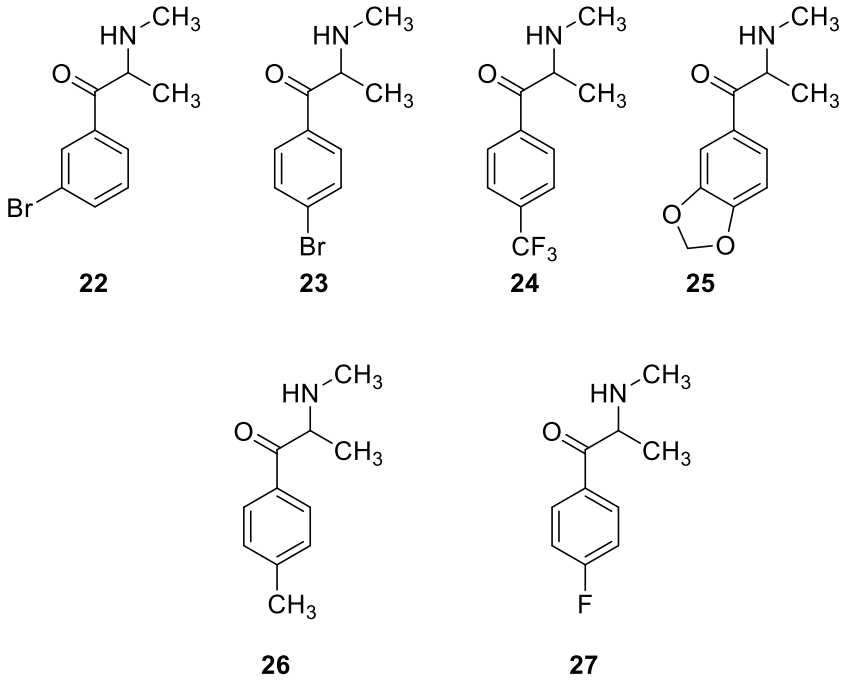

Figure 13. Structure of methcathinone analogs with selected aryl substitutions.

Compound **22** stimulated locomotor activity in rats at 10 mg/kg, double the dosage of methcathinone (**7**), 5 mg/kg.[53] Analogs **23** and **24** were found to not produce any hyperactivity at all doses tested.[53,54] The cathinone analog of MDMA, **25**, generalized for both amphetamine (**4**) trained rats and MDMA trained rats.[52] It was, however, 6-fold less potent than methcathinone (**7**) in the amphetamine (**4**) discrimination assay. [52] Mephedrone (**26**) has been shown to be a DA releasing agent with a similar EC_{50} (1.19 μM) but with less percent of maximum release (68%) when compared to methcathinone

(**7**) (3.57 μM, 83.3%) in a [^{3}H]DA release assay using HEK-293 cells expressing hDAT.[55] Compound **27** on the other hand, exhibited opposite behavior to mephedrone (**26**) with a larger EC_{50} (17.8 μM) but a higher percent maximum release (98%).[55]

2. α-Methyl Modification

α-Desmethylcathinone (**28**) was not active and failed to substitute at up to 10 times the ED_{50} dose of cathinone (**6**) both in rats trained to discriminate amphetamine (**4**) and rats trained to discriminate cathinone (**6**) from saline vehicle.[49,51] When tested as a releasing agent with [^{3}H]DA in rat synaptosomes, **28** was found to be about one-fourth to one-third as potent as cathinone (**6**).[56,57]

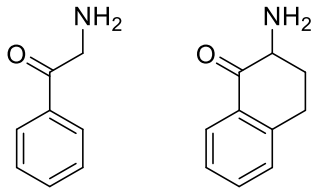

28 **29**

Figure 14. Structure of cathinone analogs with selected α-methyl modifications.

Conformationally constraining the α-methyl group into a ring **29** also failed to substitute at 10 times the ED_{50} dose of cathinone in discrimination studies.[56] Analog **29** was about one-fifth as potent as cathinone in a tritiated DA release experiment.[56]

3. Amine Modification

Homologation at the amine beyond N-methyl to N-ethyl (i.e., **30**) and N-propyl (i.e., **31**) lowered stimulant potency in drug discrimination studies.[52]

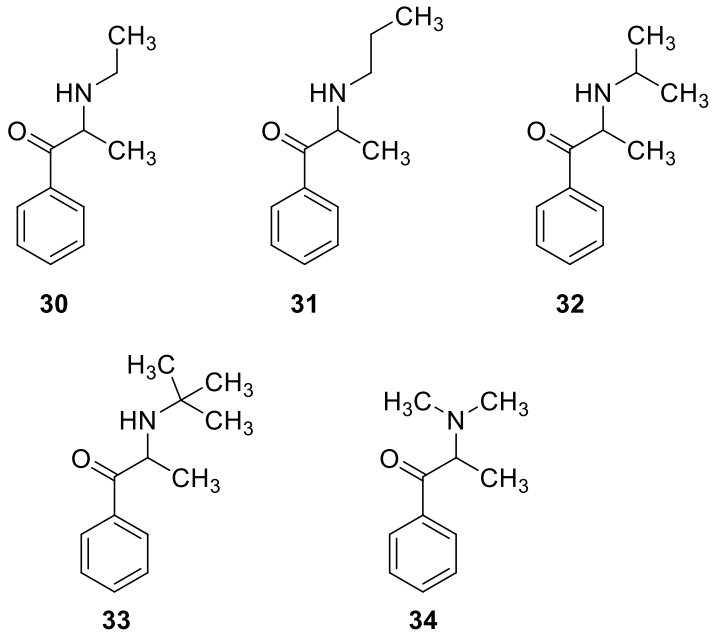

Figure 15. Structure of cathinone analogs with selected amine modifications.

Increased branching of the amine substituent with an isopropyl group (i.e., **32**) or tert-butyl (i.e., **33**) resulted in diminished potency in locomotor activity assays compared to methcathinone (**7**).[53] It was also found *N*,*N*-dimethylcathinone (**34**) was about half as potent as methcathinone and it was later discovered that in human subjects about 45% of this agent is metabolically converted to methcathinone (**7**) when taken orally.[52,58]

4. Inhibitor Cathinone Deconstruction

MDPV (**10**) being the first DAT inhibitor cathinone found on the clandestine market promoted research on the deconstruction of this cathinone to examine the structural features that contribute to its DAT inhibitory effects.[59] All MDPV (**10**) deconstruction analogs tested behaved as DAT reuptake inhibitors although with varying degrees of potency (Figure 16).[39] MDPV (**10**) itself was found to be the most potent.[39]

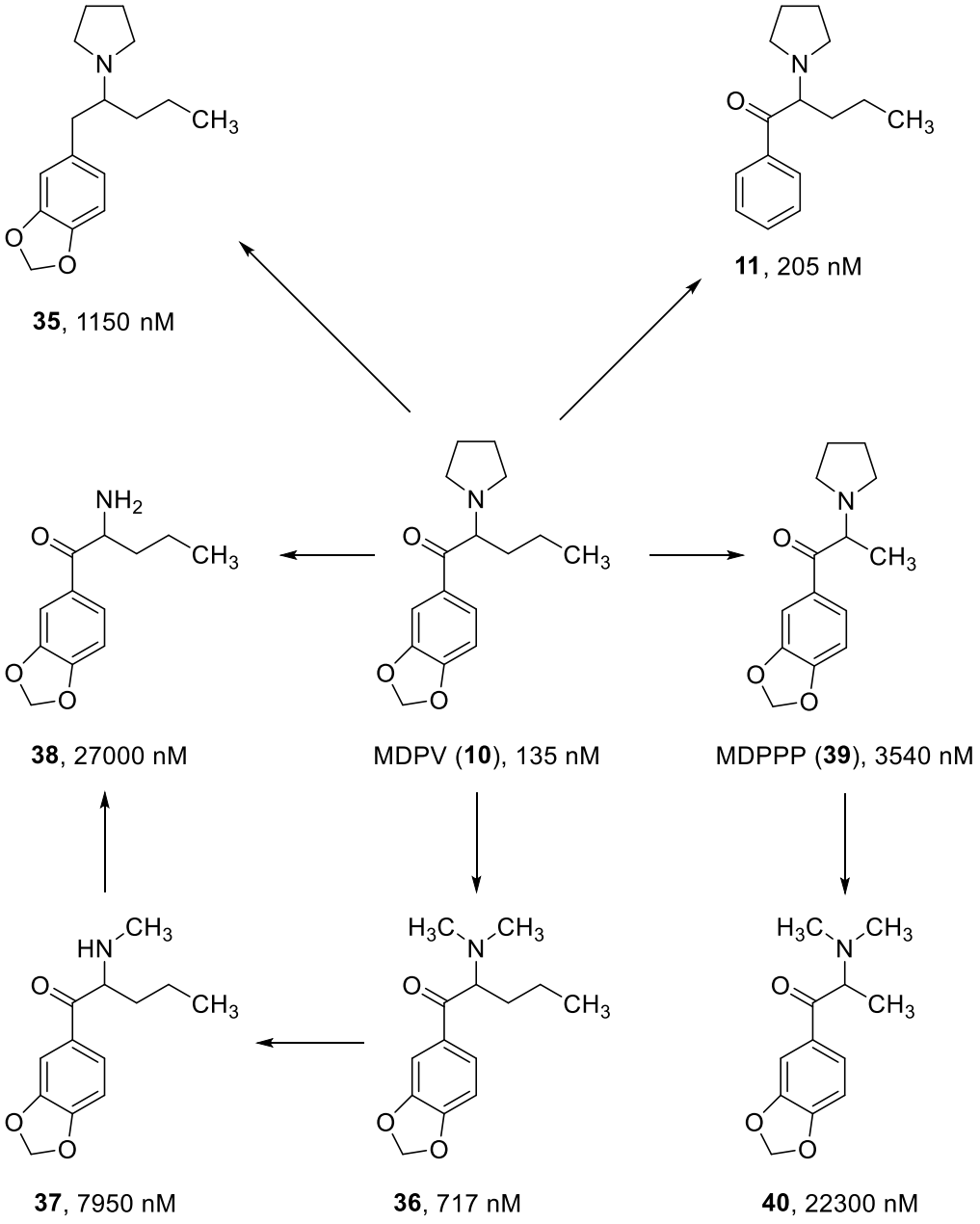

Figure 16. Deconstruction of MDPV (**10**). IC_{50} values represent potency to block reuptake of DA. Each arrow represents one structural modification.[39]

The loss of the methylenedioxy ring to form α-PVP (**11**) showed little change in inhibitory activity compared to the parent compound which provides evidence that the ring is not

necessary.[39] All other deconstructions (i.e., **35**-**40**) were much less potent than MDPV (**10**).[39] Removal of the carbonyl oxygen (i.e., **35**) showed around a 10-fold loss in potency.[39] This is unique for inhibitor drugs of abuse as a large potency drop is not seen in the releasing agents (i.e., methcathinone (**7**) to methamphetamine (**5**)).[60] The other analogs reduced potencies demonstrate the two most important features for high DAT inhibition activity. The first is bulk of the pyrrolidine ring. Alteration of this ring to a simpler tertiary (i.e., **36**), secondary (i.e., **37**), or primary (i.e., **38**) amine greatly reduces DAT inhibition potency in a stepwise manner with the primary amine **38** being the weakest inhibitor compound.[39] The second most important feature is the extended α-alkyl side chain. Truncation of this chain alone (i.e., **39**) reduces potency by 25-fold.[39] Modification to both the pyrrolidine ring and the alkyl side chain (i.e., **40**) showed the second largest drop in potency with an IC_{50} of 22,300 nM.[39]

5. Inhibitor Cathinone Elaboration

α-PVP (**11**), the des-methylenedioxy analog of MDPV (**10**) and roughly equipotent in DAT inhibition, was used as a scaffold in a series of elaborations to explore the SAR of the alkyl side chain and the pyrrolidine ring size of these inhibitor cathinones (Table 4).[61] It was found that reducing the length of the side chain (i.e., **41**-**43**) decreased potency in a stepwise manner.[61] Branching from n-propyl (i.e., **11**) to iso-propyl (i.e., **44**) reduced potency as well.[61] Elongation from n-propyl (i.e., **11**) to n-butyl (i.e., **45**) increased potency.[61] Adding a cyclopentyl ring (i.e., **46**) was equipotent to the parent compound while elaboration to a cyclohexyl ring (i.e., **47**) increased potency and was the most potent

compound of the series.[61] Modifying the pyrrolidine ring to a piperidine ring decreased potency for both compounds tested (i.e., **48**, **49**).[61] As seen with other cathinones conformationally constraining the alkyl side chain back to the aryl ring (i.e., **50**) showed a large drop in potency.[61]

Table 4. Inhibition of [^{3}H]dopamine uptake in synaptosome assay by elaborated analogs of α-PVP (**11**).[61]

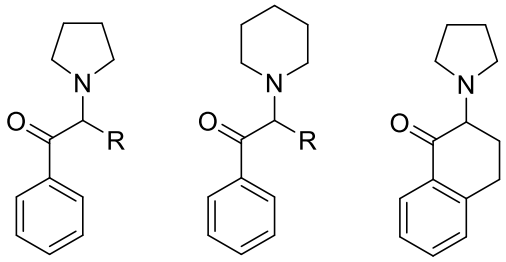

11,41-47 **48,49** **50**

Compound	-R	IC_{50}, nM
41	-H	3250.0
42	$-CH_3$	196.7
43	$-CH_2CH_3$	63.3
11	$-CH_2CH_2CH_3$	17.5
44	$-CH(CH_3)_2$	92.3
45	$-CH_2(CH_2)_2CH_3$	11.6
46	$-C_5H_9$	17.1
47	$-C_6H_{11}$	8.3
48	$-CH_3$	2490.0

49	-$CH_2CH_2CH_3$	128.0
50		12900.0

To summarize what is currently known about the SAR of cathinones: by adding bulk to the alpha carbon (R_2) or changing the primary amine to a bulky secondary or tertiary amine (R_3) caused the action of these agents to change from a releaser to an inhibitor (Figure 11).[5] Also, selectivity for the different transporters can be affected through molecular modification. Cathinone (**6**) is a releaser for all of the monoamine transporters.[5] Adding bulk onto the alpha carbon (R_2) shifts selectivity more towards DAT and NET.[5] In contrast, adding a methylenedioxy ring or a trifluoromethyl substituent on the aromatic ring (R_1) shifts the selectivity of the compounds more towards SERT than DAT or NET.[5,12] All these different alterations to the backbone of the molecules do interplay with each other. MDPV (**10**), the potent DAT inhibitor, that has the methylenedioxy ring on the aromatic ring (R_1) has no activity towards SERT due to its large alpha alkyl side chain (R_2) and its tertiary amine (R_3) from the pyrrolidine ring.[5] Cathinone (**6**) has a chiral center as well (α) (Figure 11). The stereochemistry does affect the overall potency of cathinones. Both R and S isomers have been shown to be active with S being shown to be the eutomer in most cases.[5]

G. Methylphenidate SAR

Methylphenidate (**9**), a well-studied and widely prescribed drug on the market, is primarily used for the treatment of ADHD.[62] It was first synthesized in 1944 but was not discovered to have stimulant activity until 10 years later.[63,64] The first clinical use of methylphenidate (**9**) was as an analeptic from barbiturate-induced coma.[41] The original patent of methylphenidate (**9**) was for its preparation by CIBA pharmaceuticals in 1950 then later patented for method of use in 1954 as a treatment of psychiatric disorders.[65] It has a bulky secondary amine and an extended alpha alkyl side chain that connects back to the amine to make up a piperdine ring. These features contribute to the compound's character as an inhibitor that is selective towards DAT and NET as well as showing little to no activity at SERT.[66] There are four stereoisomers of methylphenidate (**9**) (Figure 17) and there is a high eudysmic ratio between the RR and SS enantiomers.[67] Dexmethylphenidate (d-threo-methylphenidate), the RR enantiomer of methylphenidate (**9**), is the eutomer of the four isomers.[6,67,68]

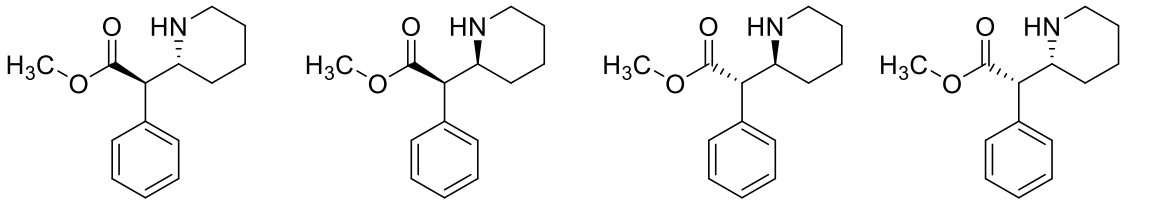

Figure 17. Four stereoisomers of methylphenidate (**9**).

A crystal structure of the inactive conformation of *l-threo*-methylphenidate (**9**) has been solved (Figure 18) with the monoclinic crystal in the $P2_1$ space group.[69] In addition, with the use of this crystal and the MM2-87 program a global minimum of the active *d-threo*-methylphenidate (**dt9**) was also obtained.[69] In the active *d-threo*-methylphenidate (**dt9**) conformation it can be observed that the protonated piperidine nitrogen can form an interaction with the carbonyl oxygen at a distance of 3.32 Å.[69]

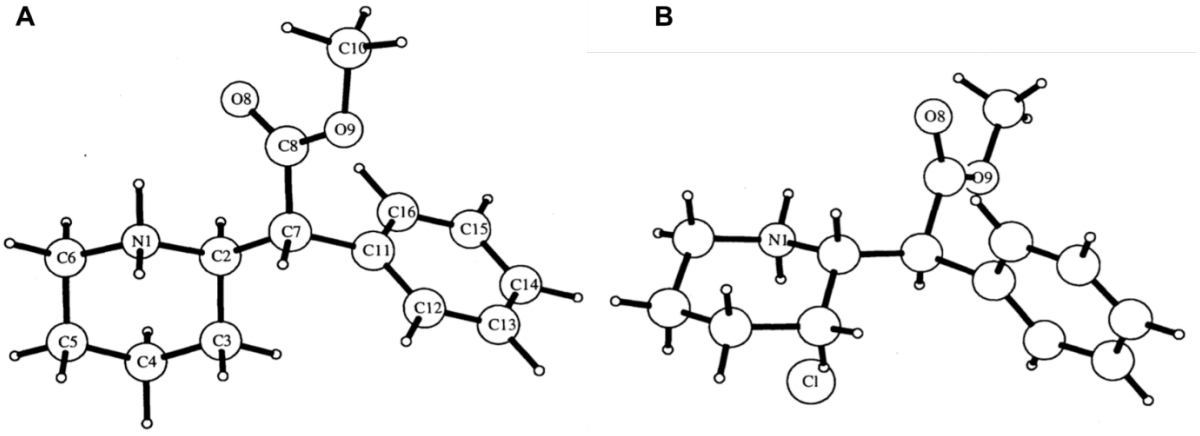

Figure 18. (A) Global minimum of *d-threo*-methylphenidate (**dt9**) (B) Solved crystal structure of *l-threo*-methylphenidate (**lt9**).[69]

The chemical space of methylphenidate has been explored exhaustively (Figure 19).[6] A quantitative SAR analysis of 80 methylphenidate (**9**) analogues has previously been conducted.[6]

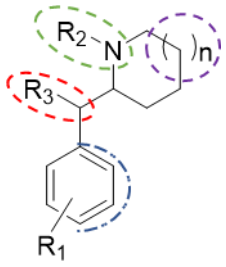

Figure 19. SAR features that have been quantitatively explored for **dt9**.[70]

Substituents have been added and tested on the aromatic ring, the ester has been modified, and the piperdine ring has been added to as well as ring size altered (Figure 19).[6] All further discussion of methylphenidate analogs will be concerned with the racemic mixture of *threo*-methylphenidate (**t9**).

1. Aryl Substitution

A series of aryl substituted analogs of methylphenidate (**9**) were examined for [^{3}H]WIN 35,428 binding and [^{3}H]DA uptake.[6,71] All 2-substituted compounds had weaker binding and were less potent than **t9** at uptake inhibition.[71] In the 3-position all halogens and hydrophobic groups evaluated were more potent than **t9** while all hydrophilic electron donating groups (EDG) were less potent.[71] The 4-position reveals a similar trend as the 3-position substituents having halogens and hydrophobic groups showing more potency than **t9** but with less increases in potency.[71] A hydrophilic EDG, 4-NH_3•HCl analog (i.e., **73**), was twice as potent as **t9** indicating that hydrophobicity and electronic character may not be responsible for potency at the 4-position but instead volume of the substituent.[71]

Table 5. DAT binding affinity (IC_{50}, nM) and uptake inhibition potency (IC_{50}, nM) of aryl substituted methylphenidate (**9**) analogs **51-79**.[6,71]

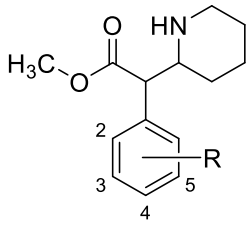

Compound	-R	Binding[a] (IC_{50}, nM)	Uptake[b] (IC_{50}, nM)
t9	-H	83	224
51	2-F	1420	2900
52	3-F	41	160
53	4-F	35	142
54	4-CF_3	615	-
55	2-Cl	1950	2660
56	3-Cl	5	23
57	4-Cl	21	74
58	3,4-diCl	5	7
59	3,5-diCl	67	-
60	2-Br	1870	3410
61	3-Br	4	13
62	4-Br	7	26
63	4-I	14	65
64	2-OH	23100	35800

65	3-OH	321	790
66	4-OH	98	340
67	2-MeO	101000	81000
68	3-MeO	288	635
69	4-MeO	83	293
70	3,4-diMeO	810	1760
71	4-NO_2	494	1610
72	3-NH_2•HCl	265	578
73	4-NH_2•HCl	35	115
74	3-Me	21	100
75	4-Me	33	126
76	3,5-diMe	4690	-
77	4-Et	737	-
78	3,4-benzo	11	53
79	4-*t*-Bu	13500	9350

[a][^{3}H]WIN 35,428 radioligand. [b][^{3}H]DA substrate.

Also, there was an exception of 4-NO_2 and 4-*t*-Bu analogs (i.e., **71** and **79**) being less potent than compound **t9** suggesting that there is a limit to the size of the substituents at the 4 position.[71] A hydrophobic electron withdrawing group (EWG), 4-CF_3 analog **54**, with a similar size to 4-Me and 4-Cl, was less potent than compound **t9**.[6] This substituent has a higher polarizability or negative hyperconjugation that might explain the difference seen in 4-CF_3 from the other substituents at the 4-position. For disubstituted compounds, 3,4

and 3,5 were the only positions tested.[6,71] All disubstituted compounds evaluated saw an increase in potency from EWGs and a decrease in potency from EDGs compared to (**t9**).[6,71]

2. Amine Substitution

Alkylation of the piperidine amine group has been examined.[6] Alkylation such as methyl **80**, allyl **81**, and propynyl **82** reduced affinity.[6] Addition of benzyl type groups had mixed results (i.e., **83-94**). The only substitutions that had better binding than compound **t9** were benzyl **83** and *p*-Cl-benzyl **92**. *p*-MeO-Benzyl (**94**) was similar in potency to **t9** whereas all other benzyl substitutions were weaker.

Table 6. [^{3}H]WIN 35,428 binding affinities (IC_{50}, nM) of methylphenidate (**9**) analogs with amine substituents.[6]

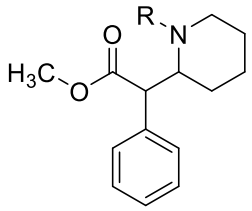

Compound	-R	(IC_{50}, nM)
t9	-H	83
80	-CH_3	499
81	-CH_2CHCH_2	597
82	-CH_2CCH	821
83	-Bn	53
84	-MeBn	678
85	-EtBn	267
86	-PrBn	205
87	-BuBn	1570
88	-PeBn	656
89	-Bn-*p*-NCS	422
90	-Bn-*m*-Cl	106
91	-Bn-*o*-Cl	243
92	-Bn-*p*-Cl	31
93	-Bn-*p*-NO_2	113
94	-Bn-*p*-MeO	79

95	-2-Pyridyl	369
96	-3-Pyridyl	173
97	-4-Pyridyl	128
98	-2-furyl	536
99	-3-furyl	459
100	-2-thienyl	224
101	-3-thienyl	143

2-, 3-, and 4-Pyridyl groups were also examined (i.e., **95-97**) of which all were weaker in comparison to **t9**.[6] Likewise, 2- and 3-furyl **98**, **99** and thienyl **100**, **101** analogs were tested as well with weaker affinities.[6]

3. Ester Modifications

Several substituents have been examined in place of the ester group on methylphenidate (**t9**) (Table 7).[6,72] All modifications tested showed lower affinity when compared to the parent compound.[6,72] The methyl Et_2O **103** was the only compound tested with a similar binding affinity to methylphenidate (**t9**).[6]

Table 7. [^{3}H]WIN 35,428 binding affinities (IC_{50}, nM) of ester-modified methylphenidate (**9**) analogs.[6,72]

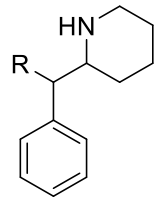

9

Compound	**-R**	**(IC_{50}, nM)**
t9	$-CO_2CH_3$	83
102	$-CH_2OH$	448
103	$-CH_2OCH_3$	97
104	$-CO_2Bn$	1020
105	$-CH_2O(CO)CH_3$	690
106	$-CO_2NH_2$	1730
107	-H	6360

4. Ring Modifications

Modification of the piperidine ring has also been explored from a 5-membered ring all the way up to an 8-membered ring as well as a change to a morpholine ring (Table 8).[73] The piperidine ring of **t9** was the most efficacious followed by the 7-membered ring analog which had 2-fold lower affinity and 3-fold lower potency.[73] While the morpholine analog contains a 6-membered ring like the parent compound **t9**, it had the lowest affinity and

activity of all the analogs tested.[73] It can be concluded then that the oxygen atom of the morpholine ring is not well tolerated by DAT.[73]

Table 8. DAT binding affinity (IC_{50}, nM) and uptake inhibition potency (IC_{50}, nM) of piperidine ring modified methylphenidate (**t9**) analogs **108-111**.[73]

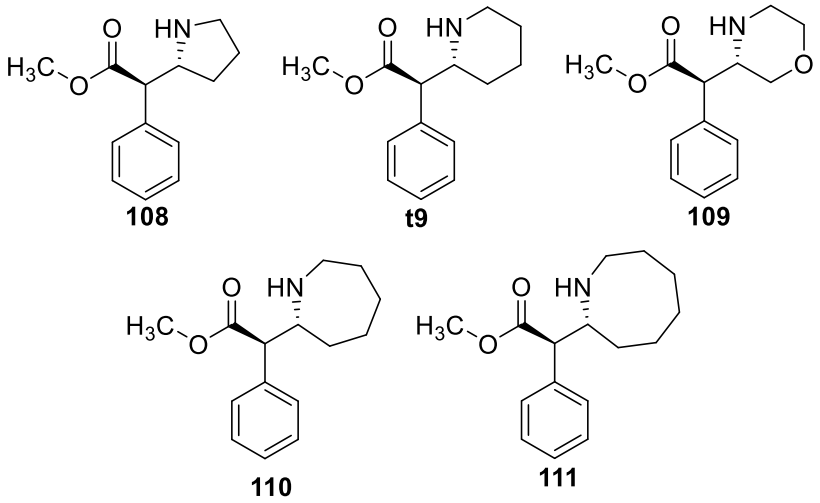

Compound	Ring Size	Binding[a] (IC_{50}, nM)	Uptake[b] (IC_{50}, nM)
108	5	355	885
t9	6	83	224
109	6-morpholine	1250	9930
110	7	197	701
111	8	623	1590

[a][^{3}H]WIN 35,428 radioligand. [b][^{3}H]DA substrate.

Of all the modifications explored for methylphenidate, only EWG substitutions at the meta or para position that are within the plane of the phenyl ring correlate with increased DAT affinity and activity.[6] Large substituents in the ortho position, substituents above and below the plane of the aryl ring, substitutions on the piperdinyl nitrogen atom, and decreasing polarity near the carbonyl moiety all correlated with decreased DAT activity.[6]

H. New Methylphenidate/Cathinone Hybrids

Portoghese proposed that if two different series of compounds with the same change in substituents have parallel changes in binding affinity then they likely bind in a similar manner.[74] With the large number of synthetic cathinones coming onto the grey market as drugs of abuse, is it possible to predict new cathinone activity by using the SAR of the well-studied methylphenidate compounds? Our lab developed a hybrid cathnione/methylphenidate compound (i.e., **112**; Figure 20).[7]

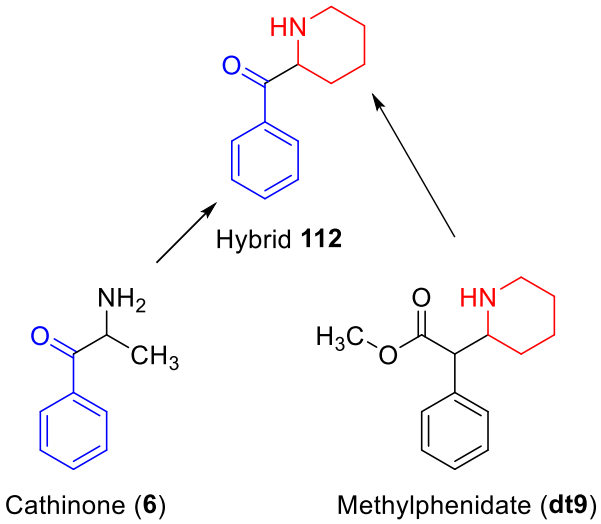

Figure 20. Cathinone (**6**)/methylphenidate (**t9**) hybrid compound **112**.[7]

The hybrid **112** has the ketone of cathinones as well as the piperidine ring of methylphenidate. The hybrid was evaluated for reuptake inhibition using the APP^+ assay as well as for DAT releaser or inhibitor properties using the Ca^{2+} assay (Figure 21).[7] It was found that the hybrid **112** was active, but less potent than methylphenidate (**t9**), at reuptake inhibition.[7]

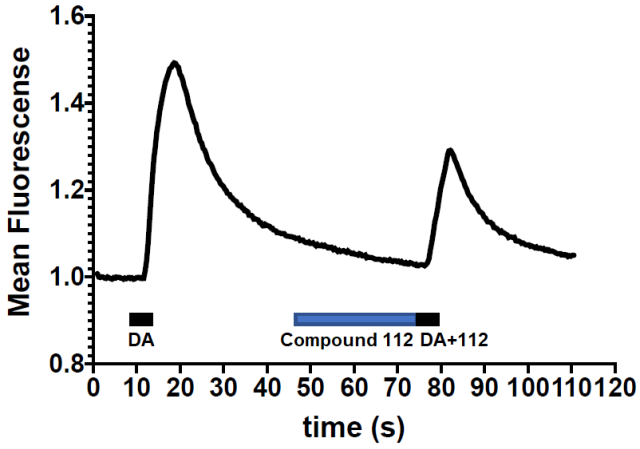

Figure 21. Ca^{2+} efflux assay of selected hybrid compound **112** showing DAT inhibitor properties.[7]

It was also determined that **112** was not a releaser and shared the inhibitor properties of methylphenidate (Figure 21).[7] Using a series of 8 hybrid compounds (i.e., **112**-**119**) it was shown that parallel activity existed in substituent alterations at the aromatic ring of the hybrid compound's potencies compared to the corresponding methylphenidate analog's binding affinities (Table 9).[7]

Table 9. DAT uptake inhibition potency (IC_{50}, nM) of aryl ring modified hybrid (i.e., **112**) compounds and DAT binding affinity (IC_{50}, nM) of corresponding aryl-ring modified methylphenidate (**9**) analogs.[7]

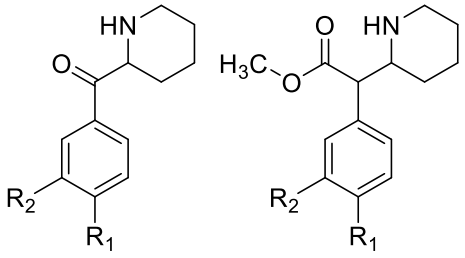

112-119 **t9** Analogs

Hybrid Compound	-R_1	-R_2	Uptake (IC_{50}, nM)	t9 Analogs	Binding (IC_{50}, nM)
112	-H	-H	1080	**9**	83
113	-CH_3	-H	380	**75**	33
114	-C_2H_5	-H	6900	**77**	737
115	-Cl	-H	520	**57**	21
116	-Br	-H	590	**62**	7
117	-OCH_3	-H	2340	**69**	83
118	-CF_3	-H	14300	**54**	615
119	-Cl	-Cl	47	**58**	5

[a]APP^+ substrate. [b][^{3}H]WIN 35,428 radioligand.

A plot comparing the hybrid series inhibition pIC_{50}'s to the affinity pIC_{50}'s of the methylphenidate analogs revealed a correlation coefficient of 0.91 (Figure 22). [7]

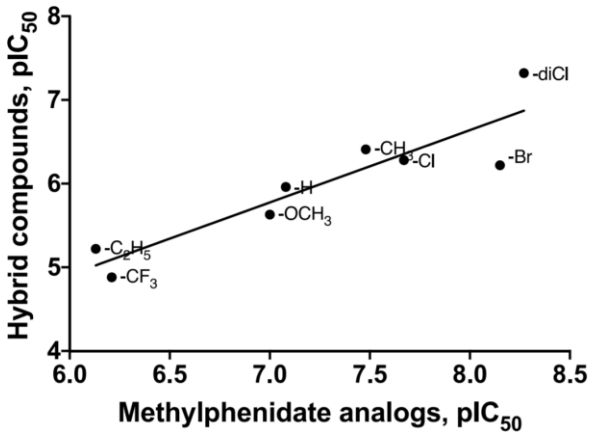

Figure 22. Correlation (r = 0.91) of APP^+ uptake assay data of hybrid (i.e., **112**) compounds and binding data of methylphenidate (**t9**) analogs.[7]

III. Specific Aims and Rationale

A. Project 1.

Aim 1. Construct a new hDAT homology model

DAT is an important transporter that is implicated in a multitude of neuropsychiatric disorders. The function and crystal structures of MATs has only been established in the past 20 years. Even with the advancements in structural biology, hDAT has still not been crystallized. In order to better understand this important transporter several different methods will be used to approach the exploration of hDAT from different perspectives. One strategy is to understand how novel agents (see below) bind at hDAT, and the second is to examine several known DAT reuptake inhibitors at dDAT mutants transitioning from dDAT to hDAT. Both of these projects will utilize a new DAT homology model that we propose to construct. **Hypothesis:** Using the most recent MAT homologues with high identity compared to hDAT it should be possible to develop a more accurate model than what has been used in the past. Using this new homology model, docking and HINT analysis can be used to study the innerworkings of hDAT.

Aim 2. Elucidate factors determining the potency of 3,4-disubstituted cathinone/methylphenidate hybrids

a. Synthesis

Synthetic cathinones are a newer drug abuse problem that is causing alarm worldwide. With greater than 150 synthetic cathinones already identified and even more emerging every year there is great interest in better understanding the SAR of these compounds. MDPV (**10**) was the first discovered abused reuptake inhibitor synthetic cathinone. What is known about the SAR of the DAT reuptake inhibitor cathinones mainly involves the nature of the bulky amine and extended α-alkyl side chain. Little is known about substituents around the aryl ring. Methylphenidate (**9**) is a well-known DAT reuptake inhibitor with extensive SAR established. Our lab developed a cathinone/methylphenidate hybrid that exhibits DAT reuptake inhibition. A series of these hybrid compounds was developed and used to explore DAT SAR in comparison to corresponding methylphenidate analogs. The most potent compound of the hybrid series (i.e., **112**) was shown to be even more potent than methylphenidate: the 3,4-dichlorobenzoylpiperdine analog **119**. What is it about this compound that makes it so potent? To exam this phenomenon we designed two additional hybrid compounds that will help elucidate why the dichloro substituents of **119** increase DAT inhibition potency (Figure 23).

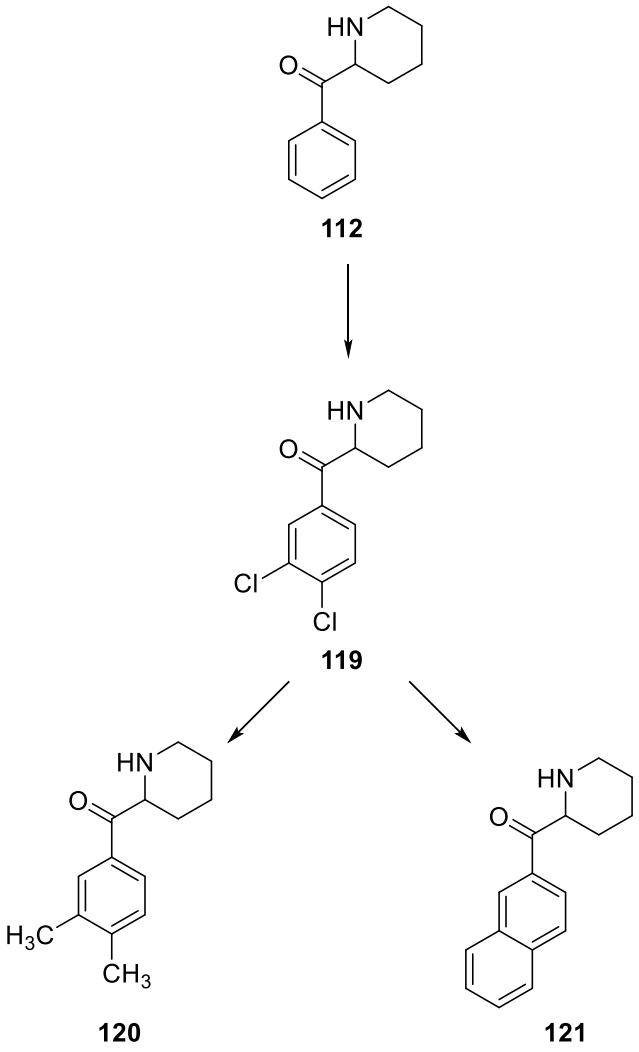

Figure 23. Structures of hybrid compound **112**,[74] potent hybrid compound **119**,[74] and two proposed new compounds **120** and **121**.

The two new compounds take into account steric, electrostatic, hydrogen bonding, and halogen bonding effects (Table 10). The first compound is 3,4-dimethylbenzoylpiperdine **120**. The two methyl groups are about the same size as the chloro groups of **119** but with opposite electronic character. Chloro groups are weakly electron withdrawing while methyl groups are electron donating. **Hypothesis:** If electronic character is driving the

increase in activity the 3,4-dimethylbenzoylpiperdine **120** should be less potent than the dichloro **119** compound. If electronic character is not important for activity, then the dimethyl compound should have similar activity. The second compound is the 2-naphthoylpiperdine **121**. This compound has the additional conjugated ring to the phenyl ring at the 3,4 positions.

Table 10. Lipophilic (π), electronic (σ), steric (Vol), hydrogen bond (HB) acceptor, and halogen bond formation properties of compounds **119**-**121**.

Parameter	119	120	121
π	1.46[a]	1.03[b]	1.32[a]
σ	0.60[c]	-0.24[c]	0.08[a]
Vol ($Å^3$)[d]	90.9	88.2	100.0
HB Acceptor	Yes	No	Yes
Halogen Bond	Yes	No	No

[a] Values as reported by Hansch et al.[75] [b] Values as reported by Fujita et al.[76] [c] Values as reported by Jaffé.[77] [d] Volume measured using SybylX 2.1.1.

It is slightly larger in size compared to the dichloro substituents of **119** and has similar electron withdrawing character. It is usually seen as a bioisotere for 3,4-dichlorophenyl substituents. What is different about **121** is that it does not have the ability to form halogen bonds. This halogen bond activity is due to the anisotropic nature of halogen substituents.

The halogen forms a σ-hole that has positive electronic nature and can be viewed as a Lewis acid (Figure 24). This σ-hole can then interact with a Lewis base such as a lone pair from a hetero atom. **Hypothesis:** If **121** is less potent than the dichloro compound **119** then the dichloro compound might have increased potency through hydrogen or halogen bond formation. If the naphthoyl compound **121** has similar potency to the dichloro compound then halogen bond formation is less likely and only the size (i.e., volume) of the substituents, hydrogen bonding, or possibly electronic σ character is important for activity. The extended aromatic ring of compound **121** has a delocalized π cloud above and below the face of the ring (Figure 24). This π cloud has negative electronic character and can participate in interactions with positively charged species such as hydrogen bond donors.[78] This can be viewed in the same way as edge-to-face interactions of aromatic rings.

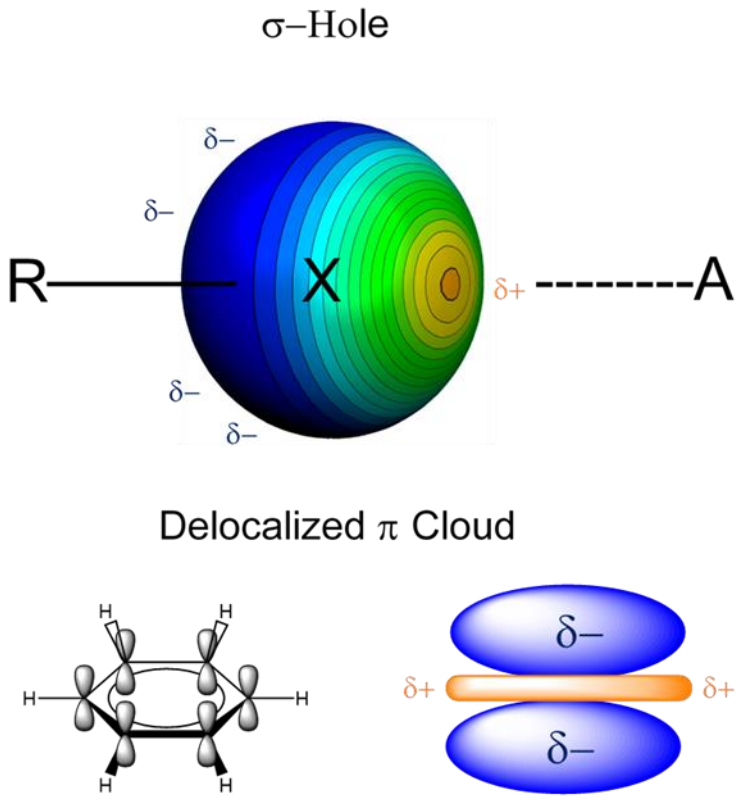

Figure 24. Representation of positive and negative electrostatic interactions involving a halogen bonds (above) and aromatic rings (below).

b. Biological Studies

After the synthesis of each target compound (i.e., **120**, **121**) the APP^+ assay will be used to evaluate their potencies. HEK Flp-In T-REx 293 cells stably expressing hDAT will be cultured and plated in a 96-well plate. Using an imaging solution, selected concentrations of the target agents will be constantly perfused followed by a mixture of the target agent and APP^+. The entire experiment will be observed and recorded using fluroescence microscopy. Data obtained through the recording will then be analyzed and inhibtion IC_{50}

plots will be generated. Compound **119** will be resynthesized and used as control in this assay.

c. Docking

After developing a hDAT homology model all three compounds will be docked and scored using Hydrophilic INTeraction (HINT) analysis. On a molecular level, the specific interactions with the amino acids within hDAT and the compounds will be examined. The particular substituent properties important for increased or decreased hDAT reuptake inhibition can then be possibly elucidated. The modeling data will then be compared to the biological data and new insights on cathinone reuptake inhibitor SAR will be established.

B. Project 2.

Aim. Evaluate binding modes of selected cathinones at DAT mutant transporters utilizing 3D molecular modeling

Another approach to better understand DAT is mutagenesis. dDAT might be thought of as a natural mutant to hDAT that might display unique SAR with cathinone reuptake inhibitors. While both dDAT and hDAT transport the endogenous ligand DA with similar potencies, the potent hDAT cathinone reuptake inhibitor MDPV (**10**) is essentially inactive at dDAT (DeFelice, unpublished data). Evidently, structural differences between dDAT and hDAT must account for this difference. In a collaboration with Dr. Eltit's lab, using

constructed four point mutations transitioning dDAT to hDAT, three synthetic cathinones known to be effective hDAT reuptake inhibitors will be examined at the dDAT mutant transporters: MDPV (**10**), α-PVP (**11**), and MDPPP (**39**) (Figure 25).

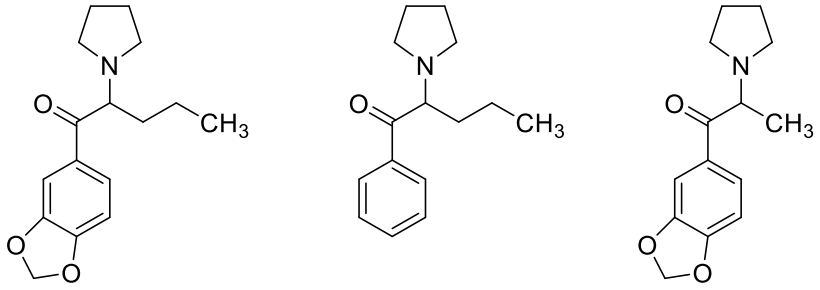

Figure 25. Structures of agents to be examined at dDAT mutant transporters: MDPV (**10**), α-PVP (**11**), and MDPPP (**39**).

Compounds **11** and **39** might be viewed as deconstructed analogs of MDPV (**10**). Compound **11** lacks the methylenedioxy ring of **10** whereas **39** possesses a shorter side chain. Evaluation of these compounds will assist in determining which of these two structural features (i.e., the methylenedioxy ring or the extended side chain) account for the difference in action of MDPV (**10**) at dDAT versus hDAT.

Hypothesis: As the structure of dDAT transitions to hDAT favorable molecular interactions between ligand and protein should improve.

Using the previous (see Project 1) generated hDAT homology model and in addition the crystal structure of dDAT and a mutant model with the four mutations, docking studies and HINT analysis on all three agents within the models will be performed.

Overall, this two-pronged approach, which can be summarized by Figure 26, will help develop a better understanding of the innerworkings of DAT.

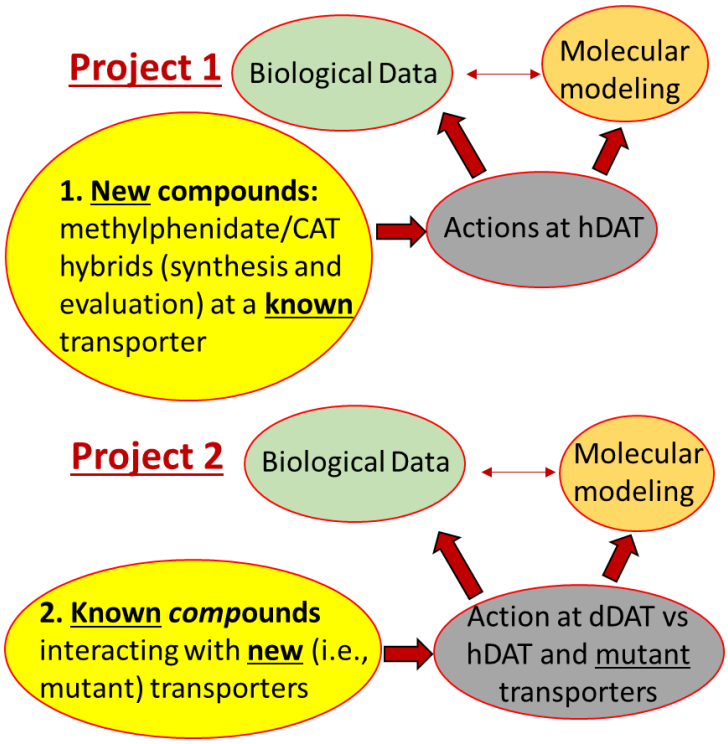

Figure 26. Summary of two-pronged approach to better understand DAT.

IV. Results and Discussion

A. Project 1.

Aim 1. Construct a new hDAT homology model

There is no crystal structure of hDAT, thus, a homology model of hDAT was constructed using MODELLER 9.24. This software package makes use of a crystal structure template and the amino acid sequence of the protein of interest. For this particular hDAT homology model three separate crystal structure templates were used. The reason for multiple templates is based on three criteria: the highest sequence identity, the largest query coverage, and a crystal structure with a similar test ligand. The highest sequence identity allows for the most similar structure to be formed during the model build. The largest query coverage ensures places where there could be gaps or high amounts of ambiguity for model generation are minimized. Using a crystal structure that has a similar test ligand can help ensure that in docking studies proper interactions will take place between an agent of interest and the amino acids within the binding pocket. PDB ID: 4XPB, a dDAT crystal structure, was used due to having the highest sequence identity with hDAT at 55.35%. This is a large improvement from previous models developed from the ortholog LeuT having only a 24% identity to hDAT.[79] Also, homology model generation usually needs at least 30% identity to produce an adequate model otherwise there can be significant alignment errors and main chain positions can be greatly altered.[80] PDB ID: 6VRH, an hSERT crystal structure, was used due to having a 92% query coverage.[81] Having such a large query coverage crystal structure template that is in the SLC6 family with hDAT helps ensure that the portions of the protein that are missing from the dDAT crystal structure can still be sufficiently modeled. Lastly, PDB ID: 4XPT was used because

its co-crystallized ligand was 3,4-dichlorophenethylamine that has chloro substituents on the phenyl ring that correspond to the ones found in compound **119**. Utilizing this crystal structure that has amino acids within the binding pocket possibly interacting with the two chloro groups in the same manner as the chloro groups from compound **119**, should have considerable benefits when docking compounds **119**, **120**, and **121**. The target hDAT sequence was obtained from NCBI accession BAA22511.1. Using this target sequence and the three templates, MODELLER aligned the sequences and generated 100 hDAT models. The models were evaluated through GA341 and DOPE scoring. The best scoring model was then uploaded into SybylX 2.1.1, hydrogen atoms were added, and the structure was minimized using the Tripos Force Field with Gasteiger-Hückel charges. The finalized hDAT homology model (Figure 27) was then compared to the crystal structure of dDAT using the biopolymer suite within SybylX 2.1.1. The calculated root mean squared deviation (RMSD) of all atoms was 2.16 Å. An RMSD < 3 Å for the Cα atoms of the backbone of a template and predicted protein is considered a success.[82] With all atoms having an RMSD < 3 Å this hDAT homology model should be considered more than satisfactory.

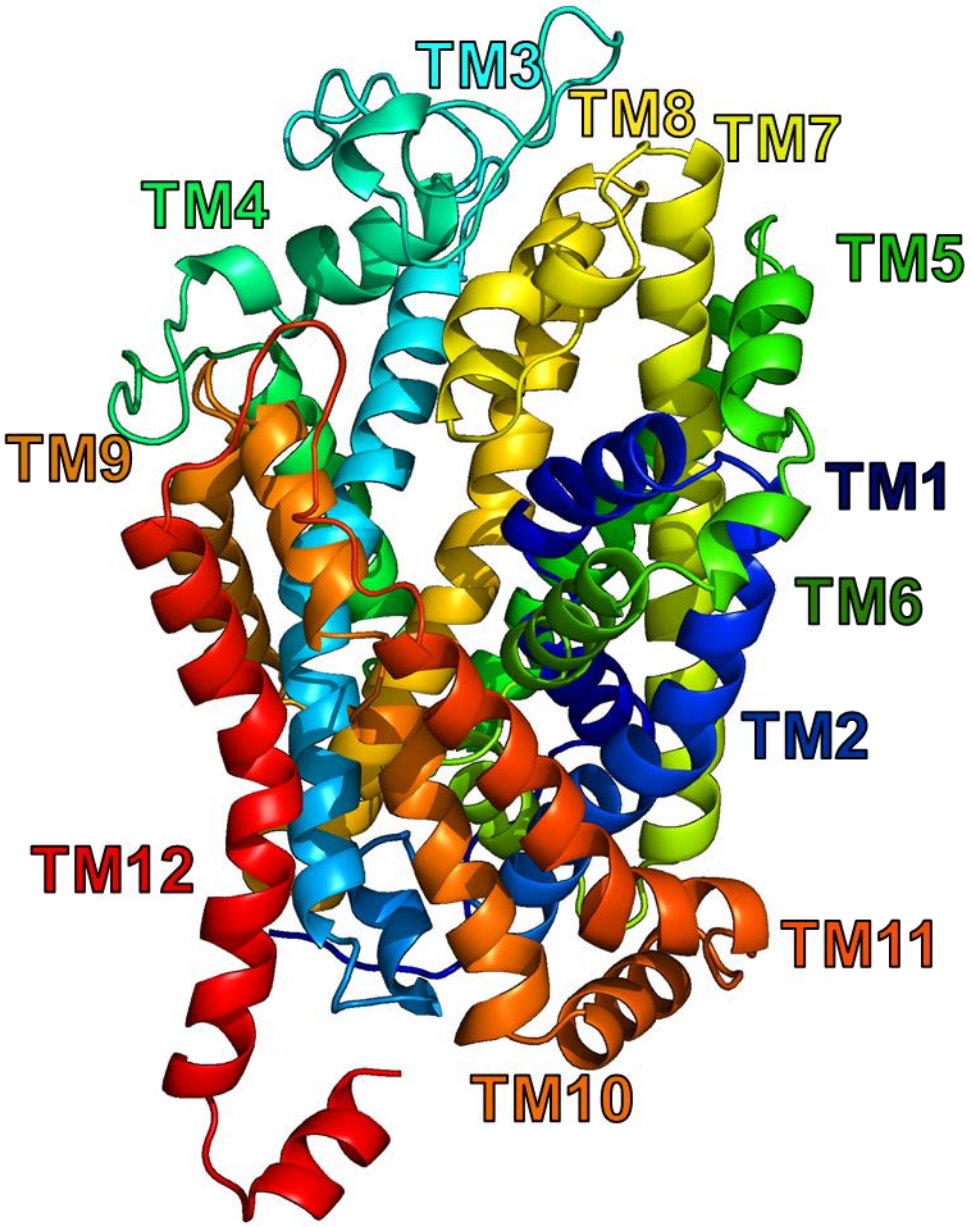

Figure 27. Generated hDAT homology model (cartoon) with labeled transmembrane (TM) helices.

The generated hDAT homology model was then used to dock methylphenidate (**dt9**) for initial homology model docking studies. Methylphenidate (**dt9**) was first sketched using SybylX 2.1.1. The sketched molecule was then energy minimized using the Tripos Force

Field with Gasteiger-Hückel charges. Using GOLD2020, methylphenidate (**dt9**) was then used as a test ligand and cocaine (**8**) was used as a reference ligand in the hDAT homology model. Methylphenidate (**dt9**) was docked 100 times and scored with ChemPLP and GOLD. The best GOLD scoring methylphenidate (**dt9**) pose formed a salt bridge interaction with an aspartate residue (D79) (Figure 28). When compared to the pose of the dDAT crystallized ligand cocaine (**8**), both phenyl rings as well as the methyl ester groups had significant overlap for each compound. While the tropane ring of cocaine (**8**) and the piperidine ring of methylphenidate (**dt9**) differ in structure the nitrogen atom of both compounds was at a distance from D79 for salt bridge formation (i.e., 3.4 and 3.1 Å, respectively).

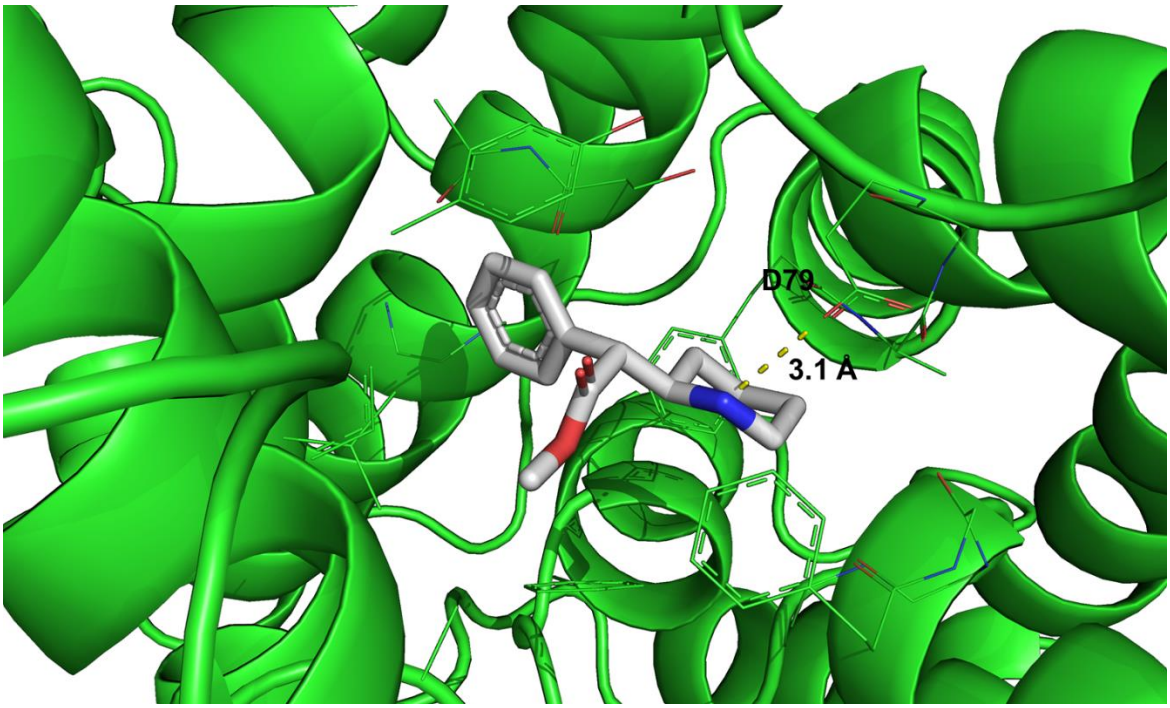

Figure 28. hDAT homology model (cartoon, green) with possible binding pose of methylphenidate (**dt9**, sticks, white) forming salt bridge (dotted line, yellow) with D79.

All 100 poses generated in GOLD2020 were then subjected to HINT analysis. Using SybylX 2.1.1 scripting programming language (SPL) each methylphenidate (**dt9**) pose was merged with the hDAT homology model. Each formed complex was then minimized using the Tripos Force Field with Gasteiger-Hückel charges. Using Sybyl 8.1, each complex had the test ligand removed and HINT analysis was performed. For the initial partitioning phase, the dictionary method was used for the protein and the calculation method was used for the ligand.[83,84] All other parameters were set to their default values. The highest HINT score was 868 (Table 11). The pose of the molecule for this high HINT score also mimicked cocaine with the phenyl ring and methyl ester group overlapping the same groups of cocaine. The highest contribution to the overall scores was from the hydrogen bond (HB) formation with the piperidine amine and D79 (3.1 Å). HINT does not consider salt bridges but a salt bridge can be viewed as a kind of HB.

Table 11. Total HINT score of **dt9** solutions with top scores for each type of molecular interaction.

	Scored Solution	
	Highest	**Lowest**
Total HINT Score	868	-104
Hydrogen Bond	646	
Acid/Base	612	
Hydrophobic	789	
Polar Clash	-1179	

Aim 2. Elucidate factors determining the potency of 3,4-disubstituted cathinone/methylphenidate hybrids

a. Synthesis

The synthesis of the target hybrid compounds (**119**-**121**) followed the same basic procedure (Scheme 1). Small differences occurred between the generation of each compound due to availability of chemicals and attempts to improve yields.

Scheme 1.[a] General procedure for target compound synthesis.

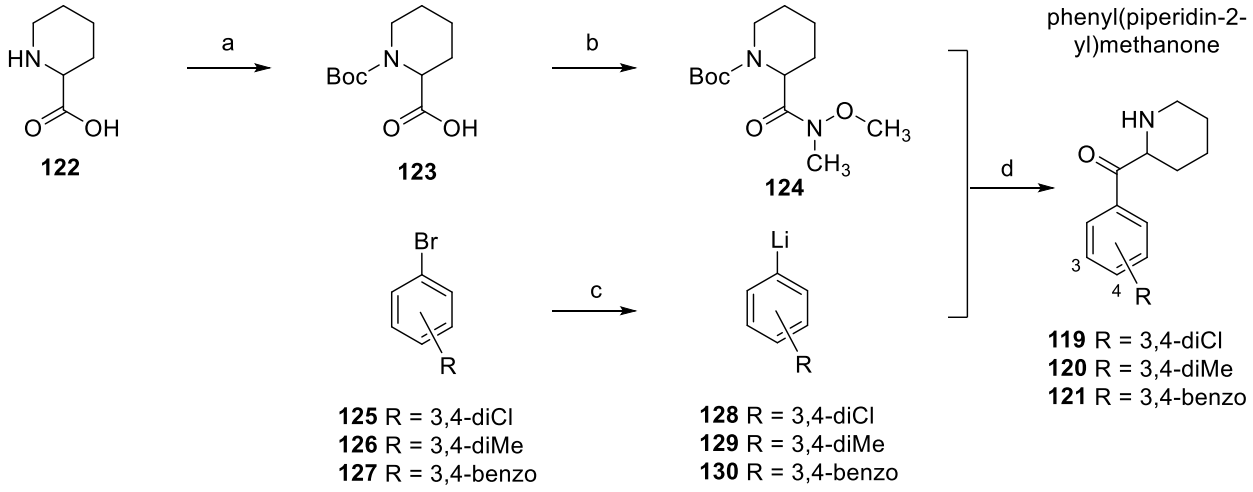

[a]Reagents and conditions: a. $(Boc)_2O$, Et_3N, MeOH, rt, 1 h; b. *N*,*O*-dimethylhydroxylamine hydrochloride, BOP, Et_3N, DCM, rt, 16 h; c. 2.5 M *n*-BuLi in hexanes, anhydrous Et_2O, -78 °C (but, see text), 3 h; d. anhydrous Et_2O, -29 °C, 24 h.

The synthesis of compound **119** had been previously accomplished in our laboratory and proceeded through what is known as a Weinreb ketone synthesis.[7] The exact procedure

was followed for the synthesis of compound **119** with the exception of the starting material being pipecolic acid (**122**) and not *N*-Boc-pipecolic acid (**123**). For the synthesis of the Boc-protected intermediate, pipecolic acid (**122**) was reacted with $(Boc)_2O$ in methanol with Et_3N used as a base at room temperature for 1 hour (Scheme 2). This reaction proceeded by generation of CO_2 gas as a side product. Several reaction iterations were used to produce this intermediate, but this particular setup had the most optimized yields of all conditions tested at 95%.

Scheme 2.[a] Synthesis of intermediate **123.**

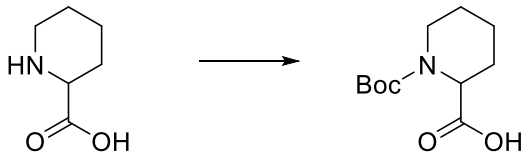

122 **123**

[a]Reagents and conditions: $(Boc)_2O$, Et_3N, MeOH, rt, 1 h.

Following the synthesis of intermediate **123**, the next step was to generate the Weinreb amide **124**. This reaction borrows from peptide chemistry and reacts the carboxylic acid of compound **123** with the amine of *N*,*O*-dimethylhydroxylamine hydrochloride in DCM using the peptide coupling agent (benzotriazol-1-yloxy)tris(dimethylamino)phosphonium hexafluorophosphate (BOP) and Et_3N as a base at room temperature for 16 hours (Scheme 3). BOP produces the carcinogenic side product hexamethylphosphoramide (HMPA) during the amide coupling reaction. In future reactions of this nature, it is

recommended that benzotriazol-1-yloxytripyrrolidinophosphonium hexafluorophosphate (PyBOP) be used as the coupling agent instead of BOP as HMPA is not formed in the process and the reaction produces the same yields under the same conditions as BOP.[85] The synthesis of intermediate **124** was also repeated several times and the most optimized setup produced a yield of 85%. The product (i.e., **124**) is in most cases reported as a clear oil. A clear oil was obtained as the final product in this reaction but after several days it solidified into a white solid with a melting point of 64-66 °C. A method that was found to enhance the solidification process was to expose the oil to a dry ice/acetone cooling bath. Upon exposure to the -78 °C temperature cooling bath the oil would solidify and upon returning to room temperature remained in solid form.

Scheme 3.[a] Synthesis of intermediate **124**.

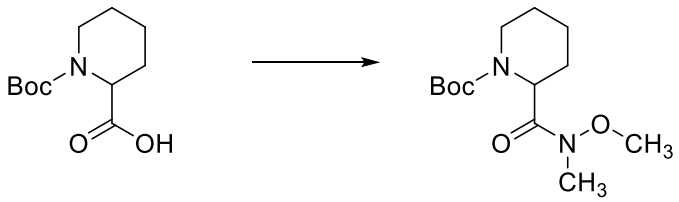

123 **124**

[a]Reagents and conditions: *N*,*O*-dimethylhydroxylamine hydrochloride, BOP, Et_3N, DCM, rt, 16 h.

An organolithium intermediate (i.e., **128**) was then needed for the second portion of the Weinreb ketone synthesis. The intermediate was synthesized using a lithium halogen exchange reaction (Scheme 4). 3,4-Dichlorobromobenzene (**125**) was used as the

starting material as the bromo substituent was the halogen in the lithium halogen exchange. Due to the extreme reactivity of organolithium compounds and their sensitivity to air and moisture the reaction flask was prepped by oven drying and then using three cycles of gas evacuation by vacuum and back filling with dry N_2 gas. Anhydrous Et_2O was added to the flask by syringe followed by the syringe addition of compound **125**. Also due to the sensitivity of organolithium reactions the reaction mixture was cooled to -78 °C using a dry ice/acetone cooling bath. *n*-Butyllithium (2.5 M) in hexanes was added via syringe in a dropwise manner over 15 minutes. This slow addition was to ensure the reaction did not exceed a safe rate. This reaction was allowed to run over a 3-hour period, although lithium halogen exchange should occur rapidly. Because organolithium products are difficult to characterize, intermediate **128** was generated *in situ* and used directly in the following reaction for the intermediate **131**.

Scheme 4.[a] Synthesis of intermediate **128**.

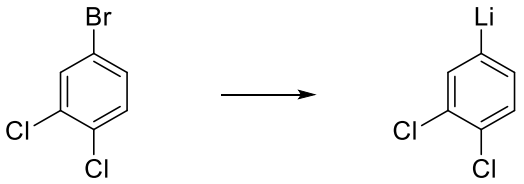

125 **128**

[a]Reagents and conditions: 2.5 M *n*-BuLi in hexanes, anhydrous Et_2O, -78 °C, 3 h.

For the synthesis of compound **131** (the N-Boc protected target compound), intermediates **124** and **128** were reacted with each other in Et_2O (Scheme 5). Compound

124 was placed in an oven-dried flask after which was evacuated by vacuum and back filled with N_2 gas three times. Afterwards, anhydrous Et_2O was added via syringe and the reaction mixture was cooled to -29 °C using a dry ice/*o*-xylene cooling bath. Once the reaction mixture was cooled, intermediate **128** was added via syringe in a dropwise manner over a 15-minute period. This slow addition time was taken to add the organolithium intermediate in order to avoid rapid exotherms. This reaction was allowed to run overnight as the Weinreb ketone reaction intermediate formed is somewhat stable. A reverse quenching method was employed to reduce any side product formation by slowly adding portions of the reaction mixture to a cold 1 M KH_2PO_4 solution.

Scheme 5.[a] Synthesis of intermediate compound **131**.

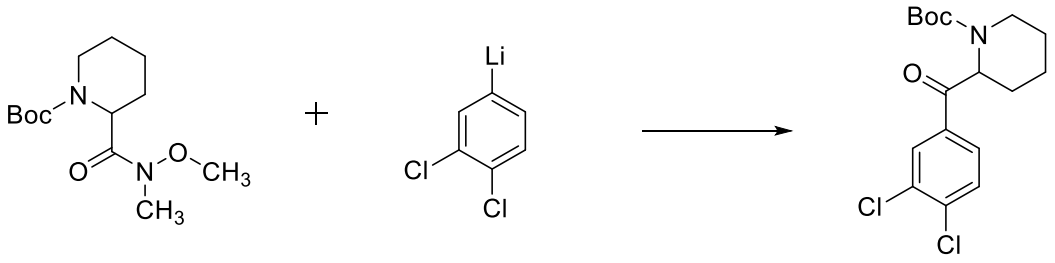

124 **128** **131**

[a]Reagents and conditions: anhydrous Et_2O, -29 °C, 24 h, 1 M KH_2PO_4 reverse quench.

In order to generate the final target compound **119**, intermediate **131** was deprotected and the freebase of **119** was converted to an HCl salt (Scheme 6). Deprotection and salt formation was accomplished in one pot by first dissolving **131** in anhydrous methanol and cooling the solution with an ice bath. Then, methanolic HCl was added in a dropwise

manner to the reaction mixture until the pH of the solution was near 1. The reaction mixture was allowed to stir overnight. Upon removal of solvent, washing with acetone, and recrystallizing using anhydrous methanol, pure target product **119** was collected with a melting point of 272-273 °C. This melting point corresponds to what was previously recorded at 273-275 °C.[7] For full characterization of the target compound **119** nuclear magnetic resonance (NMR) spectrometry, high resolution mass spectrometry (HRMS), and C, H, N analysis were utilized and each analysis method confirmed successful synthesis and purity (Figure 29). C, H, N analysis had not previously been reported for compound **119**.

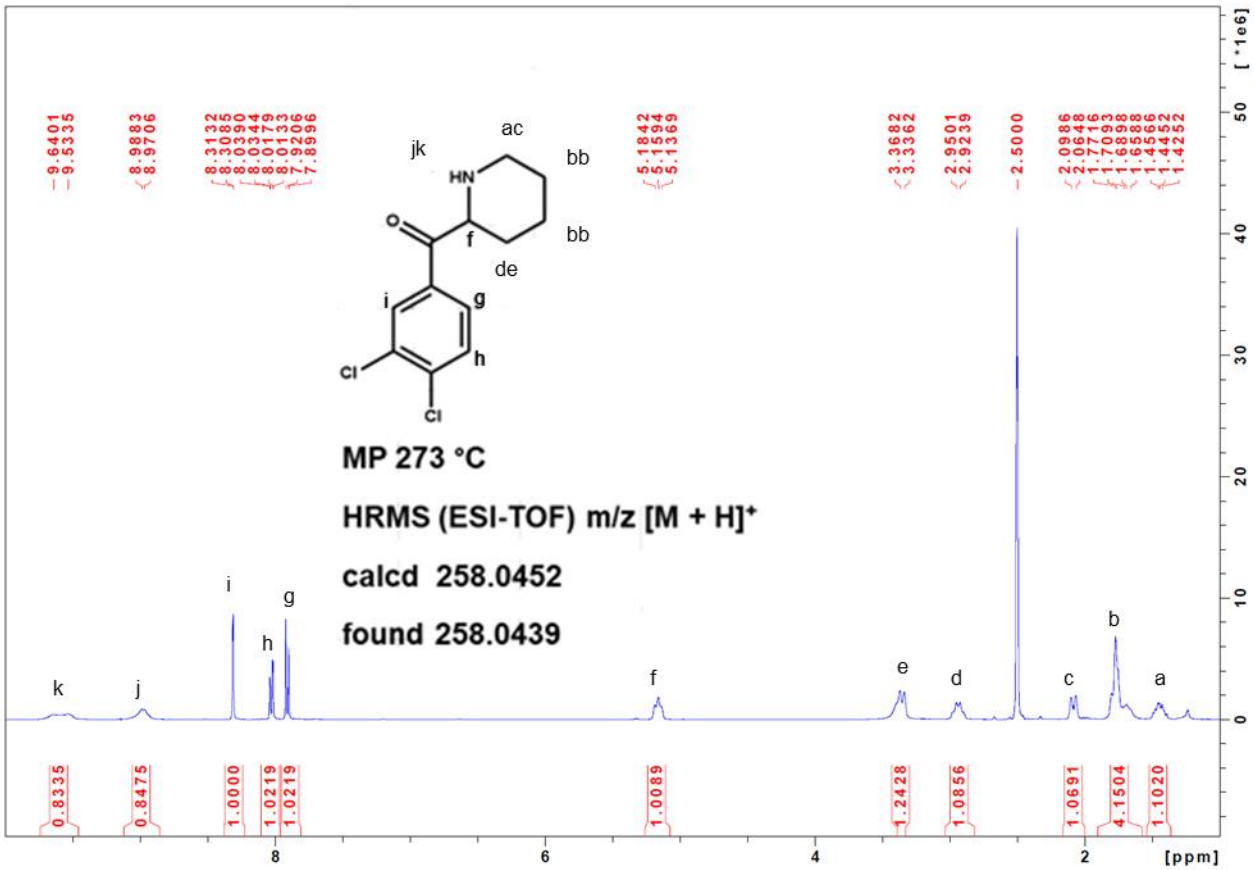

Figure 29. [1]H NMR spectrum of compound **119**.

Scheme 6.[a] Synthesis of target compound **119**.

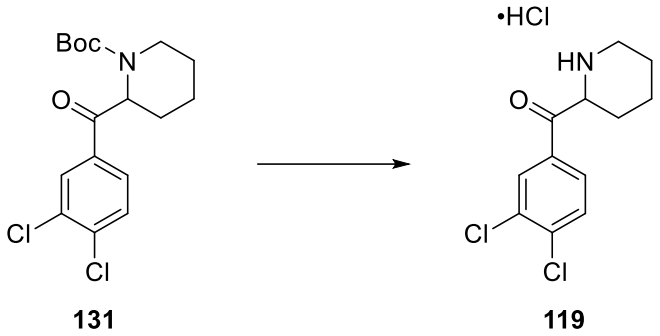

131 **119**

[a]Reagents and conditions: methanolic HCl, anhydrous methanol, 0 °C, 24 h.

After the success of the first target compound (i.e., **119**), synthesis of compound **120** was attempted. Four attempts were made to finally generate compound **120**. The first attempt proved to be successful albeit having immensely low yields. The amount of compound **120** obtained was just enough for characterization but not enough for future biological assay studies. The second attempt made use of a newer batch of the starting material 4-bromo-*o*-xylene (**126**) in an effort to increase yields. This was in case the starting material had decomposed or been compromised. The second attempt yielded a higher total amount of a white crystalline solid than the first. The thin layer chromatography (TLC) for this second compound produced the same retention factor (Rf) value as the first attempt. Even the CombiFlash Companion/TS readout produced a similar chromatogram as the first attempt. Unfortunately, when it came to the melting point it was close to 100 °C less than for the characterized first compound (i.e., **120**). Also, ^{1}H NMR characterization showed that compound **120** was not present in the test sample. Attempt two was a failure

(Scheme 7). Further characterization was not carried out and another set of reactions was set up for the third attempt.

Scheme 7.[a] Failed synthesis of target compound **120**.

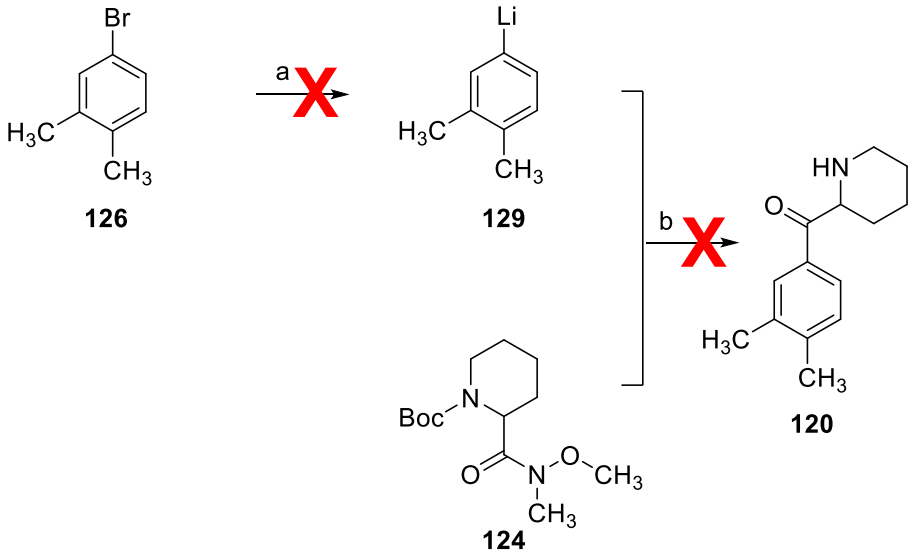

[a]Reagents and conditions: a. 2.5 M *n*-BuLi in hexanes, anhydrous Et_2O, -78 °C, 3 h; b. anhydrous Et_2O, -29 °C, 24 h.

For the third attempt, the original batch of 4-bromo-*o*-xylene was used as it was the one that produced a successful synthesis and the only variable changed between the first two attempts. Again, a white crystalline solid was isolated with similar Rf and chromatogram to compound **120**, but it had a much lower melting point. This time several recrystallizations using absolute ethanol were attempted to further purify the white solid and possibly raise the melting point and produce a clean ^{1}H NMR spectrum. The melting point stabilized at around 160 °C, compared to 263-264 °C for the original sample of **120**.

The ^{1}H NMR integrated for the number of protons that was expected for compound **120**, but the anticipated aromatic signals were missing and instead only aliphatic protons were observed (other than the proton signals from the protonated amine) (Figure 30). On further analysis it was hypothesized that the product formed was **132** (Scheme 8). This was confirmed through HRMS generating a signal within 5 ppm of the theoretical compound (i.e., **132**). A search of the literature did not yield any articles describing compound **132**.

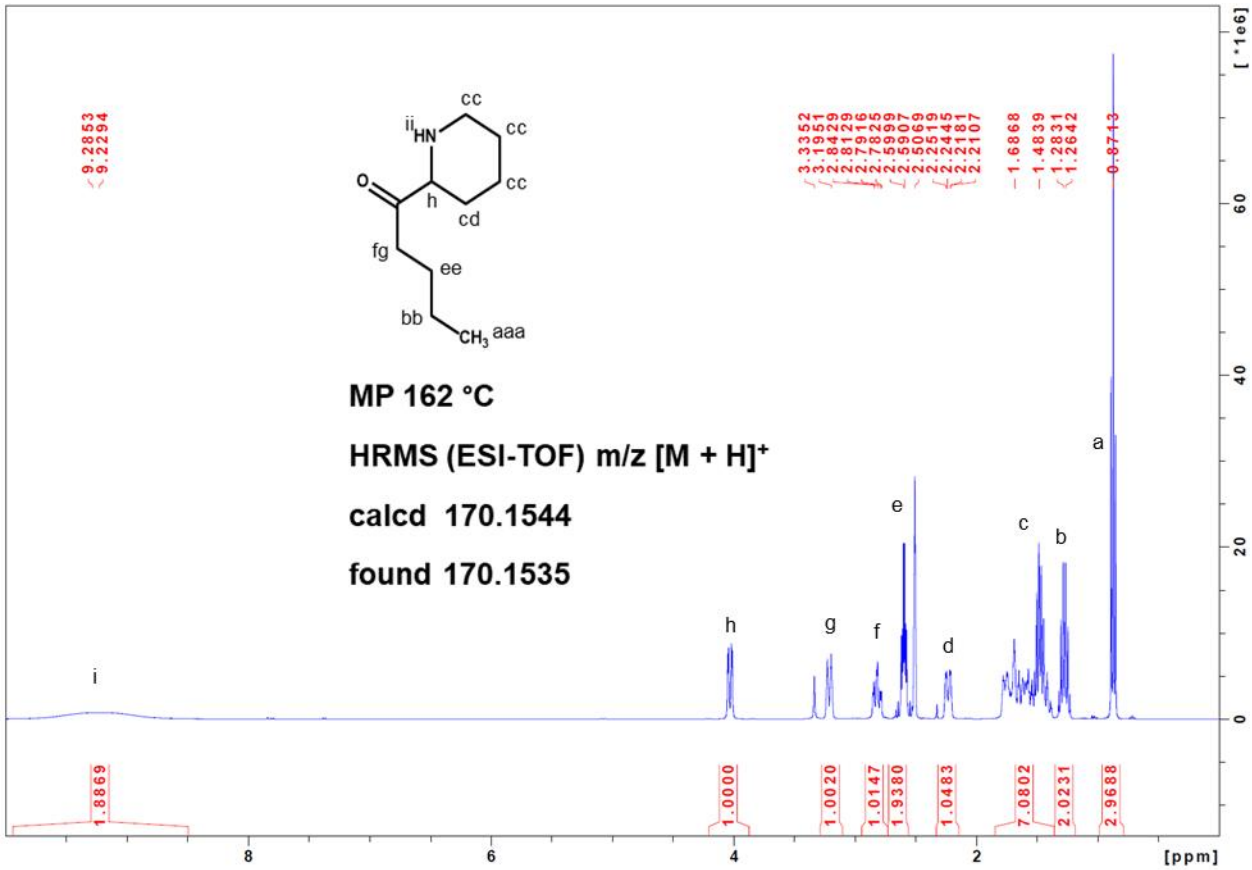

Figure 30. ^{1}H NMR spectrum of compound **132**.

Scheme 8.[a] Synthesis of off-target compound **132**.

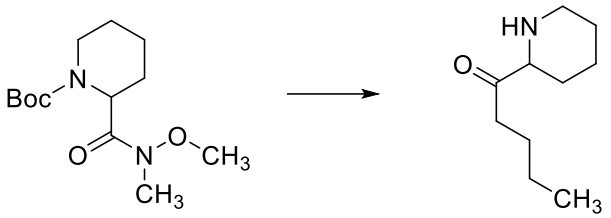

124 **132**

[a]Reagents and conditions: 2.5 M *n*-BuLi in hexanes, anhydrous Et_2O, -29 °C, 24 h.

After the identification of compound **132** it was established that the lithium halogen exchange reaction was not proceeding. Possible explanations for this reaction not taking place could be due to an improper amount of *n*-BuLi reacting either from an inaccurate titer from the reagent bottle due to degradation or moisture/air exposure to the reaction. This explanation was dismissed because compound **132** would not be able to form if this was the case. Another option would be to use *t*-BuLi for the lithium halogen exchange because it is an irreversible reaction but none was available at the time. Regardless, the lithium halogen exchange reaction should be rapid and take place for *n*-BuLi and reagent **126**. For the fourth and final attempt to produce target product **120** the lithium halogen exchange set up and reaction was meticulously monitored. Upon cooling the 4-bromo-*o*-xylene (**126**)/anhydrous Et_2O solution to -78 °C with a dry ice/acetone bath it was noted that a small amount of white solid was present in the flask. Testing this observation, a small vial was filled with a large amount of reagent **126** and anhydrous Et_2O and submerged into the cooling bath. Solid 4-bromo-*o*-xylene (**126**) instantly precipitated from

solution. It would seem that the reagent was insoluble at this temperature and not taking part in the lithium halogen exchange reaction. A literature search revealed that 4-bromo-*o*-xylene (**126**) melting point is -0.2 °C.[86] The next step was to determine if organolithium reactions can safely be run at higher reaction temperatures near 0 °C and a literature search was successful in answering that question.[87] In a study on the effects of solvent on lithium-bromine exchange of aryl bromides using *n*-BuLi at 0 °C, it was clearly shown that the lithium halogen exchange could safely take place with good yields at higher temperatures than -78 °C.[87] With this knowledge the fourth attempt was continued at 0 °C but using the same molar equivalent of *n*-BuLi as was used in the study by Bailey et al.[87] (Scheme 9).

Scheme 9.[a] Successful synthesis of target compound **120**.

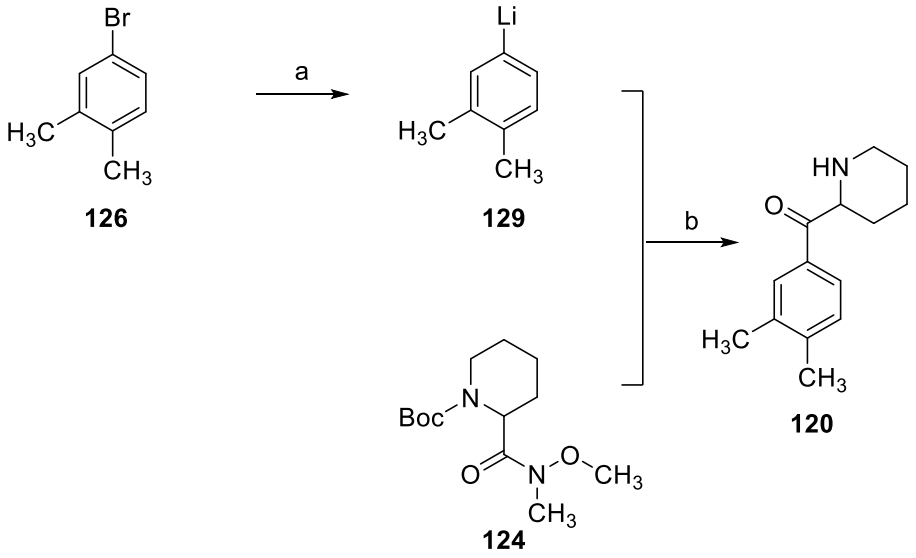

[a]Reagents and conditions: a. 2.5 M *n*-BuLi in hexanes (1.2 equiv.), anhydrous Et_2O, 0 °C, 3 h; b. anhydrous Et_2O, -29 °C, 24 h.

After quenching, extraction, and purification a white crystalline solid was obtained. Just as in the first attempt, this compound had the same Rf and chromatogram profile for compound **120**. The melting point was 262-264 °C matching the previously fully characterized target compound **120**. The ^{1}H NMR spectra displayed the anticipated proton signals in the aromatic region that were missing in the previous two attempts and integrated for the correct total number of protons (Figure 31). HRMS also confirmed the desired mass within 5 ppm. Target compound **120** was successfully synthesized and had the highest yield (27%) of this hybrid cathinone/methylphenidate series.

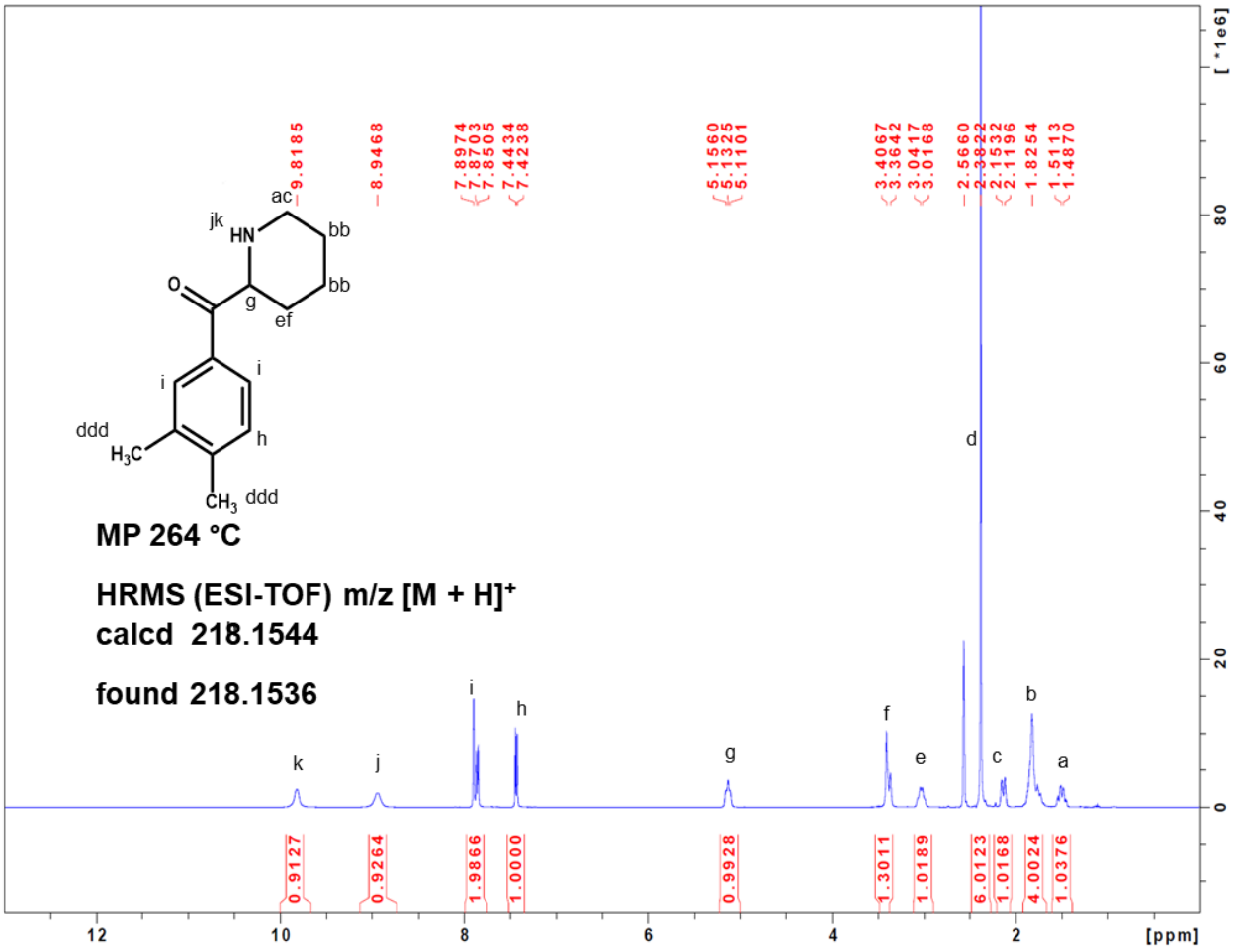

Figure 31. ^{1}H NMR spectrum of compound **120**.

The synthesis of target compound **121** followed the same procedures for the synthesis of compound **119** with the only difference in using 2-bromonaphthalene (**127**) instead of 3,4-dichlorobromobenzene (**125**). This compound had a high melting point (245-247 °C) similar to the other two target products. ^{1}H NMR, HRMS, and Fourier-transform infrared spectroscopy (FTIR) were used to characterize compound **121** (Figure 32). FTIR was able to demonstrate the band from the target product's ketone functional group at 1674 cm^{-1}.

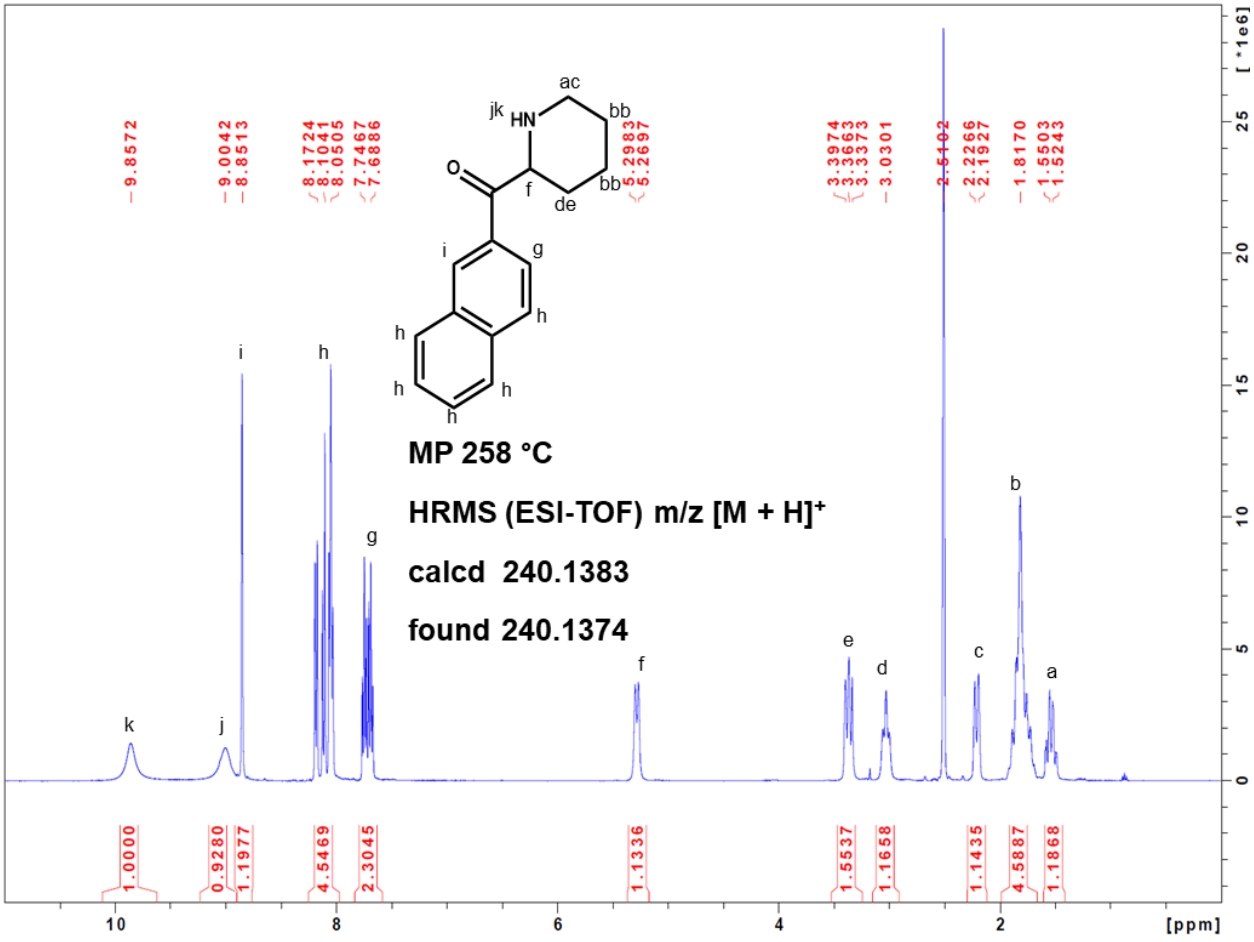

Figure 32. ^{1}H NMR spectrum of compound **121**.

b. Biological Studies

Once each compound had been successfully synthesized and fully characterized their ability to inhibit DAT was examined using biological assays. The hyrbid compound backbone and several analogues had been previously shown to be DAT reuptake inhibitors and not releasing agents using a Ca^{2+} fluorescence assay.[7] The compounds were evaluated as DAT reuptake inhibitors using an APP^{+} uptake assay. The assay was

performed on HEK Flp-In T-REx 293 cells stably expressing hDAT. Fluorescence microscopy was used to measure fluorescent intensity of the cells. APP^+, which is a DAT substrate, fluoresces at an emission wave length of 540 nm with an excitation of 460 nm after transporter mediated transport intracellularly. A stepwise loss in fluroescent intensity is seen when the APP^+ substrate is added with increasing concentrations of agents that interact with DAT. The potency of the test agent is in direct proportion to the inhibition of the fluorescence from APP^+. Methylphenidate **t9** and compound **119** were both used as standards in testing. Dose response curves (Figure 33) were obtained for the two standards and compounds **120** and **121** using six different concentrations (1 nM, 10 nM, 30 nM, 100 nM, 300 nM, and 1 μM) . Each concentration was repeated in triplicate and each experiment was repeated on separate days in order to reduce error. All data were analyzed using EasyRatioPro 3 and then plotted with GraphPad Prism 8.0.1. For each experiment 40 separate cells that showed activity were choosen as regions of interest (ROI). These ROIs were then used for the data to build the IC_{50} inhibition curves (Figure 33). Each data set was background subtracted and normalized by the average positive control for the experiment day. To fill out some of the curves more completely lower and higher concentrations of the test compounds were used. For both compounds **119** and **121** an extra set of experiments were performed to include concentrations of 0.1 nM and 3 μM. For compound **120** an extra experiment was performed at 3 μM.

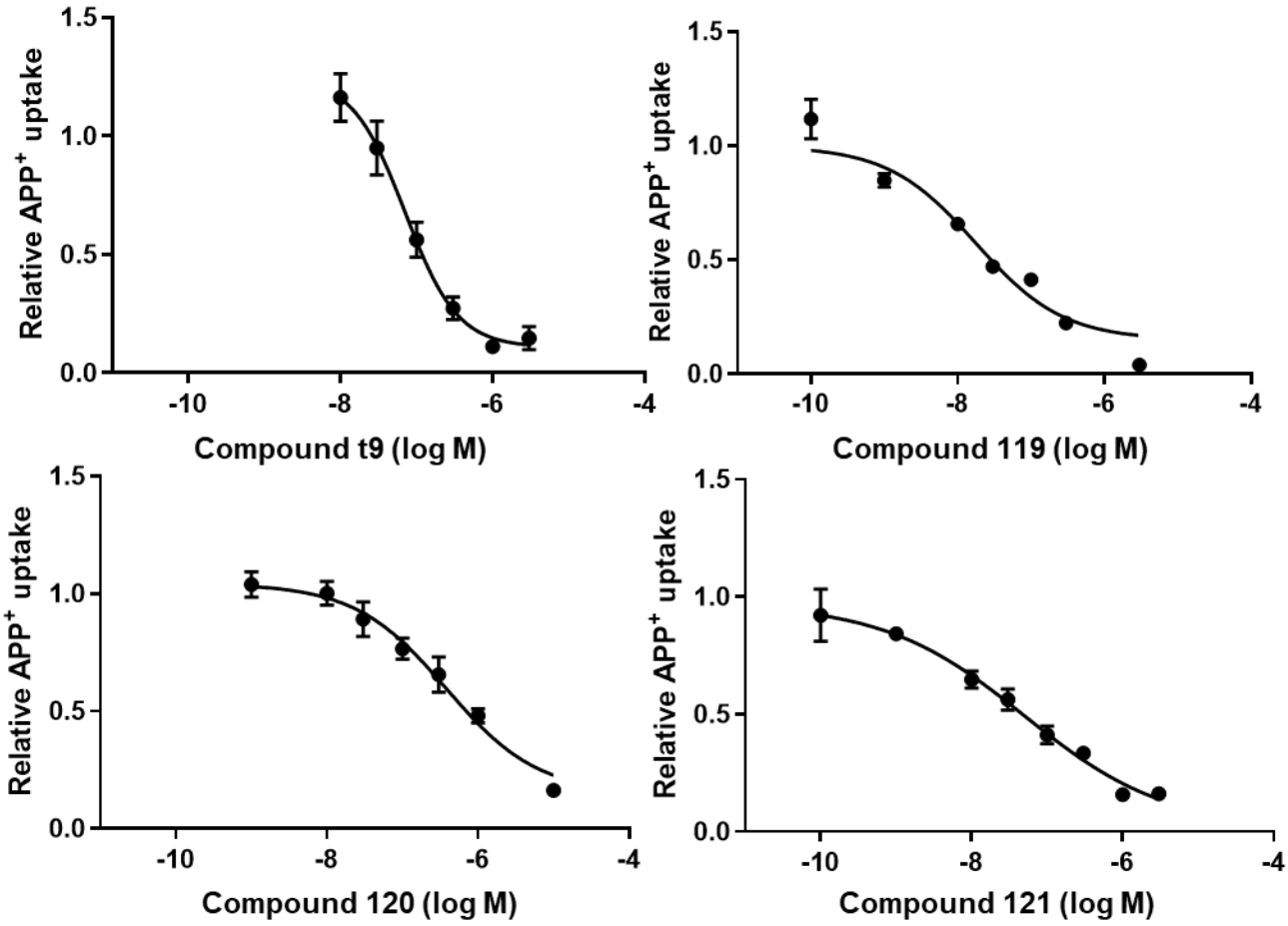

Figure 33. Dose-response curves of **t9** and hybrid compounds **119**-**121** in an APP^+ uptake assay at hDAT.

The IC_{50} value of each compound is shown in Table 12. The potency of the standard methylphenidate (**t9**, IC_{50} = 70 ± 16 nM) was similar to what had been reported previously (IC_{50} = 72 nM).[7] The hybrid compound **119** was about twice as potent (IC_{50} = 17 ± 2.34 nM) than previously reported (IC_{50} = 47).

Table 12. Uptake inhibition (IC_{50}, nM) values of methylphenidate (**t9**) and hybrid compounds **119**-**121** in the APP^+ uptake assay at hDAT.

Compound	IC_{50} ± SEM (nM)
t9*	72
t9	70 ± 16
119*	47
119	17 ± 2.34
120	379 ± 88
121	50 ± 25

*As reported previously.[7]

What can be seen with the new data is that all compounds are much more potent compared to the unsubstituted parent compound **112** (IC_{50} = 1080 nM).[7] The dimethyl compound **120** was weaker (IC_{50} = 379 ± 88 nM) than the other two test compounds. This result shows that the potency of these disubstituted benzoylpiperidines is not strictly related to lipophilicity or occupancy of the chemical space in the binding pocket of hDAT but these two factors likely contribute to greater potency. The naphthyl compound **121** with an IC_{50} = 50 ± 25 nM was more potent than the methylphenidate standard and had a similar potency to the previously published data for compound **119**. The similarity in these two compounds' (i.e, **119**, **121**) potencies demonstrate that the electron withdrawing character of these substituents is likely the cause for an even greater increase in potency from the parent compound **112** and the electron donating dimethyl compound **120**. Also due to the high potency of compound **121** it is unlikely that

compound **119** is participating in halogen bonding interactions or if these interactions are present, they contribute minimally to its overall increased potency. However, both **119** and **121** analogs could participate in hydrogen bond interactions via either the chloro substituents of compound **119** or the aromatic hydrogen atoms of compound **121**. It is not possible with this data to state whether or not the potency of these two compounds is due to their electron withdrawing properties, hydrogen bonding capabilities, or a combination of both. To be certain of these interactions modeling and future compounds will have to be explored. These data correlate with the modeling data as in both instances the dimethyl compound **120** was the lowest scoring for modeling (see "c. Docking Studies" section) and had the weakest activity in the APP^+ assay (see below). Compound **121** has a previously studied corresponding methylphenidate analog **78** with a $pIC_{50} = 7.96$. Using the previously developed plot of the hybrid analogs and the corresponding methylphenidate compounds it would be predicted that compound **121** should have a $pIC_{50} = 6.60$ or about 250 nM (Figure 34). The experimental pIC_{50} for compound **121** was 0.7 log units greater with a potency approximately five times greater than that of the prediction.

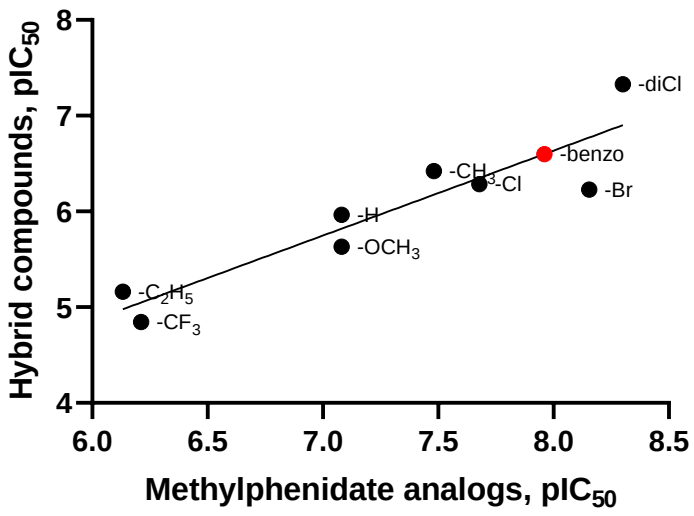

Figure 34. Correlation between the binding data of **t9** analogs (x-axis) and APP^+ uptake assay data (y-axis) for the corresponding methylphenidate hybrid compounds (r = 0.91, n = 8). Predicted pIC_{50} activity for compound **121** analog (red).

Adding the experimental compound **121** data point to previously plotted correlation data increases the number of corresponding compounds to n = 9 (Figure 35). The r value lowers to 0.89 from 0.93 but the correlation is still statistically significant. Using this new plot the predicted corresponding dimethyl methylphenidate compound to the hybrid **120**, which has not been reported, should have a binding pIC_{50} of approximately 7.57 (Figure 35). What is still undetermined from these experiments are the relative potencies between the two possible isomers of each compound and there is still not enough data for disubstituted benzoylpiperidines for statistical significance. Several compounds will still need to be explored for an n = 6. At that point individual factors involved with the structural variation between the analogs can be correlated.

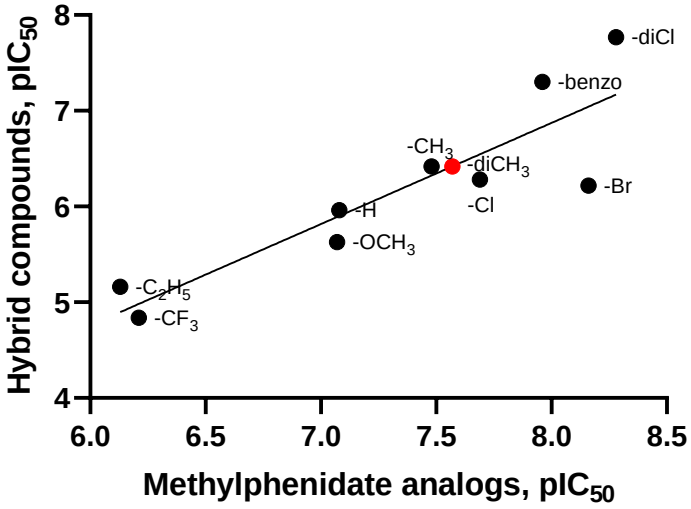

Figure 35. Correlation between the binding data of **t9** analogs (x-axis) and APP^+ uptake assay data (y-axis) for the corresponding methylphenidate hybrid compounds (r = 0.89, n = 9). Predicted pIC_{50} binding for dimethyl **t9** analog (red).

c. Docking Studies

Both S and R isomers of the three compounds **119**, **120**, and **121** were sketched in SybylX 2.1.1 and energy minimized using the Tripos Force Field with Gasteiger-Hückel charges. Using Gold2020 each compound was docked 100 times in the hDAT homology model with cocaine as a reference ligand. All poses were scored with GOLD and ChemPLP. Gold scores for each of the isomers of the three compounds were within 1 unit of each other suggesting both isomers bind at the S1 central binding site of hDAT. The highest scoring pose for each compound were in a similar pose and had a high degree of overlap (Figure 36). There was not an observed difference in the rotomer orientation of D79 for

any of the compounds tested. Each of the S isomers was within hydrogen bond distance from the D79 (i.e., 2.56, 2.55, and 2.59 Å for **119**, **120**, and **121**, respectively) while the R isomers were about half an angstrom too far for the desired interaction. These distances and scoring suggest that the S isomers of the three compounds might be more potent than their R isomer counterparts.

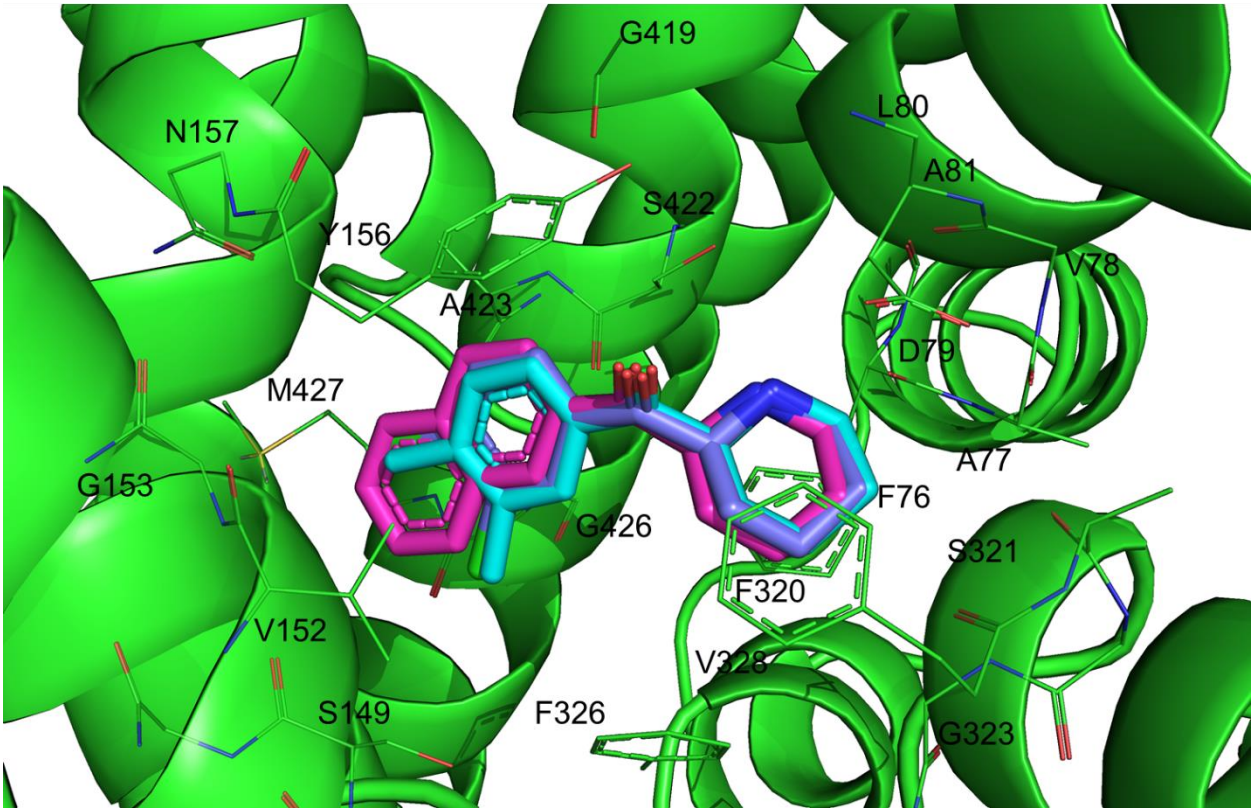

Figure 36. hDAT homology model (cartoon, green) with possible binding poses of S isomer hybrids **119** (sticks, purple), **120** (sticks, cyan), and **121** (sticks, magenta).

All poses generated were analyzed through HINT. Using SybylX 2.1.1 scripting language each pose of both S and R isomers of hybrid compounds **119**, **120**, and **121** was merged with the hDAT homology model. Each formed complex was then minimized using the

Tripos Force Field with Gasteiger-Hückel charges. Using Sybyl 8.1, each complex had the test ligand extracted into its own molecular area and HINT analysis was performed. For the initial partitioning phase, the dictionary method was used for the protein and the calculation method was used for the ligand.[83,84] All other parameters were set to their default values. The highest scoring compound in HINT was the S isomer of hybrid **121** (Table 13). While compound **121** was not the most potent of the series there is a good relationship between its high HINT score and potency. The other two compounds (i.e., **119** and **120**) had similar scores to previously docked methylphenidate (**dt9**). Both S and R isomers scored well with the S isomer of each compound scoring higher than the corresponding R isomer. These results suggest that all compounds are likely (and, in fact, were) active and that the S isomer, which has slightly better interactions within the S1 central binding site of hDAT, is probably more potent than the R isomers. While synthesis and biological studies only examined the racemates of compounds **119**-**121**, The same docking results could be used in future studies if the isomers are to be isolated.

Table 13. HINT scores in descending order of compounds **119**-**121** and **dt9**.

Compound	**HINT score**
S **121**	1040
R **121**	904
dt9	868
S **119**	842
S **120**	834

R **119**	809
R **120**	743

The HINT and GOLD scores do not reveal the relative potencies of the compounds. It has already been established that compound **119** is more potent than **dt9** yet for this modeling study **119** scored lower for both isomers than **dt9**. For the potential halogen bonding aspect of compound **119** HINT and GOLD cannot answer this question because neither software takes this particular interaction into account. This could be a reason why compound **119** is scored lower than **dt9**. If a halogen bond interaction could be scored for either of these software packages then **119** might have the highest score. Hydrogen bond interactions with the substituents were not observed in the HINT analysis tables for compounds **119** or **121**. By default, an aryl hydrogen's partial positive charge (such as the aryl hydrogens on compound **121**) is not considered in HINT. S149 in particular is aligned in such a way that the oxygen atom lone pair is in direct alignment of compound **119**'s 3-chloro substituent's terminal end where a sigma hole would occur as well as one of compound **121**'s aryl hydrogens from the extended phenyl ring. These atoms are within a distance of 3.5 Å and 3.22 Å for compounds **119** and **121**, respectively. Compound **121**'s planar hydrogen atom from the extended aryl ring with its partial positive charge could be involved in electrostatic interactions at this distance from S149's oxygen atom. There is tolerance for the large naphthyl ring mainly due to the space G153 and S149 allows in a similar manner that is seen with the methylenedioxy ring of MDPV (**10**; See Project 2). The lowest scoring compound was compound **120**. It is likely that the three

test compounds (**119**-**121**) scored somewhat similarly due to the hydrophobic nature of the substituents. Possible differences could then be due to the electron withdrawing character of the substituents of **119** and **121**. This could be a reason why compound **121** had the highest HINT score. The scores are too close in magnitude to make definitive conclusions about potency though. What these data can contribute is that all of these compounds more than likely should (and, in fact, did) interact with hDAT. The modeling allows for speculation of the actual configuration that these disubstituted compounds (**119**-**121**) take although it will not be proved unless either a constricted analog is developed that shows similar activity to the parent compounds or a crystal structure with one of these compounds is solved. Most likely though the structure's substituents probably take the same orientations of the previous solved crystal structures of DA and 3,4-dichlorophenethylamine in dDAT. All compounds in the modeling were likely to be active and the previous biological data corroborates that finding.

B. Project 2.

Aim. Evaluate binding modes of selected cathinones at DAT mutant transporters utilizing 3D molecular modeling

dDAT which can be considered a natural mutant of hDAT displays unique properties for certain inhibitor psychostimulants. MDPV (**10**), α-PVP (**11**), and MDPPP (**39**) have all been identified on the clandestine market as drugs of abuse. These three psychostimulants are potent hDAT inhibitors but show virtually no activity at dDAT (unpublished findings). With this distinction between the two species of DATs, gain-of-function experiments were performed upon where mutating one non-conserved amino acid residue at a time from dDAT to hDAT, might restore activity to the three stimulants to what is observed in hDAT. The amino acid residues chosen for mutation were A117S/D121G/P323V/F318C. Three of the amino acid residues that were chosen (i.e., A117, P323, and F318) were those that dDAT and hSERT have conserved but are not present in hDAT (Figure 37). These residues are either part of, or part of the opening to, the S1 central binding site in dDAT and hSERT crystal structures.[4,15] All three stimulants show no activity towards hSERT and these residues might be responsible for that lack of activity. The other amino acid residue D121 that was mutated was one that is unique to dDAT only and has been shown previously to be important for DAT inhibitor agent activity.[15] Although several different mutants were constructed, only a triple mutant (A117S/D121G/P323V) and quadruple mutant (A117S/D121G/P323V/F318C) are considered here. The potencies of **10**, **11**, and **39** at these two mutants, as well as at wild-type dDAT and hDAT are shown in Table 13 (Dr. Eltit; unpublished data).

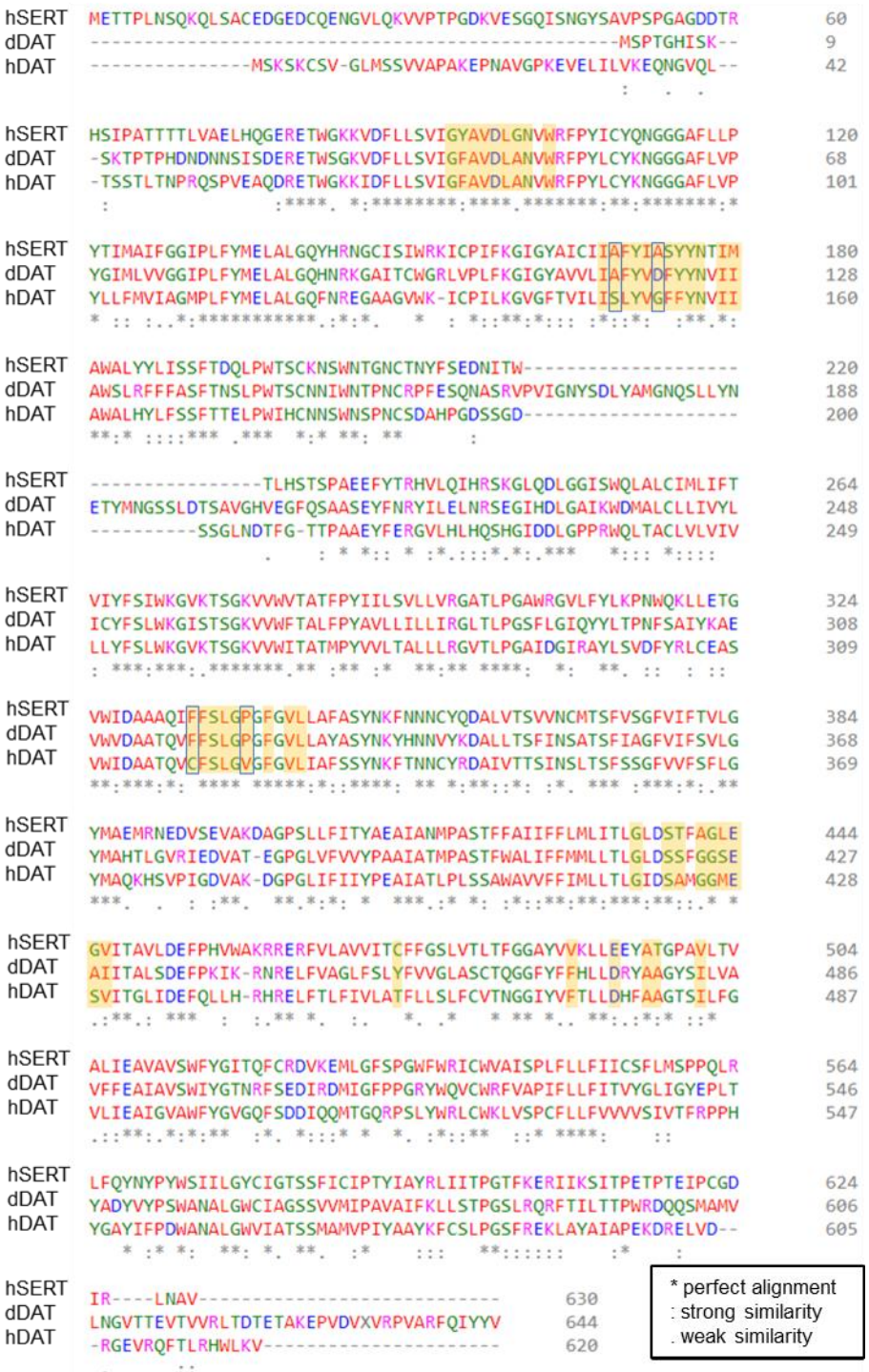

Figure 37. Sequence and alignment of hSERT, dDAT, and hDAT. Highlighted areas form the S1 central binding site and boxed amino acids are selected sites of dDAT mutations.

The largest increase in potency restoration contained all four-point mutations (Table 14). This is impressive because only four mutations were needed to see great improvement in functional activity. The functional data shows that the mutation of the four non-conserved residues from hDAT into dDAT restored activity of MDPV (**10**) by just over 100-fold compared to *wt* dDAT (Table 14; Dr. Eltit; unpublished data). Modeling studies were then used to compare the transporter structures and determine what molecular interactions were taking place between the ligands and transporters.

Table 14. Potency of MDPV (**10**), α-PVP (**11**), and MDPPP (**39**) inhibiting DA-induced Ca^{2+} signals at the indicated transporters.[a]

	Construct, pIC_{50} ± SEM (M), (IC_{50} nM; # cells analyzed)			
	***wt* dDAT**	**triple dDAT mut**	**quad dDAT mut**	***wt* hDAT**
MDPV	4.56 ± 0.02 (27,350; 437)	5.92 ± 0.02 (1,207; 438)	6.60 ± 0.04 (251; 396)	7.47 ± 0.01 (34; 459)
α-PVP	4.68 ± 0.03 (20,710; 699)	5.82 ± 0.03 (1,531; 599)	5.96 ± 0.03 (1,094; 481)	7.29 ± 0.01 (51; 569)
MDPPP	Inactive (>>30,000; 246)	4.80 ± 0.02 (16,960; 551)	4.89 ± 0.01 (12,950; 507)	5.47 ± 0.02 (3,418; 639)

[a]Unpublished data from Dr. Eltit's lab.

Of all the different combinations of dDAT mutants, the four-point mutation (i.e., the quadruple mutant) saw the largest restoration of activity and was used for the subsequent modeling studies. The models used for the molecular modeling studies were the Project 1 hDAT homology models, the available dDAT crystal structure PDB ID: 4XP4 for *wt* dDAT, and the same dDAT crystal structure as template to generate a 3D homology model of the quadruple (A117S/D121G/P323V/F318C) dDAT mutant. The three models were energy minimized using Tripos Force Field with Gasteiger-Hückel charges then compared using the Biopolymer suite within SybylX 2.1.1. The overall structure of these energy-minimized models was similar; the RMSD was 2.02 Å between hDAT and the quadruple dDAT mutant homology models, and 2.16 Å between hDAT and the *wt* dDAT structures. As expected, *wt* dDAT and the quadruple dDAT mutant models were very similar (RMSD = 0.29 Å). When the S1 central binding pockets were compared, the RMSD between hDAT and the quadruple dDAT mutant is 2.11 Å, and between hDAT and *wt* dDAT models, it was 2.12 Å. The RMSD of the binding pockets of the *wt* dDAT and quadruple dDAT mutant models was 0.36 Å. The total volume of the pockets increased from 2425 $Å^3$ for *wt* dDAT, to 2533 $Å^3$ for the dDAT mutant, to 3170 $Å^3$ for hDAT. Two of the mutations contained residues (P323V/F318C) that were not part of the S1 central binding site. For docking studies this is a difficult undertaking as the test ligand is placed within the defined binding site to start. In reality, these mutations (P323V/F318C) might affect activity due to their location on the transmembrane helices and influence entry into the S1 site. Figure 38 shows the opening to the S1 site from the extracellular space for the transporter.

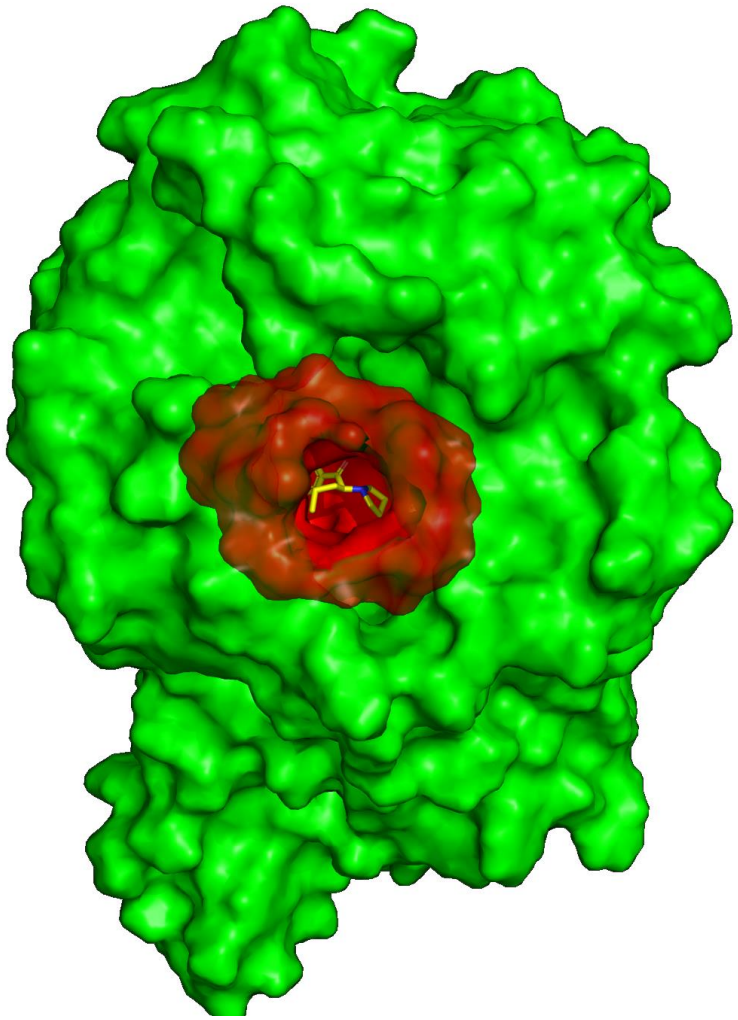

Figure 38. hDAT homology model (Connolly surface, green) with MDPV (**10**, sticks, yellow) in the S1 central binding pocket (Connolly surface, red).

The S1 site is comprised of the central portions of the transmembrane helices TM1, TM3, TM6, and TM8.[16] Helices TM3 and TM8 are uninterrupted but, helices TM1 and TM6 are subdivided into two helices (1a and 1b, and 6a and 6b, respectively) connected by a non-helical segment in the middle.[16] F318 and P323 are part of TM6 but they do not directly

face ligands. F318 is adjacent to the highly conserved F319 in the TM6a helix. F319 is considered the extracellular gate controlling access to the central cavity from the extracellular entrance.[88] This gate is “open” in the outward facing conformation, and F319 rotates to a “closed” conformation in the occluded state of the transporter.[15] The F318C P323V mutations might influence F319 operation in such a way that it allows better access of the bulky MDPV molecule to the S1 site in the outward facing state through increased structural flexibility and manipulation of F319 positioning, this positive effect of F318C is less evident for the smaller α-PVP (**11**) and MDPPP (**39**) molecules.

For the other two mutations (A117S/D121G) that lie within the S1 binding pocket, docking studies were conducted to better understand potential molecular interactions with MDPV (**10**), α-PVP (**11**), and MDPPP (**39**) within the three transporters. GOLD2020 was used to generate 100 docking solution poses of each agent in each DAT model totaling for 900 generated poses. The S1 binding site has a composition that can be divided into three subsites or subpockets (*A*, *B*, and *C*; Figure 39) that are occupied by the terminal amine, aryl portion, and α side chain, respectively.[15] Table 15 shows the amino acid residues that constitute the S1 central binding site for each of the three transporters.

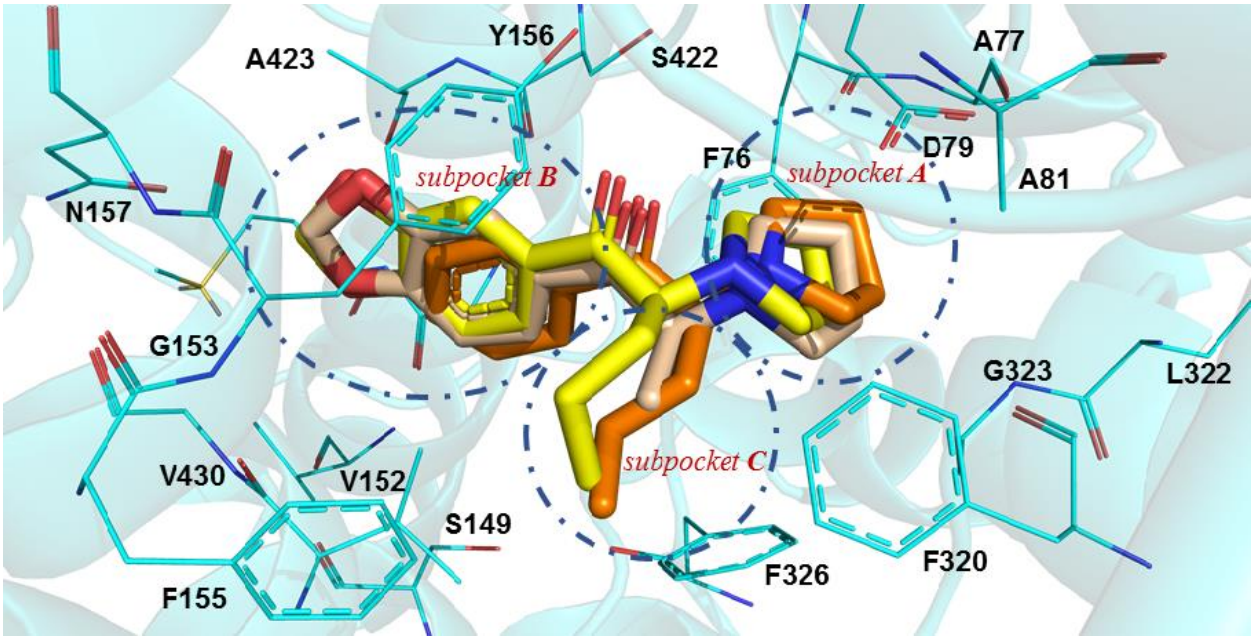

Figure 39. Divided *A*, *B*, and *C* subpockets with possible binding pose of MDPV (**10**, sticks, yellow), α-PVP (**11**, sticks, orange), and MDPPP (**39**, sticks, wheat) in hDAT (lines and cartoon, cyan) S1 central binding site.

HINT analysis was used to investigate the interactions between the aromatic and alkyl side chains of the compounds and subpockets *A*, *B*, and *C* of the dDAT and hDAT models.[84] The amino acids displayed in Table 15 were identified using the HINT analysis. For the initial partitioning phase, the dictionary method was used for the proteins and the calculation method was used for the ligands.[83,84] All other parameters were set to their default values. In the highest scoring HINT ligand-protein complex solutions, the agents showed the same orientation at all three transporters (Figure 39). These poses embody the same 3-dimensional space in the three subpockets with the same characteristics (i.e.,

aromatic ring, protonated nitrogen atom, and alkyl side chain) as the solved crystal structure pose of cocaine bound to dDAT (PDB ID: 4XP4).

Table 15. Amino acid residues corresponding to the *A*, *B*, and *C* subpockets that make up the S1 central binding site in *wt* dDAT, dDAT (i.e., quadruple) mutant, and hDAT.

Subpocket	***wt* dDAT**	**dDAT mutant**	**hDAT**
A	F43, A44, D46, A48, Y124, F319, L321, G322, S421	F43, A44, D46, A48, Y124, F319, L321, G322, S421	F76, A77, D79, A81, Y156, F320, L322, G323, S422
B	A117, V120, D121, S421, S422, G425, I429, Y455, S426, N125	S117, V120, G121, S421, S422, G425, I429, Y455, S426, N125	S149, V152, G153, S422, A423, G426, V430, T456, M427, N157
C	D46, V120, F319, F325, D475, A479, I483, Y123	D46, V120, F319, F325, D475, A479, I483, Y123	D79, V152, F320, F326, D476, A480, I484, F155

HINT scores showed low scores for MDPPP (**39**) in all models, whereas MDPV (**10**) and α-PVP (**11**) showed much higher scores at hDAT (Table 16).

Table 16. Gold and HINT scores for docking solutions of the agents MDPV (**10**), α-PVP (**11**), and MDPPP (**39**) in the *wt* dDAT, dDAT mutant, and hDAT models.

Agent	Transporter	Gold score	HINT score
MDPV	*wt* dDAT	58.08	376
MDPPP	*wt* dDAT	54.49	186
α-PVP	*wt* dDAT	51.91	605
MDPV	dDAT mutant	58.89	261
MDPPP	dDAT mutant	54.03	342
α-PVP	dDAT mutant	53.30	463
MDPV	hDAT	55.32	727
MDPPP	hDAT	52.13	287
α-PVP	hDAT	51.25	759

Each individual Interaction involving the atoms within subpockets *A*, *B*, and *C* with the three test compounds were extracted from the resulting HINT table and tabulated (Table 17). The number of positive and negative interactions between a docked molecule at each protein model showed that the total favorable interactions were highest at hDAT and the more unfavorable interactions were highest at *wt* dDAT for each agent. These results are consistent with the functional data (Table 14). A description of the potential interaction of MDPV and its analogs at each subpocket (*A*, *B*, and *C*; Figure 39) is provided below.

Table 17. Tabulated positive, negative, and sum total HINT interactions of docked solutions for the agents MDPV (**10**), α-PVP (**11**), and MDPPP (**39**) in the *wt* dDAT, dDAT (i.e., quadruple) mutant, and hDAT models.

Agent	Transporter	Positive Interactions	Negative Interactions	Sum Total
MDPV	*wt* dDAT	8	-12	-4
MDPV	dDAT mutant	8	-9	-1
MDPV	hDAT	11	-8	3
α-PVP	*wt* dDAT	8	-8	0
α-PVP	dDAT mutant	7	-7	0
α-PVP	hDAT	11	-6	5
MDPPP	*wt* dDAT	6	-10	-4
MDPPP	dDAT mutant	6	-8	-2
MDPPP	hDAT	11	-4	7

a. Interactions at *subpocket A*

MDPV (**10**), α-PVP (**11**), and MDPPP (**39**) all have the same structural feature (the pyrrolidine ring) occupying *subpocket A* (Figure 40). *Subpocket A* had the highest scoring

HINT interactions compared to the other subpockets. The cause for this high score is driven by the salt bridge formed by the essential amino acid residue D46 (dDAT)/ D79 (hDAT) and the protonated pyrrolidine nitrogen atom.

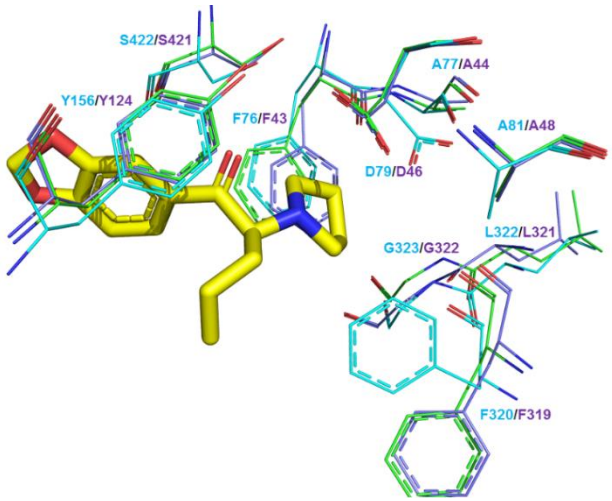

Figure 40. Amino acid residues (lines) that make up *subpocket A* for hDAT (cyan), dDAT mutant (green), and *wt* dDAT (purple). MDPV (**10**, sticks, yellow) shown as a reference.

b. Interactions at *subpocket B*

The aromatic portion (i.e., benzodioxole or phenyl ring) of the three agents was located within *subpocket B* of the transporters (Figure 41). α-PVP (**11**) differs from the other two agents in the aromatic portion of the molecules in that it lacks the methylenedioxy ring found in MDPV (**10**) and MDPPP (**39**). It has previously been shown that this difference has little effect on the potency of **11** when compared to MDPV (**10**) in hDAT.[39] The influence of this methylenedioxy ring section in *wt* dDAT and dDAT mutant should be

apparent if there is a large difference between the HINT scores of α-PVP (**11**) and the other two agents. Its scores were higher for all three models. This is contrary to the mutant transporter biological data but is likely due to fewer clashing interactions from the smaller phenyl ring compared to the benzodioxole ring in the modeling.

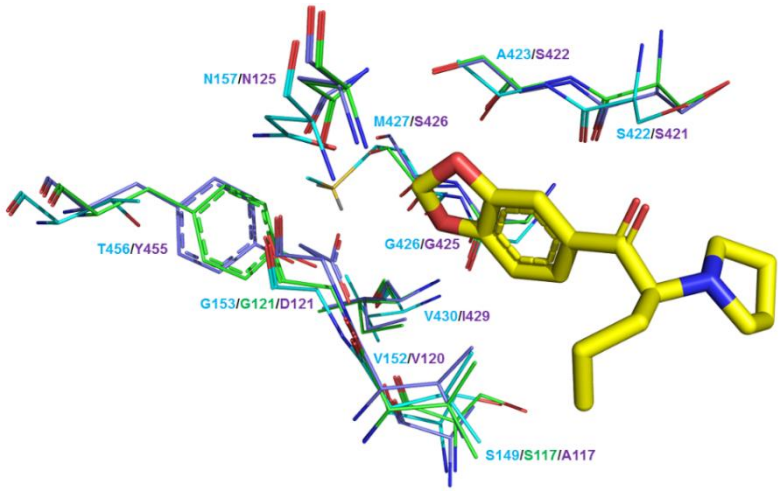

Figure 41. Amino acid residues (lines) that make up *subpocket B* for hDAT (cyan), dDAT mutant (green), and *wt* dDAT (purple). MDPV (**10**, sticks, yellow) shown as a reference.

hDAT had the most favorable interactions with the compounds at residues V152, S422, A423, G426, and M427. *wt* dDAT showed favorable interactions with residues V120, G425, I429. Two of the mutations, A117S and D121G, make up a portion of *subpocket B* and correspond to residues S149 and G153 in hDAT. These two residues have a direct effect on ligand/protein interactions at the S1 central binding site. The D121G dDAT single mutant also was the most effective at increasing MDPV's (**10**) potency in the biological assays compared to any other dDAT single mutant evaluated (data not shown). The major

clashes observed in *subpocket* B were between the docked agents' aryl portions and the residues A117 and D121 in *wt* dDAT. These interactions are more favorable with the related residues S149 and G153 in hDAT. The dDAT mutant, having the D121G mutation, exchanges the negative clash of the bulky aspartate residue to a positive interaction with the smaller neutral glycine. This allows more space for the ligand to orient and removes polar clashing interactions such as electronegative repulsion from the oxygen atoms of the methylenedioxy ring of MDPV (**10**) and the oxygen atoms of D121. The A117S mutation favors interactions with the agents by possible hydrogen bonding with one of the oxygen atoms of the methylenedioxy ring for MDPV (**10**)/MDPPP (**39**) and/or by bonding with the protein backbone, thereby increasing the size of the pocket. The measured distance of the potential hydrogen bond between the two methylenedioxy ring containing agents and the dDAT mutant and hDAT models was 3.9 Å and 7.53 Å, respectively. These distances make this interaction unlikely and just a weak electrostatic interaction if anything. If the weak but favorable interaction is occurring it would explain why that in all the biological data, α-PVP (**11**) (without the methylendioxy ring) was slightly weaker than MDPV (**10**) except for the *wt* dDAT, which has alanine and not serine at that position. It was found that S117/S149 was able to form a hydrogen bond with the backbone amide oxygen atom of F325 or F326 in the dDAT mutant and hDAT models, respectively. The measured distances of these possible hydrogen bonds are 2.6 Å and 2.8 Å for the dDAT mutant and hDAT, respectively. The possible S117 and F325/F326 hydrogen bond would pull the S117/S149 residue away from the binding pocket creating more space for the ligand to bind. This hydrogen bond interaction cannot take place with an alanine residue and would explain the clashes in the *wt* dDAT model. The dDAT mutant did have a

negative interaction at G425 with the aryl portion of the agents compared to *wt* dDAT where this interaction was not observed.

c. Interactions at *subpocket C*

Subpocket C is enveloped with hydrophobic amino acid residues (Figure 42). The only nonneutral residues are the two aspartates D476/D475 and D79/D46 for hDAT and dDATs, respectively. The hydrophobic alkyl side chains, methyl for MDPPP (**39**) and *n*-propyl for MDPV (**10**) and α-PVP (**11**), occupied *subpocket C* with nothing but favorable hydrophobic interactions. In fact, the methyl substituent of MDPPP (**39**) did not have any overall negative interactions, only fewer favorable interactions within *subpocket C* compared to the other two compounds. In the hDAT model the α-methyl substituent of MDPPP (**39**) is not long enough to interact with residues (I484 and F155), or residues (I483 and A479) in the mutant and *wt* dDAT models, respectively. The absence of these interactions is most likely the driving force for why MDPPP (**39**) is much less potent compared to the other two agents MDPV (**10**) and α-PVP (**11**). Due to only favorable interactions within *subpocket C* for both hDAT and dDATs, the difference in potency between the different transporters for MDPV (**10**) is plausibly not driven by its alkyl side chain. That is to say an extended alkyl side chain most likely benefits potency of these agents in DAT regardless of the construct (i.e., dDAT or hDAT) and is not responsible for the gain in potency observed.

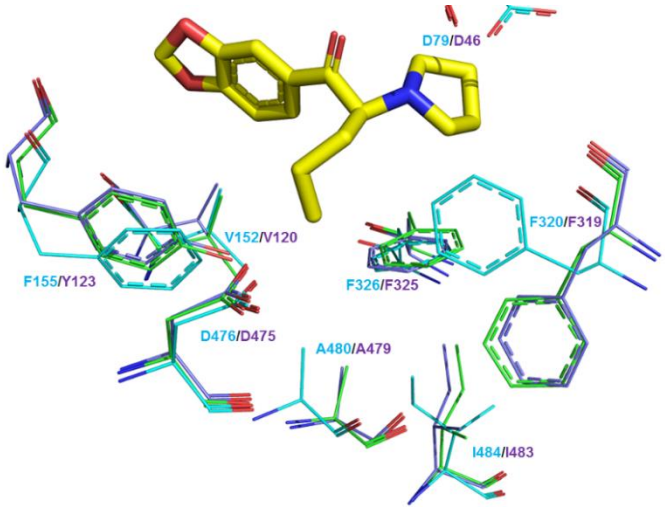

Figure 42. Amino acid residues (lines) that make up *subpocket C* for hDAT (cyan), dDAT mutant (green), and *wt* dDAT (purple). MDPV (**10**, sticks, yellow) shown as a reference.

V. Conclusions

A two-pronged approach has provided a means in which to expand the understanding of DAT SAR using new compounds and “known” transporters as well as “known” compounds and new (i.e., mutant DAT) transporters. Through this work new hDAT homology models were generated, and new potent DAT inhibitors were synthesized, characterized, and evaluated. These projects provided insight on the types of molecular interactions involved in hDAT function and small molecule inhibitors for aryl substituents

For project 1 a new homology model of hDAT was generated that was able to successfully determine that the new hybrid compounds would be active. It was found that all compounds tested were active in the nanomolar range exhibiting that lipophilicity (π) plays a role in DAT activity. Differences in magnitude of activity could be attributed to electronic character (σ value) favoring electron withdrawing substituents as 3,4-dichloro compound **119** and naphthyl compound **121** were more potent than 3,4-dimethyl compound **120**. The volume of all the substituents are tolerated but are not the cause of difference in activity as compound **121** was similar in potency compared to the smaller compound **119**. Both compounds **119** and **121** can be hydrogen bond acceptors while compound **120** cannot. Compound **119** forming a halogen bond is not likely because **121** is almost as potent.

For project 2 using modeling it was found that residues S149, V152, G426, and M427 were identified to be vital interactions within the S1 central binding site. Non-conserved

residues identified can drive MDPV (**10**) selectivity not solely by stabilizing binding, but also controlling access to its binding site. The mutations on the outside of the binding site at the entrance can lend flexibility to the transporter and the overall size of the central binding pocket can greatly affect an agent's activity.

Modeling in both projects helped identify amino acids that are important for DAT activity through both SAR of small molecules and DAT mutants. Although attempts were made to understand the functional activity/potency of benzoylpiperdines via use of molecular modeling studies, it might be noted that use of radioligand binding data might have provided an even better picture of ligand-transporter interactions. Nevertheless, the current approach can be justified because the potency of methylphenidate (**9**) analogs as DAT reuptake inhibitors has been demonstrated to be significantly correlated with their DAT affinity as determined using radioligand binding.[7]

Future work should include synthesis and evaluation of more disubstituted benzoylpiperdines as well as optical isomers to round out the SAR for the aryl portion of DAT inhibitors. Also, in vivo studies should be conducted to see if these compounds have any abuse liability or can be used for therapeutics in the treatment of dopamine dysregulation.

VI. Experimental

A. Molecular Modeling

One hundred homology models of hDAT were generated using MODELLER 9.24 and three crystal structures as a template.[89,90] The two highest identity dDAT crystal structures (PDB ID: 4XPB, 4XPT) at 55.35% and 55.33% identity, respectively, as well as the greatest query coverage hSERT crystal structure (PDB ID: 6VRH) at 92% coverage were used.[15,18,90] The alignment of the structures was conducted using BLAST.[81] The sequences of both dDATs, hSERT, and hDAT were obtained from GenPept (accession codes 4XPB_A, 4XPT_A, 6VRH_A, and BAA22511, respectively). Due to the lack of corresponding residues, the first 54 residues from the N-terminus were not modelled. The homology model with the lowest discrete optimized protein energy (DOPE) score and highest GA341 score was then used for docking.[89,91] GA341 is a multivariate scoring function that depends on compactness and combined statistical potential z-score of the model as well as the percentage sequence identity of the target-template alignment that was used to build the model.[89,91] The mutant quadruple transporter in the present study was generated using SybylX 2.1.1 (TRIPOS Associates, Inc) by replacing the dDAT (PDB ID: 4XP4) amino acids with the corresponding hDAT amino acids D121G, P323V, A117S, and F318C.[15,92] The compounds MDPV, α-PVP, and MDPPP (as their *S* isomers) were sketched using SybylX 2.1.1 and energy minimized using the Tripos Force Field with Gasteiger-Hückel charges. The automated docking program GOLDsuite2020 was used to dock the three compounds one hundred times in each of the three DAT models (*wt* dDAT, quadruple dDAT mutant, hDAT) using D46 and D79 residues and the surrounding 10-Å radius to define the binding pocket for the dDAT and hDAT models, respectively.[93]

All solutions generated from GOLD were then merged with their respective protein and energy-minimized using the Tripos Force Field with Gasteiger-Hückel charges in SybylX 2.1.1.[93,83] The Hydropathic INTeraction (HINT) analysis software within SYBYL 8.1 was used to quantify the nature and magnitude of the molecular interactions between the aromatic and alkyl side chains of the compounds and subpockets *A*, *B*, and *C* of the dDAT and hDAT models.[84] For the initial partitioning phase, the dictionary method was used for the protein and the calculation method was used for the ligands.[83,84] All other parameters were set to their default values. Atom-based interactions involving atoms within subpockets *A*, *B*, and *C* were extracted from the resulting HINT table and tabulated. MOLCAD and BioPolymer suite within SybylX 2.1.1 were used for binding pocket volume calculations and RMSD calculations, respectively.

B. Synthesis

Melting points were taken on MEL TEMP melting point apparatus in glass capillary tubes and are uncorrected. ^{1}H NMR spectra were recorded using a Bruker AXR 400 MHz spectrometer with tetramethylsilane (TMS) as an internal standard. Signal positions are given in parts per million (δ) downfield from TMS, together with their splitting pattern (s = singlet, d = doublet, t = triplet, q = quartet, dd = doublet of doublets, m = multiplet), coupling constant (J, Hz) and integration. MS were recorded using a Waters Acquity tandem quadrupole (TQD) instrument with electrospray ionization. Infrared spectra were obtained on a Thermo Nicolet iS10 FT-IR spectrophotometer. Microanalyses were performed by Atlantic Microlab Inc. (Norcross, GA) for the indicated elements and results are within 0.4% of calculated values. Reactions were routinely monitored by thin-layer

chromatography (TLC) using silica gel GHLF plates (250 mm, 2.5 x 10 cm; Analtech Inc. Newark, DE), and flash chromatography was performed on a CombiFlash Companion/TS (Teledyne Isco Inc. Lincoln, NE). All final compounds were prepared as water-soluble hydrochloride salts.

2-(3,4-Dichlorobenzoyl)piperidine Hydrochloride (119). 1-Bromo-3,4 dichlorobenzene (**125**; 0.50 g, 2.2 mmol) was dissolved in anhydrous Et_2O (7 mL) under an N_2 atmosphere and cooled to -78 °C (acetone : dry ice) and then 2.5 M n-BuLi in hexane (1.8 mL, 4.4 mmol) was added in a dropwise manner over 15 min. The reaction mixture was stirred at -78 °C for 3 h to give intermediate **128**. In another flask a stirred solution of **124** (0.59 g, 2.2 mmol) in Et_2O (5 mL) under an N_2 atmosphere was cooled to -29 °C (o-xylene : dry ice) and then **128** was added in a dropwise manner over 15 min. The reaction mixture was stirred at -29 °C for 3 h and allowed to warm to room temperature with continued stirring for 12 h. The reaction mixture was quenched using cold 1 M KH_2PO_4 (20 mL), extracted with EtOAc (3 x 30 mL), dried over $MgSO_4$, filtered, and evaporated under reduced pressure to produce a yellow oil that was chromatographed on silica gel 10 : 0 – 7 : 3 hexane : EtOAc. The collected fractions were combined and concentrated under reduced pressure. The concentrate was dissolved in anhydrous Et_2O and cooled in an ice bath. Anhydrous methanolic HCl was added in a dropwise manner until pH=1. The solution was stirred overnight and evaporated to dryness. Washing with acetone then recrystallization from MeOH gave 0.07 g of **119** as a white solid (12% yield): mp 272-273 °C (lit.[7] mp 273-275 °C); ^{1}H NMR (DMSO-d_6 , 400 Mhz) δ 1.42–1.45 (m, 1H, CH_2), 1.65–1.77 (m, 4H, 2 x CH_2), 2.06–2.09 (d, 1H, J = 12 Hz, CH_2), 2.92–2.95 (d, 1H, J = 12 Hz,

CH_2), 3.33–3.36 (d, 1H, *J* = 12 Hz, CH_2), 5.13–5.18 (m, 1H, CH), 7.89-7.92 (m, 1H, Ar-H), 8.01–8.03 (m, 1H, Ar-H), 8.30–8.31 (m, 1H, Ar–H), 8.97-8.98 (br d, 1H, NH), 9.53-9.64 (br d, 1H, NH^+); IR (diamond, cm^{-1}) 1685 (C═O); HRMS (ESI-TOF) m/z $[M + H]^+$ calcd for $C_{12}H_{13}NOCl_2$, 258.0452; found, 258.0439; Anal. Calcd for $C_{12}H_{13}NOCl_2 \cdot HCl$: C, 48.92; H, 4.79; N, 4.75. Found: C, 48.81; H, 4.80; N, 4.77.

2-(3,4-Dimethylbenzoyl)piperidine Hydrochloride (120). 4-Bromo-o-xylene (**126**; 0.35 mL, 2.6 mmol) was dissolved in anhydrous Et_2O (5 mL) under an N_2 atmosphere and cooled to 0 °C (ice-bath) and then 2.5 M n-BuLi in hexane (1.3 mL, 3.1 mmol) was added in a dropwise manner over 15 min. The reaction mixture was stirred at 0 °C (ice bath) for 3 h to give intermediate **129**. In another flask a stirred solution of **124** (0.20 g, 1.8 mmol) in Et_2O (5 mL) under an N_2 atmosphere was cooled to -29 °C (o-xylene : dry ice) and then **129** was added in a dropwise manner over 15 min. The reaction mixture was stirred at -29 °C for 3 h and then allowed to warm to room temperature with continued stirring for 12 h. The reaction mixture was quenched using cold 1 M KH_2PO_4 (25 mL), extracted with EtOAc (3 x 30 mL), dried over Na_2SO_4, filtered, and evaporated under reduced pressure to produce a yellow oil that was chromatographed on silica gel 9.5 : 0.5 hexane : EtOAc. The collected fractions were combined and concentrated under reduced pressure. The concentrate was dissolved in anhydrous MeOH and cooled in an ice-bath. Anhydrous methanolic HCl was added in a dropwise manner until pH=1. The solution was stirred overnight and evaporated to dryness. Washing with acetone then recrystallization from EtOH gave 0.12 g of **120** as a white solid (27% yield): mp 262-264 °C; ^{1}H NMR (DMSO-d_6, 400 Mhz) δ 1.48(m, 1H, CH_2), 1.82(m, 4H, 2 x CH_2), 2.11(d, 1H, *J* = 16 Hz, CH_2),

2.38(s, 6H, 2 x CH_3), 3.01(d, 1H, *J* = 12 Hz, CH_2), 3.40(d, 1H, *J* = 16 Hz, CH_2), 5.11(m, 1H, CH), 7.42(m, 1H, ArH), 7.85(m, 1H, ArH), 7.89(s, 1H, ArH), 8.94(br s, 1H, NH), 9.81(br s, 1H, NH^+); IR (diamond, cm^{-1}) 1683 (C═O); HRMS (ESI-TOF) m/z $[M + H]^+$ calcd for $C_{14}H_{19}NO$, 218.1545; found, 218.1536.

2-(Naphtho-2-yl)piperidine Hydrochloride (121). 2-Bromonaphthalene (**127**; 0.50 g, 2.43 mmol) was dissolved in anhydrous Et_2O (10 mL) under an N_2 atmosphere. The stirred mixture was cooled to -78 °C (acetone : dry ice). n-BuLi in hexanes (2.5 M, 5.93 mL, 4.83 mmol) was added in a dropwise manner over 15 min. The reaction mixture was stirred at -78 °C for 3 h to give intermediate **130**. In another flask a stirred solution of **124** (0.62 g, 2.74 mmol) in Et_2O (5 mL) under an N_2 atmosphere was cooled to -23 °C (CCl_4 : dry ice bath). Compound **130** was added in a dropwise manner over 15 min. The reaction mixture was stirred at -23 °C (CCl_4 : dry ice bath) for 3 h and then allowed to warm to room temperature with continued stirring for 12 h. The reaction mixture was quenched using cold 1 M KH_2PO_4 (20 mL), extracted with EtOAc (3 x 30 mL), dried over $MgSO_4$, filtered, and evaporated under reduced pressure to produce a yellow oil that was chromatographed on silica gel 10 : 0 – 2 : 8 hexane : EtOAc. The collected fractions were combined and stirred in anhydrous methanolic HCl overnight and evaporated to dryness. Recrystallization from MeOH gave 0.13 g of **121** as a white solid (20% yield): mp 245-247 °C; ^{1}H NMR (DMSO-d_6, 400 Mhz) δ 1.49–1.59 (q, 1H, CH_2), 1.73–1.89 (m, 4H, 2 x CH_2), 2.19–2.23 (d, 1H, *J* = 16 Hz, CH_2), 3.00–3.06 (t, 1H, *J* = 12 Hz, CH_2), 3.34–3.40 (t, 1H, *J* = 12 Hz, CH_2), 5.27–5.30 (d, 1H, *J* = 12 Hz, CH), 7.67-7.76 (m, 2H, Ar-H), 8.03–8.07 (m, 2H, Ar-H), 8.10–8.13 (d, 1H, *J* = 12 Hz, Ar–H), 8.17–8.19 (d, 1H, *J* = 8 Hz, Ar–

H), 8.85 (s, 1H, Ar–H), 9.00 (br s, 1H, NH), 9.86 (br s, 1H, NH^+); IR (diamond, cm^{-1}) 1674 (C═O); HRMS (ESI-TOF) m/z $[M + H]^+$ calcd for $C_{16}H_{18}NO$, 240.1383; found, 240.1374.

***N*-Boc-pipecolic acid (123)**. Pipecolic acid (**122**) (2.0 g, 15.5 mmol) was added to MeOH (22 mL) followed by the addition of Et_3N (2.4 mL, 17.2 mmol). Room temperature $(Boc)_2O$ (7.12 mL, 31.0 mmol) was then added to the stirred reaction mixture via syringe. The reaction mixture was stirred for 1 h at room temperature. The mixture was then concentrated under reduced pressure and suspended between EtOAc (75 mL) and sat. $NaHCO_3$ (75 mL). The organic layer was extracted with sat. $NaHCO_3$ (2 x 30 mL) and H_2O (30 mL). The aqueous portions were combined and brought to pH 2 using 3 M HCl and extracted with EtOAc (4 x 30 mL). The combined organic portion was dried over $MgSO_4$, filtered, and evaporated under reduced pressure to yield 3.4 g of *N*-Boc-2-pipecolic acid (**123**) as a white solid (95% yield): mp 130-133 °C. (lit.[67] 123-124 °C).

***N*-Boc-pipecolate *N*-(methylmethoxyl)amide (124)**. *N*-Boc-2-pipecolic acid (**123**; 3.38 g, 14.7 mmol) was dissolved in DCM (50 mL) followed by the addition of *N*,*O*-dimethylhydroxylamine hydrochloride (1.72 g, 17.7 mmol) and Et_3N (7.18 mL, 51.5 mmol). BOP (7.16 g, 16.2 mmol) was then added and the mixture was stirred at room temperature for 16 h. The reaction mixture was then diluted with DCM (150 mL) and added to a separatory funnel containing 1 M HCl (75 mL). The organic layer was washed with sat. $NaHCO_3$ (3 x 30 mL), brine (2 x 30 mL), H_2O (2 x 30 mL), and 5% HCl (2 x 30 mL), dried over $MgSO_4$, filtered, and evaporated under reduced pressure. The resultant oil was then

chromatographed on silica gel 4 : 1 hexanes : EtOAc to give 3.35 g of **124** as a colorless oil that crystallized to a white solid over 48 h (84% yield): mp 64-66 °C (lit.[94] 66-68 °C).

2-(1-Pentoyl)piperidine Hydrochloride (132) 4-Bromo-o-xylene (**126**; 0.35 mL, 2.6 mmol) was dissolved in anhydrous Et_2O (5 mL) under an N_2 atmosphere and cooled to -78 °C (acetone : dry ice) and then 2.5 M n-BuLi in hexane (2.08 mL, 5.2 mmol) was added in a dropwise manner over 15 min. The reaction mixture was stirred at -78 °C for 3 h to give intermediate **128**. In another flask a stirred solution of **124** (0.57 g, 2.6 mmol) in Et_2O (5 mL) under an N_2 atmosphere was cooled to -29 °C (o-xylene : dry ice) and then **128** was added in a dropwise manner over 15 min. The reaction mixture was stirred at -29 °C for 3 h and allowed to warm to room temperature with continued stirring for 12 h. The reaction mixture was quenched using cold 1 M KH_2PO_4 (20 mL), extracted with EtOAc (3 x 30 mL), dried over $MgSO_4$, filtered, and evaporated under reduced pressure to produce a yellow oil that was chromatographed on silica gel 10 : 0 – 7 : 3 hexane : EtOAc. The collected fractions were combined and concentrated under reduced pressure. The concentrate was dissolved in anhydrous Et_2O and cooled in an ice bath. Anhydrous methanolic HCl was added in a dropwise manner until pH=1. The solution was stirred overnight and evaporated to dryness. Washing with acetone then recrystallization from MeOH gave 0.13 g of **132** as a white solid: mp 162-163 °C; ^{1}H NMR (DMSO-d_6 , 400 Mhz) δ 0.87 (s, 3H, CH_3), 1.26–1.28 (m, 2H, CH_2), 1.48–1.68 (m, 7H, CH_2), 2.21–2.24 (m, 1H, CH_2), 2.59 (m, 1H, CH_2), 2.78-2.84 (m, 1H, CH), 3.19 (d, 1H, J = 12 Hz, CH_2), 4.01-4.04 (dd, 1H, J = 12 Hz, CH), 9.22-9.28 (br s, 1H, NH), 9.22-9.28 (br s, 1H, NH^+); HRMS (ESI-TOF) m/z $[M + H]^+$ calcd for $C_{12}H_{13}NOCl_2$, 170.1544 found 170.1535.

C. APP^+ Uptake Assay

1. Preparation of HEK293 cells

A HEK293 Flp-In T-REx cell line stably expressing hDAT was developed previously in the laboratory.[46] Cells were prepared in Dulbecco's modified Eagle's medium (DMEM) supplemented with 10% fetal bovine serum and hygromycin. The cells were plated on 96-well plates and were transiently transfected with red fluorescent protein (DsRed, TaKaRa Bio USA, Mountain View, CA) which is used to focus cells to a monolayer plane in the fluorescence microscope before the addition of APP^+. Doxycycline (1 μg/mL) was added to the culturing media 3 days before the experiment to induce expression of DAT.

2. Solution for the experiment

Imaging solution (IS) was prepared and was used to dissolve all the analogs and as a vehicle. It consisted of NaCl (130 mM), KCl (4 mM), $CaCl_2$ (2 mM), $MgCl_2$ (1 mM), Hepes (10 mM), and glucose (10 mM). The pH of the IS was adjusted between 7.3-7.4 using a saturated solution of NaOH.

3. Agents

threo-Methylphenidate was purchased as its hydrochloride salt from

Sigma-Aldrich, St. Louis, MO.

4. Live-cell imaging

The cells were placed on the stage of the epifluorescent microscope (Olympus IX71) equipped with a light source DeltaRAM X Random Access Monochromator (HORIBA Scientific, Piscataway, New Jersey), a Lightning-Cam camera (HORIBA Scientific, Piscataway, New Jersey), and an automated perfusion system Pressurized Superfusion (AutoMate Scientific, Berkeley, California) regulated by Clampex 10.2 (Molecular Devices, San Jose, California). The imaging system was coordinated using the EasyRatioPro 3 (HORIBA Scientific, Piscataway, New Jersey). The entire experiment was done at room temperature. The DsRed signal of transfected cells were used to find the focal plane of the cell monolayer. The wavelength of 460 nm was used for excitation of the APP+ and 540 nm to detect the emission. The experiment consisted of three phases over 70 seconds and was under constant perfusion. The cells were exposed with the IS for 10 seconds followed by the compound of interest for 30 seconds and finally compound of interest plus APP^+ (3 μM) for 30 seconds. All the hybrid analogs were evaluated at six different concentrations in order to obtain a complete dose-response curve.

5. Analysis

The data obtained from the APP^+ assay were analyzed using EasyRatioPro 3 (HORIBA Scientific, Piscataway, New Jersey) and the dose-response curves were plotted using GraphPad Prism 8.0.

VII. Bibliography

1. Pramod, A. B.; Foster, J.; Carvelli, L.; Henry, L. K. SLC6 Transporters: Structure, Function, Regulation, Disease Association and Therapeutics. *Mol. Aspects Med.* **2013**, *34*, 197–219.
2. Yamashita, A.; Singh, S. K.; Kawate, T.; Jin, Y.; Gouaux, E. Crystal Structure of LEUTAA, a Bacterial Homolog of Na+/Cl^--Dependent Neurotransmitter Transporters. *Nature* **2005**, *437*, 215–223.
3. Gouaux, E.; Penmatsa, A.; Wang, K. X-Ray Structure of Dopamine Transporter Elucidates Antidepressant Mechanism. *Nature* **2013**, *503*, 85–90.
4. Coleman, J. A.; Green, E. M.; Gouaux, E. X-Ray Structures and Mechanism of the Human Serotonin Transporter. *Nature* **2016**, *532*, 334–339.
5. Glennon, R. A.; Dukat, M. Structure-Activity Relationships of Synthetic Cathinones. In *Neuropharmacology of New Psychoactive Substances (NPS). Current Topics in Behavioral Neurosciences*; vol 32; Baumann M., Glennon R. A., Wiley J., Eds.; Springer International Publishing: New York City, 2017; pp 19–47.
6. Misra, M.; Shi, Q.; Ye, X.; Gruszecka-Kowalik, E.; Bu, W.; Liu, Z.; Schweri, M. M.; Deutsch, H. M.; Venanzi, C. A. Quantitative Structure–Activity Relationship Studies of Threo-Methylphenidate Analogs. *Bioorg. Med. Chem.* **2010**, *18*, 7221–7238.
7. Yadav-Samudrala, B. J.; Eltit, J. M.; Glennon, R. A. Synthetic Cathinone Analogues Structurally Related to the Central Stimulant Methylphenidate as Dopamine Reuptake Inhibitors. *ACS Chem. Neurosci.* **2019**, *10*, 4043–4050.

8. Hertting, G.; Axelrod, J. Fate of Tritiated Noradrenaline at the Sympathetic Nerve Endings. *Nature* **1961**, *192*, 172–173.
9. Betke, K. M.; Wells, C. A.; Hamm, H. E. GPCR Mediated Regulation of Synaptic Transmission. *Prog. Neurobiol.* **2012**, *96*, 304–321.
10. Torres, G. E.; Gainetdinov, R. R.; Caron, M. G. Plasma Membrane Monoamine Transporters: Structure, Regulation and Function. *Nat. Rev. Neurosci.* **2003**, *4*, 13–25.
11. Jaber, M. Monoamine Transporters. In *Psychopharmacogenetics*; Gorwood, P., Hamon, M. D., Eds.; Springer US: New York City, NY, 2006; pp 333–355.
12. Niello, M.; Cintulova, D.; Hellsberg, E.; Jäntsch, K.; Holy, M.; Ayatollahi, L. H.; Cozzi, N. V.; Freissmuth, M.; Sandtner, W.; Ecker, G. F.; Mihovilovic, M. D.; Sitte, H. H. Para-Trifluoromethyl-Methcathinone Is an Allosteric Modulator of the Serotonin Transporter. *Neuropharmacology* **2019**, *161*, 107615.
13. Kristensen, A. S.; Andersen, J.; Jørgensen, T. N.; Sørensen, L.; Eriksen, J.; Loland, C. J.; Strømgaard, K.; Gether, U. SLC6 Neurotransmitter Transporters: Structure, Function, and Regulation. *Pharmacol. Rev.* **2011**, *63*, 585–640.
14. Guastella, J.; Nelson, N.; Nelson, H.; Czyzyk, L.; Keynan, S.; Miedel, M.; Davidson, N.; Lester, H.; Kanner, B. Cloning and Expression of a Rat Brain GABA Transporter. *Science* **1990**, *249*, 1303–1306.
15. Wang, K. H.; Penmatsa, A.; Gouaux, E. Neurotransmitter and Psychostimulant Recognition by the Dopamine Transporter. *Nature* **2015**, *521*, 322–327.

16. Penmatsa, A.; Wang, K. H.; Gouaux, E. X-Ray Structures of Drosophila Dopamine Transporter in Complex with Nisoxetine and Reboxetine. *Nat. Struct. Mol. Biol.* **2015**, *22*, 506–508.
17. Coleman, J. A.; Yang, D.; Zhao, Z.; Wen, P.-C.; Yoshioka, C.; Tajkhorshid, E.; Gouaux, E. Serotonin Transporter–Ibogaine Complexes Illuminate Mechanisms of Inhibition and Transport. *Nature* **2019**, *569*, 141–145.
18. Coleman, J. A.; Navratna, V.; Antermite, D.; Yang, D.; Bull, J. A.; Gouaux, E. Chemical and Structural Investigation of the Paroxetine-Human Serotonin Transporter Complex. *eLife* **2020**, *9*, e56427.
19. Coleman, J. A.; Gouaux, E. Structural Basis for Recognition of Diverse Antidepressants by the Human Serotonin Transporter. *Nat. Struc. Mol. Biol.* **2018**, *25*, 170–175.
20. Sitte, H. H.; Freissmuth, M. Amphetamines, New Psychoactive Drugs and the Monoamine Transporter Cycle. *Trends Pharmacol. Sci.* **2015**, *36*, 41–50.
21. Hasenhuetl, P. S.; Bhat, S.; Freissmuth, M.; Sandtner, W. Functional Selectivity and Partial Efficacy at the Monoamine Transporters: A Unified Model of Allosteric Modulation and Amphetamine-Induced Substrate Release. *Mol. Pharmacol.* **2018**, *95*, 303–312.
22. U.S. Department of Justice, Drug Enforcement Administration. Drugs of Abuse A DEA Resource Guide. **2020**; pp 1-112.
23. Goodwin, J. S.; Larson, G. A.; Swant, J.; Sen, N.; Javitch, J. A.; Zahniser, N. R.; De Felice, L. J.; Khoshbouei, H. Amphetamine and Methamphetamine

Differentially Affect Dopamine Transporters in Vitro and in Vivo. *J. Biol. Chem.* **2009**, *284*, 2978–2989.

24. Al-Motarreb, A.; Al-Habori, M.; Broadley, K. J. Khat Chewing, Cardiovascular Diseases and Other Internal Medical Problems: The Current Situation and Directions for Future Research. *J. Ethnopharmacol.* **2010**, *132*, 540–548.
25. Al-Maweri, S. A.; Warnakulasuriya, S.; Samran, A. Khat (Catha Edulis) and Its Oral Health Effects: An Updated Review. *J. Investig. Clin. Dent.* **2017**, *9*, e12288.
26. Hyde, J. F.; Browning, E.; Adams, R. Synthetic Homologs of *d*,*l*-Ephedrine. *J. Am. Chem. Soc.* **1928**, *50*, 2287–2292.
27. Glennon, R. A.; Yousif, M.; Naiman, N.; Kalix, P. Methcathinone: A New and Potent Amphetamine-like Agent. *Pharmacol. Biochem. Behav.* **1987**, *26*, 547–551.
28. Emerson, T. S.; Cisek, J. E. Methcathinone: A Russian Designer Amphetamine Infiltrates the Rural Midwest. *Ann. Emerg. Med.* **1993**, *22*, 1897–1903.
29. Prosser, J. M.; Nelson, L. S. The Toxicology of Bath Salts: A Review of Synthetic Cathinones. *J. Med. Toxicol.* **2011**, *8*, 33–42.
30. Calatayud, J.; González, Á. History of the Development and Evolution of Local Anesthesia Since the Coca Leaf. *Anesthesiology* **2003**, *98*, 1503–1508.
31. Goldstein, R. A.; DesLauriers, C.; Burda, A. M. Cocaine: History, Social Implications, and Toxicity—A Review. *Dis. Mon.* **2009**, *55*, 6–38.
32. Morton, W. A.; Stock, G. G. Methylphenidate Abuse and Psychiatric Side Effects. *Prim. Care Companion J. Clin. Psychiatry* **2000**, *02*, 159–164.
33. U.S. Department of Justice, Drug Enforcement Administration. Lists of: Scheduling Actions Controlled Substances Regulated Chemicals. **2021**; pp 1-96.

34. Gatley, S. J.; Pan, D.; Chen, R.; Chaturvedi, G.; Ding, Y.-S. Affinties of methylphenidate derivatives for dopamine, norepinephrine, and serotonin transporters. *Life Sci.* **1996**, *58*, 231–239.
35. Baumann, M. H.; Partilla, J. S.; Lehner, K. R.; Thorndike, E. B.; Hoffman, A. F.; Holy, M.; Rothman, R. B.; Goldberg, S. R.; Lupica, C. R.; Sitte, H. H.; Brandt, S. D.; Tella, S. R.; Cozzi, N. V.; Schindler, C. W. Powerful Cocaine-Like Actions of 3,4-Methylenedioxypyrovalerone (MDPV), a Principal Constituent of Psychoactive 'Bath Salts' Products. *Neuropsychopharmacology* **2012**, *38*, 552–562.
36. Simmler, L. D.; Wandeler, R.; Liechti, M. E. Bupropion, Methylphenidate, and 3,4-Methylenedioxypyrovalerone Antagonize Methamphetamine-Induced Efflux of Dopamine According to Their Potencies as Dopamine Uptake Inhibitors: Implications for the Treatment of Methamphetamine Dependence. *BMC Res. Notes* **2013**, *6*, 1–5.
37. Baumann, M. H.; Partilla, J. S.; Lehner, K. R. Psychoactive "Bath Salts": Not so Soothing. *Eur. J. Pharmacol.* **2013**, *698*, 1–5.
38. Katselou, M.; Papoutsis, I.; Nikolaou, P.; Spiliopoulou, C.; Athanaselis, S. α-PVP ("Flakka"): a New Synthetic Cathinone Invades the Drug Arena. *Forensic Toxicol.* **2015**, *34*, 41–50.
39. Kolanos, R.; Solis, E.; Sakloth, F.; De Felice, L. J.; Glennon, R. A. "Deconstruction" of the Abused Synthetic Cathinone Methylenedioxypyrovalerone (MDPV) and an Examination of Effects at the Human Dopamine Transporter. *ACS Chem. Neurosci.* **2013**, *4*, 1524–1529.

40. Rothman, R. B.; Partilla, J. S.; Baumann, M. H.; Lightfoot-Siordia, C.; Blough, B. E. Studies of the Biogenic Amine Transporters. 14. Identification of Low-Efficacy “Partial” Substrates for the Biogenic Amine Transporters. *J. Pharmacol Exp. Ther.* **2012**, *341*, 251–262.
41. Solis, E.; Partilla, J. S.; Sakloth, F.; Ruchala, I.; Schwienteck, K. L.; De Felice, L. J.; Eltit, J. M.; Glennon, R. A.; Negus, S. S.; Baumann, M. H. N-Alkylated Analogs of 4-Methylamphetamine (4-MA) Differentially Affect Monoamine Transporters and Abuse Liability. *Neuropsychopharmacology* **2017**, *42*, 1950–1961.
42. Solis, E.; Zdravkovic, I.; Tomlinson, I. D.; Noskov, S. Y.; Rosenthal, S. J.; De Felice, L. J. 4-(4-(Dimethylamino)Phenyl)-1-Methylpyridinium (APP^+) Is a Fluorescent Substrate for the Human Serotonin Transporter. *J. Biol. Chem.* **2012**, *287*, 8852–8863.
43. Steele, T. W.; Eltit, J. M. Using Ca^{2+}-Channel Biosensors to Profile Amphetamines and Cathinones at Monoamine Transporters: Electro-Engineering Cells to Detect Potential New Psychoactive Substances. *Psychopharmacology* **2018**, *236*, 973–988.
44. Karpowicz, R. J.; Dunn, M.; Sulzer, D.; Sames, D. APP^+, a Fluorescent Analogue of the Neurotoxin MPP^+, Is a Marker of Catecholamine Neurons in Brain Tissue, but Not a Fluorescent False Neurotransmitter. *ACS Chem. Neurosci.* **2013**, *4*, 858–869.
45. Wilson, J. N.; Ladefoged, L. K.; Babinchak, W. M.; Schiøtt, B. Binding-Induced Fluorescence of Serotonin Transporter Ligands: A Spectroscopic and Structural

Study of 4-(4-(Dimethylamino)Phenyl)-1-Methylpyridinium (APP+) and APP+Analogues. *ACS Chem. Neurosci.* **2014**, *5*, 296–304.

46. Cameron, K. N.; Solis, E.; Ruchala, I.; De Felice, L. J.; Eltit, J. M. Amphetamine Activates Calcium Channels through Dopamine Transporter-Mediated Depolarization. *Cell Calcium* **2015**, *58*, 457–466.
47. Gonçalves, J. L.; Alves, V. L.; Aguiar, J.; Teixeira, H. M.; Câmara, J. S. Synthetic Cathinones: an Evolving Class of New Psychoactive Substances. *Crit. Rev. Toxicol.* **2019**, *49*, 549–566.
48. Kalix, P. Cathinone, an Alkaloid from Khat Leaves with an Amphetamine-like Releasing Effect. *Psychopharmacology* **1981**, *74*, 269–270.
49. Glennon, R. A.; Schechter, M. D.; Rosecrans, J. A. Discriminative Stimulus Properties of S(−)- and R(+)-Cathinone, (+)-Cathine and Several Structural Modifications. *Pharmacol. Biochem. Behav.* **1984**, *21*, 1–3.
50. Glennon, R. A.; Showalter, D. The Effect of Cathinone and Several Related Derivatives on Locomotor Activity. *Res. Comm. Subst. Abuse* **1981**, *2*, 186–192.
51. Glennon, R. A.; Young, R.; Hauck, A. E.; McKenney, J. D. Structure-Activity Studies on Amphetamine Analogs Using Drug Discrimination Methodology. *Pharmacol. Biochem. Behav.* **1984**, *21*, 895–901.
52. Dal Cason, T. A.; Young, R.; Glennon, R. A. Cathinone: An Investigation of Several N-Alkyl and Methylenedioxy-Substituted Analogs. *Pharmacol. Biochem. Behav.* **1997**, *58*, 1109–1116.
53. Foley, K. F.; Cozzi, N. V. Novel Aminopropiophenones as Potential Antidepressants. *Drug Dev. Res.* **2003**, *60*, 252–260.

54. Cozzi, N. V.; Brandt, S. D.; Daley, P. F.; Partilla, J. S.; Rothman, R. B.; Tulzer, A.; Sitte, H. H.; Baumann, M. H. Pharmacological Examination of Trifluoromethyl Ring-Substituted Methcathinone Analogs. *Eur. J. Pharmacol.* **2013**, *699*, 180–187.
55. Eshleman, A. J.; Wolfrum, K. M.; Hatfield, M. G.; Johnson, R. A.; Murphy, K. V.; Janowsky, A. Substituted Methcathinones Differ in Transporter and Receptor Interactions. *Biochem. Pharmacol.* **2013**, *85*, 1803–1815.
56. Kalix, P.; Glennon, R. A. Further Evidence for an Amphetamine-like Mechanism of Action of the Alkaloid Cathinone. *Biochem. Pharmacol.* **1986**, *35*, 3015–3019.
57. Reith, M. E. A.; Blough, B. E.; Hong, W. C.; Jones, K. T.; Schmitt, K. C.; Baumann, M. H.; Partilla, J. S.; Rothman, R. B.; Katz, J. L. Behavioral, Biological, and Chemical Perspectives on Atypical Agents Targeting the Dopamine Transporter. *Drug Alcohol Depend.* **2015**, *147*, 1–19.
58. Markantonis, S. L.; Kyroudis, A.; Beckett, A. H. The Stereoselective Metabolism of Dimethylpropion and Monomethylpropion. *Biochem. Pharmacol.* **1986**, *35*, 529–532.
59. Cameron, K. N.; Kolanos, R.; Solis, E.; Glennon, R. A.; De Felice, L. J. Bath Salts Components Mephedrone and Methylenedioxypyrovalerone (MDPV) Act Synergistically at the Human Dopamine Transporter. *Br. J. Pharmacol.* **2013**, *168*, 1750–1757.
60. Young, R.; Glennon, R. A. Discriminative Stimulus Effects of S (−)-Methcathinone (CAT): a Potent Stimulant Drug of Abuse. *Psychopharmacology* **1998**, *140*, 250–256.

61. Kolanos, R.; Sakloth, F.; Jain, A. D.; Partilla, J. S.; Baumann, M. H.; Glennon, R. A. Structural Modification of the Designer Stimulant α-Pyrrolidinovalerophenone (α-PVP) Influences Potency at Dopamine Transporters. *ACS Chem. Neurosci.* **2015**, *6*, 1726–1731.
62. Barkley, R. A. A Review of Stimulant Drug Research With Hyperactive Children. *J. Child Psychol. Psychiatry* **1977**, *18*, 137–165.
63. Panizzon, L. La preparazione di piridil- e piperidil-arilacetonitrili e di alcuni prodotti di trasformazione (Parte I). *Helv. Chim. Acta* **1944**, *27*, 1748–1756.
64. Heal, D. J.; Pierce, D. M. Methylphenidate and Its Isomers. *CNS Drugs* **2006**, *20*, 713–738.
65. Hartmann, M.; Panizzon, L. R. Pyridine and Piperidine Compounds and Process of Making Same, US Patent 2,507,631. January 19, 1964.
66. Markowitz, J. S.; Patrick, K. S. Differential Pharmacokinetics and Pharmacodynamics of Methylphenidate Enantiomers. *J. Clin. Psychopharmacol.* **2008**, *28*, S54–S61.
67. Thai, D. L.; Sapko, M. T.; Reiter, C. T.; Bierer, D. E.; Perel, J. M. Asymmetric Synthesis and Pharmacology of Methylphenidate and Its Para-Substituted Derivatives. *J. Med. Chem.* **1998**, *41*, 591–601.
68. Ding, Y.-S.; Gatley, S. J.; Thanos, P. K.; Shea, C.; Garza, V.; Xu, Y.; Carter, P.; King, P.; Warner, D.; Taintor, N. B.; Park, D. J.; Pyatt, B.; Fowler, J. S.; Volkow, N. D. Brain Kinetics of Methylphenidate (Ritalin) Enantiomers after Oral Administration. *Synapse* **2004**, *53*, 168–175.

69. Froimowitz, M.; Patrick, K. S.; Cody, V. Conformational Analysis of Methylphenidate and Its Structural Relationship to Other Dopamine Reuptake Blockers Such as CFT. *Pharm. Res.* **1995**, *12*, 1430–1434.
70. Wenthur, C. J. Classics in Chemical Neuroscience: Methylphenidate. *ACS Chem. Neurosci.* **2016**, *7*, 1030–1040.
71. Deutsch, H. M.; Shi, Q.; Gruszecka-Kowalik, E.; Schweri, M. M. Synthesis and Pharmacology of Potential Cocaine Antagonists. 2. Structure−Activity Relationship Studies of Aromatic Ring-Substituted Methylphenidate Analogs. *J. Med. Chem.* **1996**, *39*, 1201–1209.
72. Kim, D.-I.; Deutsch, H. M.; Ye, X.; Schweri, M. M. Synthesis and Pharmacology of Site-Specific Cocaine Abuse Treatment Agents: Restricted Rotation Analogues of Methylphenidate. *J. Med. Chem.* **2007**, *50*, 2718–2731.
73. Deutsch, H. Synthesis and Pharmacology of Site Specific Cocaine Abuse Treatment Agents: a New Synthetic Methodology for Methylphenidate Analogs Based on the Blaise Reaction. *Eur. J. Med. Chem.* **2001**, *36*, 303–311.
74. Portoghese, P. S. A New Concept on the Mode of Interaction of Narcotic Analgesics with Receptors. *J. Med. Chem.* **1965**, *8*, 609–616.
75. Hansch, C.; Leo, A.; Unger, S. H.; Kim, K. H.; Nikaitani, D.; Lien, E. J. "Aromatic" Substituent Constants for Structure-Activity Correlations. *J. Med. Chem.* **1973,** *16*, 1207-1216.
76. Fujita, T.; Iwasa, J.; Hansch, C. A New Substituent Constant, π, Derived from Partition Coefficients. *J. Am. Chem. Soc.* **1964**, *86*, 5175–5180.

77. Jaffé, H. H. A Reëxamination of the Hammett Equation. *Chem. Rev.* **1953**, *53*, 191–261.
78. Meyer, E. A.; Castellano, R. K.; Diederich, F. Interactions with Aromatic Rings in Chemical and Biological Recognition. *ChemInform* **2003**, *34*, 1210–1250.
79. Stockner, T.; Montgomery, T. R.; Kudlacek, O.; Weissensteiner, R.; Ecker, G. F.; Freissmuth, M.; Sitte, H. H. Mutational Analysis of the High-Affinity Zinc Binding Site Validates a Refined Human Dopamine Transporter Homology Model. *PLoS Comput. Biol.* **2013**, *9*, e1002909.
80. Vitkup, D.; Melamud, E.; Moult, J.; Sander, C. Completeness in Structural Genomics. *Nat. Struct. Biol.* **2001**, *8*, 559–566.
81. Altschul , S. F.; Gish, W.; Miller, W.; Myers, E. W.; Lipman, D. J. Basic Local Alignment Search Tool. *J. Mol. Biol.* **1990**, *215*, 403–410.
82. Reva, B. A.; Finkelstein, A. V.; Skolnick, J. What Is the Probability of a Chance Prediction of a Protein Structure with an RMSD of 6 Å? *Folding Des.* **1998**, *3*, 141–147.
83. Sakloth, F.; Kolanos, R.; Mosier, P. D.; Bonano, J. S.; Banks, M. L.; Partilla, J. S.; Baumann, M. H.; Negus, S. S.; Glennon, R. A. Steric Parameters, Molecular Modeling and Hydropathic Interaction Analysis of the Pharmacology of Para-Substituted Methcathinone Analogues. *Br. J. Pharmacol.* **2015**, *172*, 2210–2218.
84. Kellogg, G. E.; Abraham, D. J. Hydrophobicity: Is LogPo/w More than the Sum of Its Parts? *Eur. J. Med. Chem.* **2000**, *35*, 651–661.
85. Coste, J.; Le-Nguyen, D.; Castro, B. PyBOP®: A New Peptide Coupling Reagent Devoid of Toxic by-Product. *Tetrahedron Lett.* **1990**, *31*, 205–208.

86. Richard, A. M.; Wolf, M. Dsstox (Distributed Structure-Searchable Toxicity Database Network) Project and Website. Presented at board of scientific counselors 2005, RTP, NC, June 19 - 20, 2006.
87. Bailey, W. F.; Luderer, M. R.; Jordan, K. P. Effect of Solvent on the Lithium−Bromine Exchange of Aryl Bromides: Reactions of *n*-Butyllithium and *tert*-Butyllithium with 1-Bromo-4-*tert*-butylbenzene at 0 °C. *J. Org. Chem.* **2006**, *71*, 2825–2828.
88. Cheng, M. H.; Bahar, I. Molecular Mechanism of Dopamine Transport by Human Dopamine Transporter. *Structure* **2015**, *23*, 2171–2181.
89. 89 Šali, A.; Blundell, T. L. Comparative Protein Modelling by Satisfaction of Spatial Restraints. *J. Mol. Biol.* **1993**, *234*, 779–815.
90. Haddad, Y.; Heger, Z.; Adam, V. Guidelines for Homology Modeling of Dopamine, Norepinephrine, and Serotonin Transporters. *ACS Chem. Neurosci.* **2016**, *7*, 1607–1613.
91. Melo, F.; Sali, A. Fold Assessment for Comparative Protein Structure Modeling. *Protein Sci.* **2007**, *16*, 2412–2426.
92. Sybyl-X Molecular Modeling Software Packages, Version 2.0; TRIPOS Associates, Inc: St. Louis, MO, USA, 2012.
93. Jones, G.; Willett, P.; Glen, R. C.; Leach, A. R.; Taylor, R. Development and Validation of a Genetic Algorithm for Flexible Docking. *J. Mol. Biol.* **1997**, *267*, 727–748.

94. Gal, K.; Weber, C.; Wagner, A. G.; Bobok, A. A.; Nyeki, G.; Vastag, M.; Keserue, G.; Hada, V.; Koti, J. Tetrazole Derivatives as Modulators of Metabotropic Glutamate Receptors, U.S. Patent WO2007039782. April 12, 2007.

VIII. Vita

Charles Bernard Jones III was born to Charles and Nancy Jones December 20, 1989 in Lynn Haven, Florida. He received his Bachelor of Science in Chemistry from University of Central Florida, Orlando, Florida in December 2014. After receiving his bachelor degree, he worked as a research scientist on high purity quartz at Unimin in Red Hill, North Carolina. In 2019 he enrolled in Virginia Commonwealth University's School of Pharmacy Medicinal Chemistry graduate program.